A Thermodynamic Investigation of Commercial Kitchen Operations and the Implementation of a Waste Heat Recovery System

A THERMODYNAMIC INVESTIGATION OF COMMERCIAL KITCHEN OPERATIONS AND THE IMPLEMENTATION OF A WASTE HEAT RECOVERY SYSTEM

BY

PAUL RICCIUTI, B.Eng. Mgmt.

A THESIS

SUBMITTED TO THE DEPARTMENT OF MECHANICAL ENGINEERING

AND THE SCHOOL OF GRADUATE STUDIES

OF MCMASTER UNIVERSITY

IN PARTIAL FULFILMENT OF THE REQUIREMENTS

FOR THE DEGREE OF

MASTER OF APPLIED SCIENCE

Master of Applied Science (2017)		McMaster University
(Mechanical Engineering)		Hamilton, Ontario, Canada

TITLE: A Thermodynamic Investigation of Commercial Kitchen Operations and the Implementation of a Waste Heat Recovery System

AUTHOR: Paul Ricciuti
B.Sc., (Mechanical Engineering)
McMaster University, Hamilton Ontario

SUPERVISOR: Dr. J. S. Cotton

NUMBER OF PAGES: xx, 166

Abstract

A modeling tool was developed capable of evaluating the thermal performance of a commercial building, for the purpose of objectively quantifying the impacts of both operational changes and technological retrofits. The modeling tool was created using a steady state energy balance approach, discretized into half hour time steps to capture the time varying characteristics of the rate of heat transfer through the building envelope, the ventilation systems, appliance heat gains, heat generated by electricity consumption, solar energy transfer and space heating through exhaust gas energy recovery with the TEG POWER system.

Several experimental facilities were used to validate the modeling tool, and to provide inputs to the case studies presented. Data from two separate commercial baking operations was collected, and was shown to be in agreement with the model predictions with a 7% error. Several energy conservation measures were simulated, including switching to idealized methods of exhaust ventilation, sealing and insulating appliances, shutting down appliances during unoccupied hours, and the inclusion of exhaust gas energy harvesting. Implementing all four conservation measures at a single restaurant had the effect of reducing electricity consumption by 14% or approximately 17,700 kWh (64 GJ), and reducing natural gas consumption by 60% or approximately 18,200 m^3 (608 GJ) annually. In contrast, proceeding directly to the energy harvesting solution, and

bypassing other conservation measures, only allowed for 20% of the total potential energy savings to be realized.

If the concepts identified are implemented across 2000 comparable restaurants in Ontario, there is a potential to reduced electricity consumption by 44.4 million kWh and natural gas consumption by 33.7 million cubic meters annually. The measures would effectively eliminate 65,500 metric tonnes of CO_2 emissions every year.

Acknowledgments

I would like to express my sincere gratitude to my supervisor, Dr. Jim Cotton, for his guidance and motivation. I always appreciated your critical feedback and suggestions, and thoroughly enjoyed the opportunity to work on the TEG POWER project. I have learned many valuable behaviors and skills that will make me a stronger independent researcher and engineer as I move forward in my career.

I would like to thank my grandparents; Katherine Mayer, for her loving support, and Frank Mayer, who has been my greatest role model as both a mechanical engineer and a gentleman. I would also like to thank to my parents, Sue and Rick Ricciuti, for their continuous support and encouragement, and for setting the family precedent of engineering excellence. And to Eva, for her mostly well timed distractions.

Thank you to all the members of the TMRL team, for fostering such a supportive, and most importantly, fun, learning environment. A special thank you to Jeff Girard and Dr. Vick Lakhian, for their considerable expertise and assistance on many parts of this project, and to Ali and Zaher, for experiencing the joy of Advanced Heat Transfer with me, and the legendary Dr. Judd.

Lastly, I would like to thank NSERC, the Ontario Government and the Ontario Society of Professional Engineers, for providing the financial support to successfully complete this project over the last two years, and to Pizza Pizza Ltd. for providing several of the research facilities.

Contents

List of Figures

List of Tables

Nomenclature

Symbol	Description	Units
A	surface area	m^2
$AFUE$	annual fuel utilization efficiency	$\%$
$C_{p_{air}}$	specific heat capacity of air	$kJ/kg \cdot K$
$C_{p_{water}}$	specific heat capacity of water	$kJ/kg \cdot K$
$C_1, C_2, C_3, C_4, C_5, C_6$	Hyland and Wexler equation coefficients	-
COP	coefficient of performance	-
E_d	diffuse solar irradiance	W/m^2
E_{DN}	direct normal solar irradiance	W/m^2
$\dot{E}_{in}$	sum of all individual energy flows into the building	kW
$\dot{E}_{out}$	sum of all individual energy flows out of the building	kW
g	gravitational constant	m/s^2
h_{fg}	enthalpy of condensation of saturated water	kJ/kg
h_{in}	inner surface heat transfer coefficient (convection and radiation)	$\frac{W}{m^2K}$

h_{out}	outer surface heat transfer coefficient (convection and radiation)	$\frac{W}{m^2K}$
H	height of chimney	m
HDD	heating degree days	$°C$
I_{phase}	phase current	A
LHV_{CH_4}	lower heating value of natural gas	MJ/kg
$\dot{m}_{chimney}$	average mass flow rate of air through chimney	kg/s
$\dot{m}_{dilution}$	average mass flow rate of dilution air	kg/s
$\dot{m}_{exhaust}$	average mass flow rate of air exiting the oven exhaust vent	kg/s
$\dot{m}_{makeup}$	mass flow rate of unconditioned air introduced into the building in the vicinity of the exhaust system	kg/s
$\dot{m}_{net\ ventilation}$	mass flow rate of air traveling through the building that must be conditioned by the HVAC system	kg/s
$\dot{m}_{oven,leakage}$	average mass flow rate of air leaking through the oven door	kg/s
$\dot{m}_{total\ ventilation}$	mass flow rate of air exhausted from the building	kg/s
M_{da}	mass of dry air in moist air mixture	kg
M_w	mass of water vapour in moist air mixture	kg
$M(dry\ air)$	molar mass of dry air	g/mol
$M(H_2O)$	molar mass of water vapour	g/mol
n	total moles in moist air mixture	mol

n_{da}	moles of dry air	mol
n_w	moles of water vapour	mol
p	total pressure of moist air mixture	Pa
p_{da}	partial pressure of dry air	Pa
p_w	partial pressure of water vapour	Pa
p_{ws}	water vapour saturation pressure	Pa
$p_0 - p$	dynamic pressure	Pa
P_{atm}	atmospheric pressure	Pa
P_{phase}	real power measured in a single phase	W
P_{total}	total real power	W
$\dot{q}_b$	direct normal (or beam) solar energy flux	W/m^2
$\dot{q}_d$	diffuse solar energy flux	W/m^2
$Q_{DHW,Electricity(avg)}$	electrical energy input to the hot water tank	kJ
$\dot{Q}_{Building\ Skin}$	rate of heat transfer through the building walls, windows, roof and floor	kW
$\dot{Q}_{DHW}$	rate of energy transfer required to meet the domestic hot water load	kW
$\dot{Q}_{Electrical}$	heat generated through electricity consumption	kW
$\dot{Q}_{floor}$	rate of heat transfer through the floor	kW
$\dot{Q}_{Heating\ or\ Cooling\ Requirement}$	energy flow into or out of the building required to maintain equilibrium	kW
$\dot{Q}_{oven,exhaust}$	rate of energy loss from the oven in the form of exhaust gas	kW

$\dot{Q}_{Oven\ Gain}$	rate of heat transfer from the oven to the room	kW
$\dot{Q}_{oven,gas\ in}$	rate of energy transfer to the oven through the complete combustion of natural gas	kW
$\dot{Q}_{oven,leakage}$	rate of energy loss from oven door exfiltration	kW
$\dot{Q}_{oven,structure}$	rate of energy loss from the oven through convection and radiation	kW
$\dot{Q}_{oven,structure\ (rad)}$	rate of energy loss from the oven through radiation	kW
$\dot{Q}_{oven,structure\ (convection)}$	rate of energy loss from the oven through convection	kW
$\dot{Q}_{recovered}$	rate of thermal energy extraction from the exhaust stream during oven operation	kW
$\dot{Q}_{Solar}$	rate of solar energy transfer to the building	kW
$\dot{Q}_{Space\ Heating}$	recovered thermal energy that is allocated for space heating purposes	kW
$\dot{Q}_{Ventilation\ Latent}$	energy required to dehumidify and condense out a portion of the water vapour in the outside air	kW
$\dot{Q}_{Ventilation\ Sensible}$	rate of heat transfer required to change the temperature of the net ventilation air from the outside temperature to the building set-point temperature	kW
$\dot{Q}_{water,electrical\ (avg)}$	electrical power input to the water tank averaged over a 24-hour time interval	kW
$\dot{Q}_{water,loss\ (avg)}$	average rate of heat loss from the water tank	kW
$\dot{Q}_{water,thermal\ (avg)}$	thermal energy content of the hot water delivered by the water tank averaged over a 24-hour time interval	kW
$\bar{R}$	universal gas constant	$kJ/kmol \cdot K$

$SHGC(\theta)$	solar heat gain coefficient	-
$\langle SHGC\rangle_D$	hemispherically averaged solar heat gain coefficient	-
$t_{oven\ operation}$	length of time the oven was operating	s
T	temperature of moist air mixture	K
T_b	average oven surface temperature	K
$T_{chimney}$	temperature of the exhaust gases in the chimney	$°C$
$T_{dilution}$	temperature of dilution air	$°C$
$\bar{T}_{gr}$	ground surface temperature	$°C$
T_{oven}	oven temperature	$°C$
T_{in}, T_{room}	room temperature	$°C$
T_{out} , $T_{outside}$	outside air temperature	$°C$
T_s	temperature of surroundings	K
U	heat transfer coefficient of the specific surface under consideration	$\frac{W}{m^2K}$
$(UA)_{oven}$	overall heat transfer coefficient of the oven (convection and radiation)	$\frac{W}{K}$
$\vec{v}$	velocity	m/s
V	total volume of moist air mixture	m^3
V_{phase}	phase voltage	V
$V_{water\ (avg)}$	average volume of hot water used by a restaurant each day	L
$\dot{V}$	volume flow rate	m^3/s

$\dot{V}_{coolant\ water}$	volume flow rate of coolant water	L/min
$\dot{V}_{Fryer}$	volume flow rate of natural gas to the fryer	m^3/day
W	humidity ratio of the inside and outside air	kg/kg
x_{da}	mole fraction of dry air	-
x_w	mole fraction of water vapour	-
ε	emissivity	-
θ	incident angle	$degrees$
θ	power factor	-
ρ	density of air	kg/m^3
$\rho_{chimney}$	density of the air in the chimney	kg/m^3
ρ_{CH_4}	density of natural gas	g/m^3
$\rho_{outside}$	density of outside air	kg/m^3
ρ_{water}	density of coolant water	kg/m^3
σ	Stefan-Boltzmann constant	$\frac{W}{m^2K^4}$
ϕ	relative humidity	-

Chapter 1
Introduction and Problem Statement

1.1 Introduction

Over the last 50 years, there has been sustained growth in the world economy. The exponential increase in world population since the 1800s coupled with steadily rising living standards is placing great strain on natural resources and the environment [1]. This growth is supported by a significant increase in global energy consumption, which has more than quadrupled since the year 1950 [2].

Canada alone consumed a total of 14,700 PJ in primary energy resources in 2013, of which 30% was lost in the electricity generation process, 18% was used for transportation, and 16%, 11% and 6% was consumed for industrial, residential and commercial use respectivlty [3]. Within the commercial segment, the overall weighted average efficiency, for the conversion of input energy to useful outputs, was 71%, according to the latest research studies conducted by CESAR (Canada Energy Systems Analysis Research) [3]. However, the results presented within provide considerable doubt that the current assumption of a 71% commercial building energy efficiency, based on current technologies, is accurate in all situations.

The aim of this primary research study was to present a representation of the true energy efficiency of a commercial building, by examining the details of the building energy balance through a thermodynamic first principles analysis. The study had a direct focus on the thermal performance of commercial baking operations, which were proven to have two distinctive operating characteristics; a high heating and cooling design load, and a large untapped source of waste heat. Until now, no significant attempt has been made to address these two design issues, albeit if they are considered simultaneously, there is a great potential to improve energy efficiency, and to reduce waste. The primary data collection and thermodynamic analysis was tailored for commercial baking operations specifically, and these results and the methodology are directly transferable to other commercial buildings which employ natural gas fired appliances. The analysis tool developed to conduct this study, which is grounded in the fundamentals of thermodynamics, heat and mass transfer, provides a quick and simple means of evaluating the net impact of any operational change or technological retrofit on the energy performance of a commercial building.

The significance of this problem, the excessive demand for and wasted supply of thermal energy, and the need for a simplified analysis tool, is evident when simply observing the historical natural gas consumption from a random sample of twenty pizza restaurants located in Southern Ontario [4].

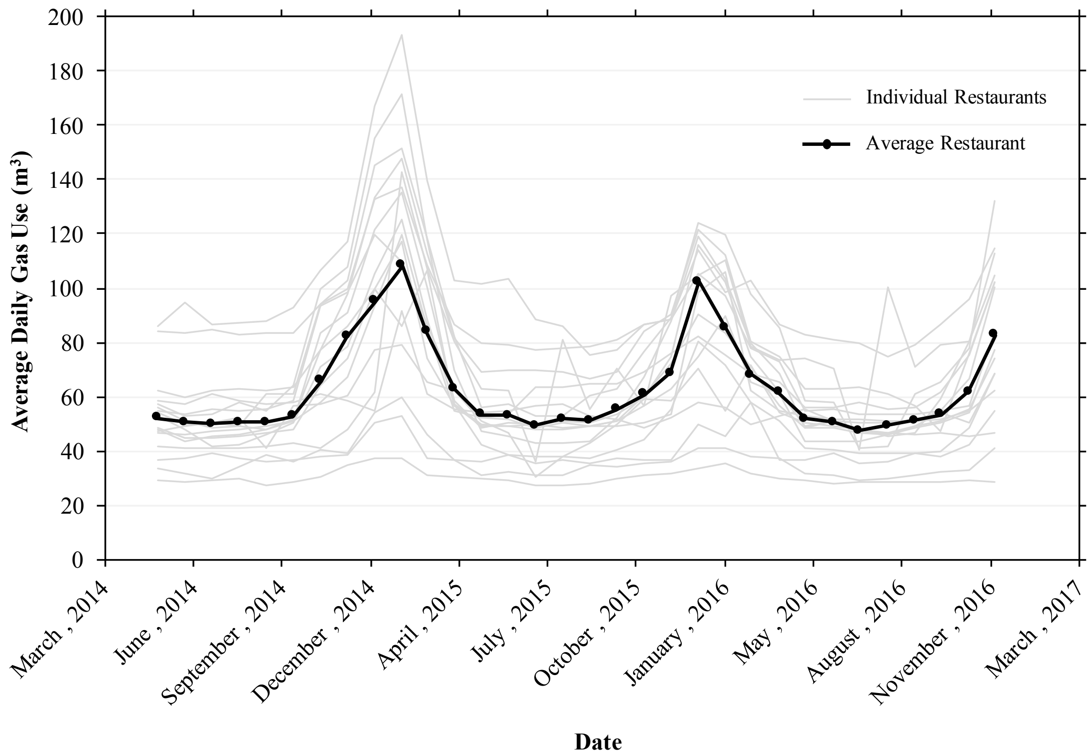

Figure 1.1: Sample of Restaurant Natural Gas Use [4]

Figure 1.1 above provides a rough insight into both of the aforementioned issues, as pizzerias are a prime example of popular commercial baking operations. Observing the summer months, where no building heating was required, revealed that the average natural gas consumption associated with operating the cooking appliances was approximately 50 m^3 per day, or 18,250 m^3 per year. To put this value into context, the quantity of natural gas required to operate the ovens would be able to provide heating to approximately seven average Canadian homes for one year [5]. Considering that the majority of the energy content of the natural gas is exhausted from the building, this represents a significant source of waste heat. Next, observing the natural gas use in the winter months after identifying the base appliance load revealed that an average of 5,000 m^3 was used per year for building heating; the equivalent of heating two average Canadian homes [5]. The operating characteristics that lead to a higher heating demand in the winter, consequently lead to a high cooling demand in the summer.

The goal of this thesis, was to create a simplified modeling tool capable of identifying and objectively evaluating methods of reducing the total energy consumption of a commercial building.

1.2 Motivation – The TEG POWER Research Project

The motivation for this study stems from the **T**hermal **E**lectric **G**enerator **P**izza **O**ven **W**aste **E**nergy **R**ecovery (TEG POWER) research project, which began at McMaster University in 2010. Over the last seven years, the TEG POWER system has been in development at the McMaster Thermal Management Research Laboratory (TMRL), and has been designed with the ability to efficiently capture the wasted heat from a natural gas oven, and repurpose it for hot water and space heating needs, while converting a portion of the energy into electricity to sustain operation. The core of the system is the air-to-liquid exhaust gas heat exchanger, which transfers thermal energy from the hot exhaust gases of the appliance, through a collection of Thermoelectric Generators (TEGs) in parallel, to the coolant water which flows through the surrounding cold side heat exchanger.

The TEG POWER project began with the design of an experimental facility capable of measuring the power generation characteristics and thermal conductivity of commercially available TEGs, for the purpose of integration into the heat exchanger design [6]. Since project inception, the exhaust gas heat exchanger has seen transformational improvements through numerous projects, with the focuses of: improving the hot side and cold side heat exchanger performance independently, designing components for manufacturability, investigating the coupled effects between waste heat recovery and buoyancy driven flow [7], and modeling the systems transient thermal storage characteristics.

This thesis takes a step back from the detailed design of the system, and sheds light on the energy balance of the restaurant as a whole, using the building energy analysis tool developed to identify the potential energy savings that may be achieved, through a combination of operational changes and the TEG POWER Solution. The research presented is valuable, as it provides direct insight into the systems economic viability, social acceptance and greenhouse gas reduction potential.

1.3 Scope

The scope of this thesis was to develop a modeling tool capable of determining the total annual energy savings that can be realized by a commercial building, and investigate the impact of operational changes and energy conservation measures. The main text describing these accomplishments has been divided into five chapters:

Chapter 2 begins by summarizing the current literature, with a focus on building energy modeling methods, commercial kitchen ventilation best practices, relevant codes and standards, and the oven operating characteristics that directly impact the energy balance of the building.

Chapter 3 introduces the thermodynamic model, designed to predict the energy consumption of a building Heating Ventilation and Air Conditioning (HVAC) system. The mathematical models for each component of the energy balance, including heat transfer through the building skin, ventilation, oven heat gains, heat generated by electricity consumption, solar energy transfer and space heating through exhaust gas energy recovery are described.

Chapter 4 highlights the main experimental facilities that were designed to provide inputs to the building energy model, as well as to provide a means of model validation. Two separate restaurants in Hamilton, referred to as Store A and Store B, were selected to investigate the impact of exhaust system configuration on building energy performance. Experiments were also conducted on the test oven at the TMRL, to quantify the effects of oven heat loss, and the rate of thermal energy extraction from the oven through the TEG POWER system. A section on model validation has also been included, where the results of the building HVAC energy model described in Chapter 3 were compared against the experimental data collected from Store A and Store B.

Chapter 5 presents a case study of Store A and Store B employing the modeling tools to quantify the effects of implementing four potential energy conservation measures. The first measure, is to substitute exhaust canopies with chimneys for oven ventilation. The second, is to seal and insulate all ovens, to mitigate the increased heat loss side effects that arise from chimney based oven ventilation. The third, is to turn off all ovens at night, and fully seal the exhaust vent with a mechanically actuated exhaust damper. The fourth, and final conservation measure, is the inclusion of energy harvesting, to recover a portion of the waste heat from the exhaust stream, and to repurpose it for space heating in the winter, and oven preheating in the summer.

Chapter 6 draws conclusions from the research study, and presents recommendations for future work with substantive impact moving forwards.

Chapter 2
Literature Review

2.1 Introduction

This chapter presents a critical review of the literature that was most relevant in developing the energy model presented in this thesis. An analysis of the current state of the art building energy modeling methods is presented, along with an assessment of the commercial software currently available. The most significant research studies in the area of commercial kitchen ventilation practices are evaluated, along with the relevant codes and standards that must be abided for a new design. Lastly, the oven energy balance and exhaust system fundamentals are summarized, with specific emphasis on the operating characteristics of a typical gas fired oven that directly affect the energy balance of the building it operates within.

2.2 Review of Building Energy Modeling Methods

Computer simulation of building energy performance has been a prominent research field since the mid 1970's, and today's analysis tools provide practical engineering design support [8]. Energy models have found their use for two main areas:

1) In the design phase of new building projects, to predict the energy performance for design optimization.
2) Simulating the performance of an existing building, to establish baseline operating characteristics and to predict retrofit savings.

Regardless of the end use, all physical models are comprised of the same three components: input variables (outside and inside dry bulb temperatures, operating schedules, etc.), system characteristics (geometry, thermal conductivity, etc.), and output variables (typically energy consumption). With knowledge of two of these components, the model may be solved for the unknown variable.

2.2.1 Model Classification

Models can be classified by the methodology used to create them, which can be created using either a first principles approach, or an approach based on empirical test data.

First principles models start by creating a description of the physical system, according the well-established physical laws of thermodynamics, heat and mass transfer. A detailed knowledge of the building structure, and the physical phenomenon that significantly affect its energy performance are required. Input variables are then selected to represent the conditions that the system will be subject to, and the model is executed to calculate the output variables. They are typically employed in the design analysis stage of a project, as they do not require empirical test data from a physical structure to develop the model.

Empirical models are created when knowledge of the input and output variables is available, and the goal is to determine a mathematical description of the system characteristics. These models are relevant when the structure has already been built, and data from its normal operation has been measured. Empirical models are generally simpler (i.e. a polynomial function of one or multiple regressor variables) since many individual parameters are combined within coefficients, and provide a more accurate prediction of future energy performance compared to a first principles model, since objects in the physical world seldom behave in accordance with idealized theoretical predictions. However, these models are black-box in nature, and are not grounded by the fundamental laws of physics, which limits their flexibility in modeling the future energy performance of the building outside of the specific condition the model was built to represent. This hampers an empirical model's ability to confidently predict retrofit savings associated with multiple design changes. For this reason, the majority of commercial building energy modeling software available has been built on the first principles approach.

2.2.2 Review of Commercial Software Developments

A wide range of Building Performance Simulation (BPS) tools used for full building and energy systems analysis are currently available for commercial use. The most popular include: e-QUEST, ESP-r, TRNSYS and EnergyPlus [9]. However, no individual tool possesses the capabilities required to address all of the significant aspects that must be considered to accurately model the energy performance of a building which implements novel technologies, where the user requirements exceed the functionality of the tool [10]. For example, ESP-r's strength lies in its ability to model thermal energy transfer within a building and with its surroundings [11]. However, the component library lacks depth, and developing models of novel technologies requires a detailed knowledge of the source-code [12]. On the other hand, TRNSYS was originally developed as a tool for modeling thermal and electrical energy systems, namely solar thermal hot water systems [13]. However, it lacks the thoroughness of ESP-r and other BPS tools for modeling complex thermal interactions within the building structure [12]. Although it is possible to link the two tools to perform a co-simulation, it introduces may new modeling complexities [12].

The applicability of using EnergyPlus was specifically investigated as a means of modeling the retrofit savings of the restaurants. EnergyPlus is a whole building energy simulation tool, and has been under development by the U.S. Department of Energy Office of Energy Efficiency and & Renewable Energy since 1996 [14]. The project was built on the foundations of the BLAST and DOE-2 simulation engines, whose source codes had become fragmented over their +20 year development history by the U.S. Department of Defense and the U.S. Department of Energy respectively [14]. The mission was to, "Develop, maintain, and support a Building Energy Management engine for fair and accurate assessment of different energy efficiency measures for all types of buildings projects," targeted at, "New construction & retrofit design, HVAC selection & sizing, energy-efficiency code development & compliance, asset ratings & labels, policy analysis, commissioning, fault-detection, demand-response & model-predictive control, control design, product design, research & education [15]."

The program was created with a highly structured modular design, where the EnergyPlus Simulation Manager controls data interactions between the Heat and Mass Balance Simulation Module (which calculates zone loads), and the Building Systems Simulation Module (which determines the response of plant equipment to the zone loads). A feedback loop was implemented between the two modules, which reflects unmet zone loads as updated zone temperatures in the next time step [14]. The heat balance method, based on the first law of thermodynamics with the assumption of a uniform zone air temperature, was used to calculate the zone loads in the Heat and Mass Balance Simulation Module, which are defined as the total rate of energy transfer to or from the zone air mass. Intricacies of the solution procedure have been documented by Walton [16], and their integration into the EnergyPlus simulation engine have been published by Strand et al. [17]. Several sub-modules draw on precursor simulation tools, including COMIS (for modeling multi-zone airflows, infiltration and ventilation) [18] and WINDOW 4.1 (for determining window performance characteristics) [19].

For its longstanding history and widespread use, EnergyPlus was used in combination with the Design Builder graphical user interface to create a thermal model of the two specific restaurants under consideration. However, after experimenting with the capabilities of the software package, it was decided to move forward with the more simplified steady-state analysis method, presented in Chapter 3, for several reasons. Firstly, the largest source of error involved in the modeling process was identifying and quantifying the physical phenomenon that most significantly impacted the energy balance of the building. Regardless of the rigor of the EnergyPlus heat balance solution method, the results produced would be erroneous if inputs were not determined correctly. Since operational characteristics were shown to fluctuate in a purely random fashion based on occupant decision making, using the more accurate EnergyPlus simulation engine to solve the energy balance on smaller time-steps, would have not produced a solution that was any closer to reality. The steady-state energy balance, with simplified analytical models for each of the major energy flows between the building and its surroundings, allowed for each modeling decision to be justified. It also provided greater flexibility in modeling the effects of the TEG POWER system, where chimney flow rates were specified as a function of appliance operating mode and outdoor dry-bulb temperature. In comparison, it was not possible to specify exhaust volume or mass flow rates that varied with temperature in EnergyPlus. EnergyPlus was used solely to determine the rate of heat transfer to the building via solar radiation.

2.3 Proper Appliance Ventilation: Relevant Codes and Standards

In this section, the relevant codes and standards pertaining to appliance ventilation within a typical quick-service restaurant are discussed. As pizzerias were featured in this analysis, the focus will be on the operating requirements of both natural gas ovens and deep fryers, commonly used in tandem across the entire industry. In all cases observed, fryers were ventilated with wall mounted canopy style hoods with no makeup air introduction, while ovens were ventilated with either wall mounted canopy style hoods equipped with short-circuit makeup air introduction, and/or class B style chimneys.

The Blodgett "*Gas Deck Oven Installation, Operation, and Maintenance Manual*" specifies that both methods are acceptable for appliance ventilation, albeit for unknown, and possibly misinformed reasons, mechanically driven exhaust ventilation is recommended [20]. Regardless, installation of both styles of ventilation equipment is subject to the Ontario Building Code [21], specifically, supplementary standards:

- ASHRAE 90.1, *Energy Standard for Buildings Except Low-Rise Residential Buildings* [22], for state of the art commercial kitchen ventilation requirements.
- NFPA 96, *Standard for Ventilation Control and Fire Protection of Commercial Cooking Operations* [23], for venting system design and replacement air requirements to limit the maximum allowable building depressurization.

Ventilation system design is also subject to the following code adopted by the Technical Standards and Safety Act, 2000 [24]:

- CSA B149.1-10, *Natural Gas and Propane Installation Cod*e [25], for venting system design requirements.

2.3.1 High Performance Commercial Kitchen Ventilation

The substantial energy impact of traditional canopy based commercial kitchen ventilation (CKV) systems has come under scrutiny, leading to much research in the area of high performance CKV. This section presents a compendium of the significant publications related to commercial kitchen ventilation best practices. The most comprehensive publication to date is ASHRAE 90.1, *Energy Standard for Buildings Except Low-Rise Residential Buildings* [22], effective in 2010, which was built on the successful aspects of ASHRAE Standard 154, *Ventilation for Commercial Cooking Operations* [26].

Paragraph 6.5.7.1.1 of ASHRAE 90.1 states that, "Replacement air introduced directly into the hood cavity of kitchen exhaust hoods shall not exceed 10% of the hood exhaust air flow rate [22]." The value of 10% is consistent with a research study conducted in 2003 [27], on the effect of makeup air on the capture and containment (C&C) of cooking effluents. The study showed that makeup air in excess of 10% of the exhaust flow rate caused the thermal plume of the appliance to spill from the canopy, and as a result, the exhaust flow rate would have to be increase to maintain C&C [27]. This clause makes current pizzeria ventilation systems outdated, which have been observed to introduce up to 60% of makeup air internally. However, these experiments were conducted with under-fired broilers as opposed to ovens, and therefore are not representative of pizza restaurants, since ovens have a thermal plume that is easier to contain, as the exhaust vents are located at the back of the appliance directly below the canopy vent [20].

Paragraph 6.5.7.1.3 of ASHRAE 90.1 implies that unlisted or listed (conforming to UL Standard 710 [28]) hoods may be used where the combined exhaust flow rate is below 5000 CFM, but only listed hoods may be used when the combined exhaust flow rate is above 5000 CFM [22]. The specific exhaust flow rates for both listed and unlisted hoods for different appliance duty ratings and have been summarized in Table 2.1 and Table 2.2 below. Note that both electric and gas ovens fall under the light duty category, while both electric and gas fryers fall under the medium duty category.

Table 2.1: Minimum Net Exhaust Flow Rate for Unlisted Hoods [26]

Type of Hood	Minimum Net Exhaust Flow Rate (CFM per Linear Foot of Hood Length)			
	Light Duty Equipment	Medium Duty Equipment	Heavy Duty Equipment	Extra Heavy Duty Equipment
Wall-mounted canopy	200	300	400	550
Single island	400	500	600	700
Double island (per side)	250	300	400	550
Eyebrow	250	250	Not Allowed	Not Allowed
Backshelf/Pass-over	250	300	400	Not Allowed

Table 2.2: Maximum Net Exhaust Flow Rate for Listed Hoods [22]

Type of Hood	Maximum Net Exhaust Flow Rate (CFM per Linear Foot of Hood Length)			
	Light Duty Equipment	Medium Duty Equipment	Heavy Duty Equipment	Extra Heavy Duty Equipment
Wall-mounted canopy	140	210	280	385
Single island	280	350	420	490
Double island (per side)	175	210	280	385
Eyebrow	175	175	Not Allowed	Not Allowed
Backshelf/Pass-over	210	210	280	Not Allowed

2.3.2 Considerations for Chimney Ventilation

Chimneys must be constructed in accordance with the Ontario Building Code [21], although manufactures installation manuals should be consulted for optimal ventilation configurations for their specific appliances. For example, the gas deck oven installation manual by Blodgett specifies that, "the flue must be class B or better with a diameter of 10" (25.4 cm). The height of the flue should rise 6-8 ft (2-2.5 m) above the roof of the building or any proximate structure. The flue should be capped with a UL Listed type vent cap to isolate the unit from external environmental conditions [20]."

Lastly NFPA 96 clause 8.3.1 states that adequate replacement air must be provided to the cooking area to limit building depressurizations from exceeding 4.98 Pa [23]. The requirement is mandatory for both canopy and chimney exhaust configurations, and although negative pressures do not adversely affect the C&C efficiency of canopies, building depressurization can adversely affect the draft condition of a chimney. This could potentially lead to a reversed chimney flow, where combustion gases would be vented to the room.

2.4 Oven Energy Balance and Exhaust System Fundamentals

A comprehensive analysis of the potential for waste heat recovery from naturally ventilated exhaust streams was conducted by Girard in 2016 [7]. The purpose of this section is to summarize the operating characteristics of a typical gas fired oven, that directly affect the energy balance of the building it operates within. Most importantly, the method of estimating the rate of heat loss from the oven to the room will be identified, along with the measurement procedure to determine the mass flow rate of air through the chimney.

When configured with a chimney, the appliance consists of three main components; the combustion chamber, the draft hood and the chimney, illustrated below in Figure 2.1.

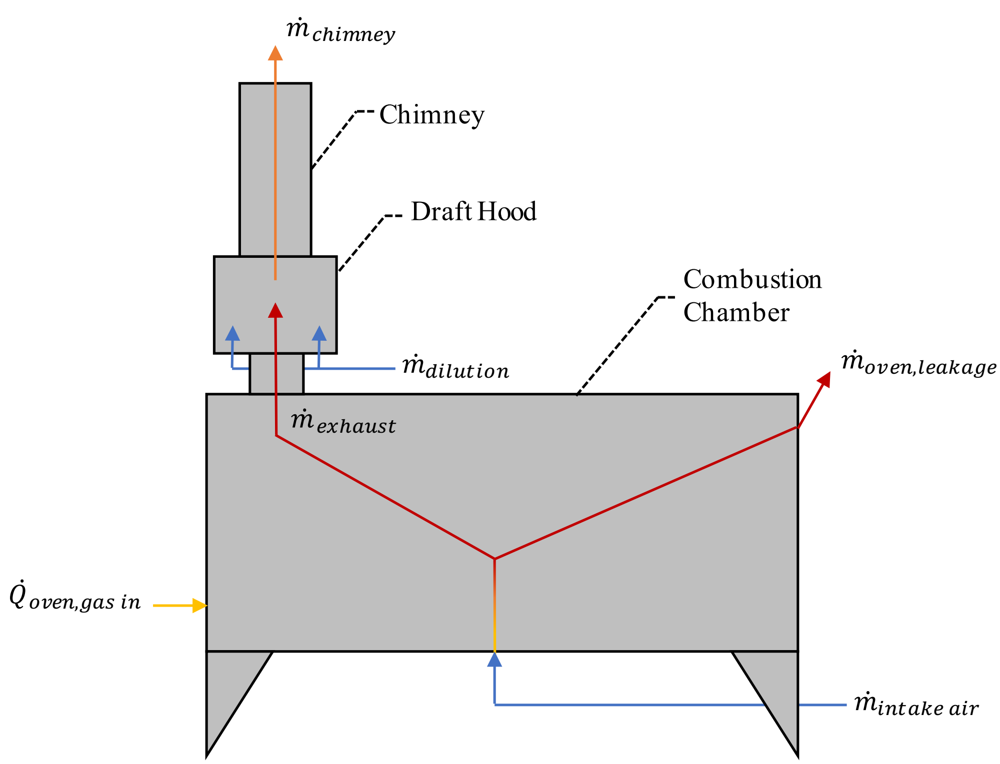

Figure 2.1: Schematic of the Oven Energy Balance

The operating principles and governing equations of each component are described in the following sections. Note that when an oven is ventilated with a canopy style hood as opposed to a chimney, the combustion chamber operating principles of Section 2.4.1 still apply, although the draft hood is not required and Section 2.4.2 and Section 2.4.3 do not apply.

2.4.1 Combustion Chamber

When operating at a steady state, the gas flow rate to the combustion chamber is controlled to maintain a desired set-point temperature, through a closed loop feedback control system, achieving the energy balance described with equation (2.1) through equation (2.4) below.

$$\dot{Q}_{oven,gas\ in} = \dot{Q}_{oven,exhaust} + \dot{Q}_{oven,structure} + \dot{Q}_{oven,leakage} \tag{2.1}$$

$$\dot{Q}_{oven,exhaust} = \dot{m}_{exhaust} C_{p_{air}} (T_{oven} - T_{room}) \tag{2.2}$$

$$\dot{Q}_{oven,structure} = (UA)_{oven} (T_{oven} - T_{room}) \tag{2.3}$$

$$\dot{Q}_{oven,leakage} = \dot{m}_{oven,leakage} C_{p_{air}} (T_{oven} - T_{room}) \tag{2.4}$$

Where:

$\dot{Q}_{oven,gas\ in}$: rate of energy transfer to the oven through the complete combustion of natural gas [kW]

$\dot{Q}_{oven,exhaust}$: rate of energy loss from the oven in the form of exhaust gas [kW]

$\dot{m}_{exhaust}$: average mass flow rate of air exiting the oven exhaust vent

Can be measured indirectly using the adjusted combustion energy balance technique described in [7].

(For a single Blodgett 1048B oven, operating at 288°C)

$$\dot{m}_{exhaust} \approx 0.03\ kg/s$$

$C_{p_{air}}$: specific heat capacity of air $\left[\frac{J}{kg\cdot K}\right]$

T_{oven}: oven temperature [°C]

T_{room}: room temperature [°C]

$\dot{Q}_{oven,structure}$: rate of energy loss from the oven through convection and radiation [kW]

$(UA)_{oven}$: overall heat transfer coefficient of the oven (convection and radiation)

Estimated through transient oven cooldown tests, for both an uninsulated and insulated case, where the oven was surrounded with a 2-inch fiberglass cover [7].

(For a single Blodgett 1048B oven)

$$(UA)_{oven,uninsulated} = 3.71\frac{W}{K}$$

$$(UA)_{oven,insulated} = 0.20\ \frac{W}{K}$$

$\dot{Q}_{oven,leakage}$: rate of energy loss from oven door exfiltration [kW]

$\dot{m}_{oven,leakage}$: average mass flow rate of air leaking through the oven door

Inferred based on the difference between the oven mass flow rate measured with the combustion energy balance technique and the waste energy balance technique described in [7].

(For a single Blodgett 1048B oven, operating at 288°C)

$$\dot{m}_{oven,leakage} \approx\ 0.016\ kg/s$$

2.4.2 Chimney

Mass flow through the chimney is caused by natural convection, and the phenomenon is commonly referred to as the stack effect. In the presence of a gravitational field, when a volume of fluid has a lower density than the density of its surroundings, a buoyancy forces is created on the fluid causing it to rise.

An approximate relation for the chimney flow rate can be derived as follows. Consider a chimney, a tall vertical column of height H, that contains a hot fluid of temperature $T_{chimney}$ and density $\rho_{chimney}$, surrounded by air at a uniform temperature of $T_{outside}$ and density $\rho_{outside}$. The chimney and its surrounds can be considered as two columns of air, exposed to the same atmospheric pressure, P_{atm}, at the top. The draft pressure, the main force driving the chimney flow, is a function of the pressure difference at the base of the two fluid columns, which may be calculated with the basic equation of fluid statics [29].

$$P_{chimney} = P_{atm} + \rho_{chimney} g H \tag{2.5}$$

$$P_{outside} = P_{atm} + \rho_{outside} g H \tag{2.6}$$

The pressure profiles along the length of the two fluid columns is illustrated in Figure 2.2 on the following page.

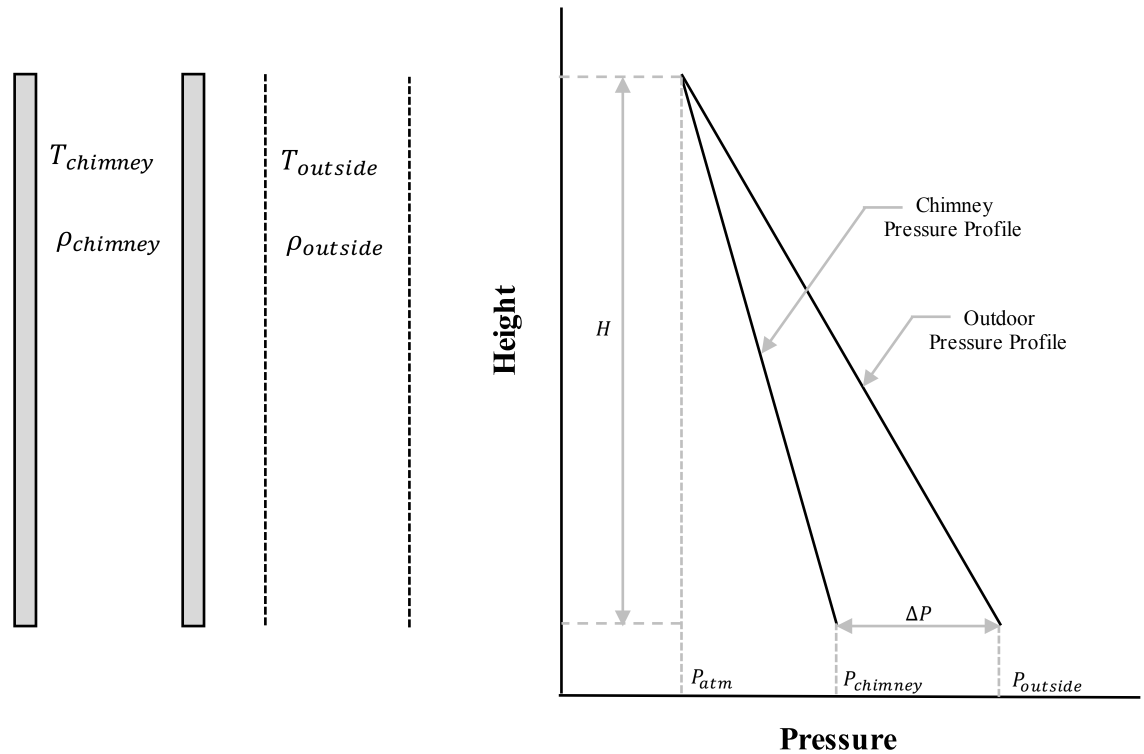

Figure 2.2: Draft Pressure Created by the Stack Effect

The draft pressure, ΔP, is derived by subtracting equation (2.5) from equation (2.6) to calculate the pressure difference at the base of the two fluid columns.

$$\Delta P = gH(\rho_{outside} - \rho_{chimney}) \tag{2.7}$$

The pressure difference can then be approximately related to the chimney mass flow rate using Bernoulli's equation, to yield equation (2.8). Note that density terms have been replaced with temperatures by assuming the ideal gas relation.

$$\dot{m}_{chimney} \propto A\sqrt{2gH\left(\frac{T_{chimney} - T_{outside}}{T_{chimney}}\right)} \tag{2.8}$$

The relation gives qualitative insight into the main parameters affecting the chimney flow rate. For example, an increase in the height of the chimney, the chimney temperature, or a decrease in the outside temperature will all cause the chimney flow rate to rise. However, the derivation excluded the effect of several important parameters, including frictional losses and the impact of waste heat recovery on the chimney temperature and pressure drop. A more comprehensive analysis of chimney flow in the presence of waste heat recovery can be viewed in [7].

The experimental measurements for the chimney flow rate collected by Girard, for cases with and without the inclusion of waste heat recovery, were used as inputs to the building energy model presented in Chapter 3. The chimney flow rate was indirectly measured using a combination of the adjusted combustion energy balance (to measure the exhaust mass flow through the appliance), along with a mass and energy balance on the draft hood (to relate the exhaust mass flow rate to the chimney mass flow rate). Draft hood operating principles are explained below in Section 2.4.3.

The mass and energy balance on the draft hood are shown below in equations (2.9) and (2.10).

$$\dot{m}_{chimney} = \dot{m}_{exhaust} + \dot{m}_{dilution} \tag{2.9}$$

$$\dot{m}_{chimney} \cdot C_P \cdot T_{chimney} = \dot{m}_{exhaust} \cdot C_P \cdot T_{exhaust} + \dot{m}_{dilution} \cdot C_P \cdot T_{dilution} \tag{2.10}$$

Solving for the chimney mass flow rate yields:

$$\dot{m}_{chimney} = \dot{m}_{exhaust} \left(\frac{(T_{exhaust} - T_{chimney})}{(T_{chimney} - T_{dilution})} + 1 \right) \tag{2.11}$$

When the oven is operating at 288°C (550°F), with an outdoor dry bulb temperature of 18°C, the experimental results can be summarized as follows [7].

Without Waste Heat Recovery:

$$\dot{m}_{chimney} \approx 0.103\ kg/s$$

With Waste Heat Recovery:

$$\dot{m}_{chimney} \approx 0.061\ kg/s$$

The flow rates may be compensated for variations in the outside temperature using equation (2.12). The equation was determined by linearly interpolating between two different results presented in [7], which were representative of two different outside temperatures (-20°C and 25°C), with consistent oven operating conditions.

$$\dot{m}_{chimney,compensated} = \dot{m}_{chimney} - 8.44\times10^{-4}(T_{outside} - 18°C) \qquad (2.12)$$

2.4.3 Draft Hood

The draft hood acts as a mixing chamber, where the hot exhaust gases exiting the exhaust vent of the oven are mixed with conditioned air from the room, before entering the chimney. The draft hood is designed with large enough dilution air openings, such that the exhaust vent of the oven remains at a neutral pressure with the room, effectively isolating the appliance from the exhaust network above. In this configuration, the exhaust flow rate through the oven is solely a function of the oven's operating temperature, and is not related to the chimney draft condition. Therefore, any increase in the flow rate through the chimney will be compensated by an equal increase in the flow rate of dilution air, with no impact on the exhaust flow rate though the appliance.

Chapter 3
The Building HVAC Energy Model

3.1 Introduction

A mathematical model has been developed that is capable of predicting the energy consumption of a building HVAC system, in response to changes in both the controllable (operating schedules, exhaust configuration, building set-point temperatures, etc.) and uncontrollable input variables (climate).

3.2 The Energy Balance

The building was modeled using a quasi-steady state energy balance, based on the fundamental principles of thermodynamics, heat and mass transfer. Two notable assumptions were made in order to simplify the analysis. A single internal thermal zone was assumed, with the air inside the zone being perfectly mixed. The quasi-steady state model also assumed that no energy was stored within the thermal mass of the building, as the building under consideration was operated at a constant set-point temperature.

To complete an energy balance on the building for a single day, the model was discretized into half hour time steps to capture the time varying characteristics of the sources and loads. The model inputs, the independent variables that have a direct causal link to the heating and cooling energy requirements of the building, are shown below in equation (3.1) in the rate form of an energy balance. The energy flows are also illustrated in Figure 3.1. Positive values indicate that the energy flow is into the building, while negative values indicate the energy flow out of the building.

$$\dot{Q}_{Heating\ or\ Cooling\ Requirement} = \pm \dot{Q}_{Building\ Skin} \pm \dot{Q}_{Ventilation\ Sensible} + \dot{Q}_{Ventilation\ Latent} + \dot{Q}_{Oven\ Gain} + \dot{Q}_{Electrical} + \dot{Q}_{Solar} + \dot{Q}_{Space\ Heating} \tag{3.1}$$

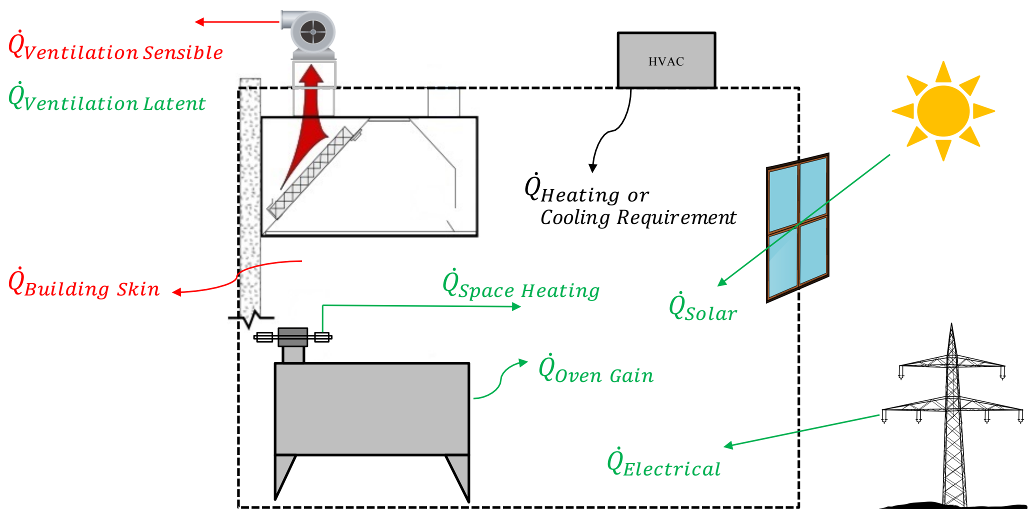

Figure 3.1: Building Energy Flow Schematic

The energy balance was solved at each time step to determine the rate of energy transfer, in kilowatts, required for the building to remain in a quasi-equilibrium state. For each time step, this rate of energy transfer was assumed to remain constant and was integrated across the domain to calculate the net heating or cooling energy requirement. The primary energy consumption of the HVAC system (in cubic meters of natural gas and kilowatt-hours of electricity) was then determined, based on the annual fuel utilization efficiency (AFUE) and the coefficient of performance (COP) of each building's specific plant equipment, which is introduced in Chapter 4. The following sub sections describe in detail the methodology used to compute each element of the energy balance.

3.2.1 Heat Transfer Through the Building Skin

The rate of heat transfer through the building walls, windows and roof was calculated using a one-dimensional steady state thermal resistance network for conduction through a plane surface with convective boundary conditions. The governing equation, shown below as equation (3.2), was solved three separate times, to determine the rate of heat transfer through the different surfaces.

$$\dot{Q}_{Building\ Skin} = \frac{A(T_{out} - T_{in})}{\left(\frac{1}{h_{in}} + \frac{1}{U} + \frac{1}{h_{out}}\right)} \tag{3.2}$$

Where:

A: surface area [m^2]

T_{out}: outside air temperature [°C]

T_{in}: inside air temperature of the building [°C]

h_{in}: inner surface heat transfer coefficient (convection and radiation) [30]

$$h_{in} = 8.29\,\frac{W}{m^2K}$$

h_{out}: outer surface heat transfer coefficient (convection and radiation)[30]

Varies between:

$$h_{out\ (summer)} = 22.7\,\frac{W}{m^2K}$$

(Corresponding to design wind conditions of 12 km/h for summer)

$$h_{out\ (winter)} = 34.0\,\frac{W}{m^2K}$$

(Corresponding to design wind conditions of 24 km/h for winter)

The average of these two surface heat transfer coefficients was selected due to the solutions insensitivity to the outside heat transfer coefficient, and the relatively insignificant effect of the heat transfer coefficient on the building energy balance.

U: heat transfer coefficient of the specific surface under consideration

Values were obtained from the EnergyPlus database, where the calculation of the heat transfer coefficient conforms to ISO standards 6946:2007 and 10292:1994 [31],[32].

$$U_{wall} = 0.350 \frac{W}{m^2K}$$

(Construction: 13 mm gypsum plaster, 100 mm concrete block, 80 mm extruded polystyrene insulation, 100 mm brick veneer)

$$U_{\mathrm{roof}} = 0.250 \frac{W}{m^2K}$$

(Construction: 13mm gypsum plaster, 200mm air gap, 145mm glass wool, 10mm asphalt)

$$U_{\mathrm{windows}} = 1.978 \frac{W}{m^2K}$$

(Construction: 3 mm clear glass, 13 mm air gap, 3 mm clear glass)

The rate of heat transfer through the floor was modeled slightly differently, using equation (3.3) below. Since there was no external convective boundary condition, only the internal surface heat transfer coefficient and the slab heat transfer coefficient were included in the thermal resistance network. Instead, a constant temperature boundary condition equivalent to the average ground temperature was applied to the underside of the concrete slab to estimate the rate of heat transfer.

$$\dot{Q}_{floor} = \frac{A\left(\bar{T}_{gr} - T_{in}\right)}{\left(\frac{1}{h_{in}} + \frac{1}{U_{floor}}\right)} \tag{3.3}$$

Where:

$\bar{T}_{gr}$: ground surface temperature, approximated from the monthly average air temperature [30], °C

Due to the relatively small contribution of foundation heat loss to the total building heat loss (~3%), any inaccuracy introduced through this assumption is negligible.

U_{floor}: heat transfer coefficient of the floor (From EnergyPlus Database)

$$U_{\text{floor}} = 0.314 \frac{W}{m^2 K}$$

(Construction: 100 mm foam insulation, 100 mm concrete, 70 mm floor screed, 30 mm timber flooring)

3.2.2 Ventilation

The flow rate of ventilation air through the building played an important role in the energy balance, affecting both the sensible and latent heat gain and loss components.

3.2.2.1 Net Ventilation Mass Flow Rate

The net ventilation flow rate, also known as the infiltration flow rate, is defined as the mass flow rate of air traveling through the building that must be conditioned by the HVAC system. It includes all air flowing through any crack, seam, open door, or other opening in the building envelope, due to the depressurization created by the exhaust ventilation system. The net ventilation flow rate was calculated by subtracting the makeup air flow rate from the total ventilation flow rate, as shown in the mass balance of equation (3.4).

$$\dot{m}_{net\ ventilation} = \dot{m}_{total\ ventilation} - \dot{m}_{makeup} \tag{3.4}$$

This is also known as the makeup air short circuit effect, which occurred when not all of the air exhausted from the building originated from the indoor mixed air space, and instead, was introduced into the building in the vicinity of the exhaust system through either a reversed chimney or the makeup air ductwork. The unconditioned makeup air was able to bypass the HVAC system, and therefore did not create a heating or cooling load. The process is illustrated below in Figure 3.2.

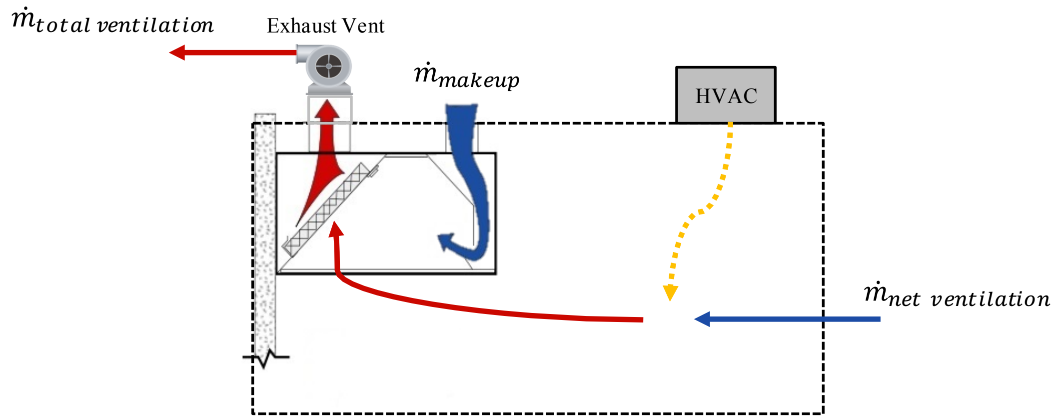

Figure 3.2: Ventilation Mass Balance

The total ventilation flow rate was determined differently in each case based on the method of exhaust ventilation. For Store A, which used exhaust blowers to ventilate the combustion appliance zone, the total ventilation flow rate was measured using a pitot static tube, traversed across the exhaust duct to indirectly measure velocity at different points in the flow. These experimental results are shown in Chapter 4. For Store B, which used chimneys to ventilate the ovens, the chimney mass flow rates introduced in Section 2.4 were used.

The total ventilation flow rate was then adjusted to account for the short circuit air, that did not require conditioning. The adjustment was made by setting a value for the amount of makeup air introduced internally, which minimized the sum of squared errors between the experimental data set and the associated model predictions. This method was chosen due to the low flow rates and geometrical constrains, which made accurate experimental measurement of the makeup air flow rate impractical. The makeup air introduced internally for each store will be discussed in Section 4.7.2 on model validation.

After determining the net ventilation flow rate, the sensible heat loss and latent heat gains could be calculated as follows.

3.2.2.2 Sensible Energy

The rate of heat transfer required to change the temperature of the net ventilation air from the outside temperature to the building set-point temperature was determined using equation (3.5). It was derived from a steady state energy balance, where the rate of heat transfer was equivalent to the rate of change of enthalpy of the fluid, using the constant specific heat assumption.

$$\dot{Q}_{Ventilation\ Sensible} = \dot{m}_{net\ ventilation} C_{p_{air}} (T_{out} - T_{in}) \tag{3.5}$$

Where:

$C_{p_{air}}$: specific heat capacity of dry air at a constant pressure at 20°C [33]

$$C_{p_{air}} = 1005 \frac{J}{kg\ K}$$

3.2.2.3 Latent Energy

In the summer as humid air is cooled, the latent energy load associated with dehumidifying, and condensing out a portion of the water vapour, in the outside air was also considered in addition to the sensible energy load described previously. Equation (3.6) was used to calculate the rate of heat transfer required to decrease the humidity of the outdoor air to indoor conditions.

$$\dot{Q}_{Ventilation\ Latent} = \dot{m}_{net\ ventilation} h_{fg} (W_{out} - W_{in}) \tag{3.6}$$

Where:

h_{fg}: enthalpy of condensation of saturated water [34]

Determined at the average of the inside and outside temperatures.

$$h_{fg} = 2501.4 - 2.366 \frac{(T_{in}+T_{out})}{2} \frac{kJ}{kg}$$

W: humidity ratio of the inside and outside air [kg/kg]

The calculation procedure is described below.

3.2.2.3.1 Humidity Ratio

This brief section describes how the humidity ratio, W, was determined, based on the measurements of air temperature, pressure and relative humidity. The measurement methodology is described in detail in Chapter 4. The humidity ratio is defined as the ratio of the mass of water vapour to dry air in a sample of moist air.

$$W = \frac{M_w}{M_{da}} = \frac{x_w}{x_{da}} \cdot \frac{M(H_2O)}{M(dry\ air)} \tag{3.7}$$

Where:

M_w: mass of water vapour [kg]

M_{da}: mass of dry air [kg]

x_w: mole fraction of water vapour

x_{da}: mole fraction of dry air

$M(H_2O)$: molar mass of water vapour [35]

$$M(H_2O) = 18.015\ 268\ g/mol$$

$M(dry\ air)$: molar mass of dry air [35]

$$M(dry\ air) = 28.966\ g/mol$$

Relations for the mole fractions were determined by assuming that moist air is a mixture of two ideal gases: water vapour and dry air. Although moist air is technically not an ideal gas, Kuehn et al. proved the validity of this assumption for practical engineering calculations, showing the maximum error in the humidity ratio does not exceed 0.7% when compared against a real gas model of moist air [36]. The assumption results in three relations assuming ideal gases, for both components of the mixture, and the mixture as a whole.

$$n_w = \frac{p_w V}{\bar{R}T} \qquad n_{da} = \frac{p_{da} V}{\bar{R}T} \qquad n = \frac{pV}{\bar{R}T} \tag{3.8}$$

Where:

n_w: moles of water vapour [mol]
n_{da}: moles of dry air [mol]
n: total moles in the mixture [mol]

$$n = n_w + n_{da}$$

p_w: partial pressure of water vapour [Pa]
p_{da}: partial pressure of dry air [Pa]
p: total pressure of the mixture [Pa]

$$p = p_w + p_{da}$$

V: total volume of the mixture [m^3]
$\bar{R}$: universal gas constant [33]

$$\bar{R} = 8.314\ kJ/kmol \cdot K$$

T: temperature of the mixture [K]

Rearranging the relations from (3.8), using the definition of a mole fraction:

$$x_w = \frac{n_w}{n} = \frac{p_w}{p} \qquad x_{da} = \frac{n_{da}}{n} = \frac{p_{da}}{p} \qquad with: \quad p = p_w + p_{da} \tag{3.9}$$

Substituting the equations from (3.9) into equation (3.7) yields the humidity ratio as a function of the total pressure and the partial pressure of water vapour:

$$W = 0.621\ 945 \frac{p_w}{p - p_w} \tag{3.10}$$

The partial pressure of the water vapour can then be determined from the definition of relative humidity, ϕ:

$$\phi = \left.\frac{p_w}{p_{ws}}\right|_{t,p} \tag{3.11}$$

Where:

ϕ: relative humidity

p_{ws}: water vapour saturation pressure [Pa]

Lastly, the water vapour saturation pressure as a function of the absolute temperature was determined, based on the Hyland and Wexler equations [37]:

$$\ln(p_{ws}) = \frac{C_1}{T} + C_2 \; + C_3 T + C_4 T^2 + C_5 T^3 + C_6 \ln{(T)} \tag{3.12}$$

Where:

p_{ws}: water vapour saturation pressure [Pa]

T: dry bulb air temperature [K]

$C_1 = -5.800\,220\,6\,E + 03$

$C_2 = \quad 1.391\,499\,3\,E + 00$

$C_3 = -4.864\,023\,9\,E - 02$

$C_4 = \quad 4.176\,476\,8\,E - 05$

$C_5 = -1.445\,209\,3\,E - 08$

$C_6 = \quad 6.545\,967\,3\,E + 00$

3.2.3 Oven Gain

The rate of heat transfer from the oven to the room was determined by separating the total rate of heat transfer into two components: the convective and radiative heat transfer resulting from conduction through the structure of the oven, and the energy losses through the oven door via mass transfer and radiation.

The method of oven ventilation was taken into consideration when calculating the thermal energy gain of the room. For chimney based oven ventilation, the total rate of heat transfer was used. However, for canopy based oven ventilation, only the heat transfer through radiation was included. Oven heat losses through convection and mass transfer were not included, since exhaust canopies ventilate the oven by removing air from the entire combustion appliance zone. Any air flowing in the vicinity of the oven that gains thermal energy would be transported out of the building, therefore imposing no impact on the HVAC energy balance. Radiation heat transfer was included in both case, since energy transfer by thermal radiation occurs between two surfaces, with an oven surface transferring energy to the walls of the room. The following subsections describe the calculation procedure.

3.2.3.1 Conduction Through Oven Structure

The overall heat transfer coefficient of the oven was determined by Girard and Hirmiz [7], for both an uninsulated and insulated case where the oven was surrounded with a 2-inch fiberglass cover. The tests resulted in the overall heat transfer coefficients of:

$$(UA)_{oven,uninsulated} = 3.71\frac{W}{K} \qquad (UA)_{oven,insulated} = 0.20\ \frac{W}{K}$$

The combined rate of heat transfer through convection and radiation can then be determined with the use of equation (3.13).

$$\dot{Q}_{oven,structure} = (UA)_{oven}(T_{oven} - T_{room}) \tag{3.13}$$

Table 3.1 below displays the rate of heat loss though the oven structure, for an oven temperature of 288°C (550°F), and a room temperature of 21°C (70°F).

Table 3.1: Rate of Heat Transfer Through Oven Structure

Case	Heat Transfer Through Oven Structure (kW)
Uninsulated	0.99
Insulated	0.05

The relative contributions of convection and radiation to the overall rate of heat transfer in the uninsulated case were estimated, by measuring the average surface temperature of the oven, and calculating the net rate of energy transfer by thermal radiation between two surfaces, using equation (3.14).

$$\dot{Q}_{oven,structure\ (rad)} = \varepsilon\sigma A(T_b^4 - T_s^4) \tag{3.14}$$

Where:

ε: emissivity of stainless steel, type 301

$$\varepsilon = 0.6$$

σ: Stefan-Boltzmann constant

$$\sigma = 5.67 * 10^{-8} \frac{W}{m^2K^4}$$

A: exposed surface area of the oven

$$A = 6.728\ m^2$$

T_b: average oven surface temperature

$$T_b = 50°C = 323.15K$$

T_s: temperature of surroundings

$$T_s = 21°C = 294.15K$$

Therefore, the rate of heat transfer from the oven to the room through radiation was:

$$\dot{Q}_{oven,structure\ (radiation)} = 0.78\ kW \quad \text{(79\% of total)}$$

And the rate of heat transfer from the oven by convection was:

$$\dot{Q}_{oven,structure\ (convection)} = 0.21\ kW \quad \text{(21\% of total)}$$

3.2.3.2 Heat Transfer from Oven Door

The rate of heat transfer from the oven to the room, through the door, was modeled using two separate components: the exfiltration from continuous door leakage, and the energy loss from door opening.

3.2.3.2.1 Continuous Door Leakage

Since the Blodgett 1048B oven door does not have perfect seal, there is always a small amount of exhaust gas that escapes through the door as opposed to the flue. This fact was observed qualitatively, since the refractive index of air decreases with increasing temperature, which manifests itself as a shimmering stream of air escaping the door. Laboratory experiments were conducted to quantify the continuous door leakage mass flow rate, specifically for a Blodgett 1048B oven. These results are presented in Section 4.4.3. With a known door leakage flow rate, the rate of heat transfer to the room through oven leakage was then calculated using equation (3.15).

$$\dot{Q}_{oven,leakage} = \dot{m}_{oven,leakage} C_{p_{air}} (T_{oven} - T_{room}) \tag{3.15}$$

3.2.3.2.2 Door Opening

The energy balance of the cooking process was also taken into consideration. Once an oven has reached operating temperature, it operates at a pseudo steady state about its set-point, where the natural gas flow rate remains constant, to balance the exiting energy flows of the exhaust, shell losses and continuous door exfiltration. This steady state is perturbed during the cooking process due to the two oven door openings required to place and remove the baked product, which increases the exfiltration rate substantially since the open door becomes the path of least resistance for the combustion gases. The steady state is also perturbed by the cooking process, where the sensible and latent heat of the product is increased. Experiments were conducted to isolate for both of these values. The determination of the oven door exfiltration will be described in Section 4.4 on laboratory testing. The study of the total energy transfer to the baked product will be reserved for Appendix A. Although this analysis provides insight into the true thermodynamic efficiency of an oven, its impact on the building energy balance is relatively insignificant. It was assumed that all energy transferred from the oven to the baked product leaves the building with the product, and that no heat is lost to the room.

3.2.3.3 Heat Gain from an Oven with Reversed Chimney Flow

Lastly, a special case of oven heat gain was considered. In the event that an oven is ventilated with a chimney, and not an exhaust canopy, the chimney has the potential to reverse its direction of flow if the building becomes overly depressurized by other elements of the exhaust network. In this case, no distinction was made between the methods of oven heat loss, since the entire thermal energy input of the oven would be exhausted into the room. In this case, the following heat gain per oven was used in the model:

$$\dot{Q}_{Oven\ Gain} = 8.57\ kW$$

The oven heat gain was calculated from the average flow rate of natural gas for an independent oven of 15.35 L/min, detailed in Appendix B, and the following properties of natural gas.

$$LHV_{CH_4} = 47.14\ MJ/kg \text{ [38]}$$

$$\rho_{CH_4} = 710.5\ g/m^3 \text{ [39]}$$

3.2.4 Heat Generated by Electricity Consumption

The heat generated by the use of electricity was discerned from the utility bills, which provided the total electricity consumption of the building on one hour time intervals. For Store A, historical electricity use was available dating back to March 31, 2016. For Store B, electricity usage data was available from August 14, 2015. Figure 3.3 and Figure 3.4 show the trends in electricity use for both stores throughout the course of one year.

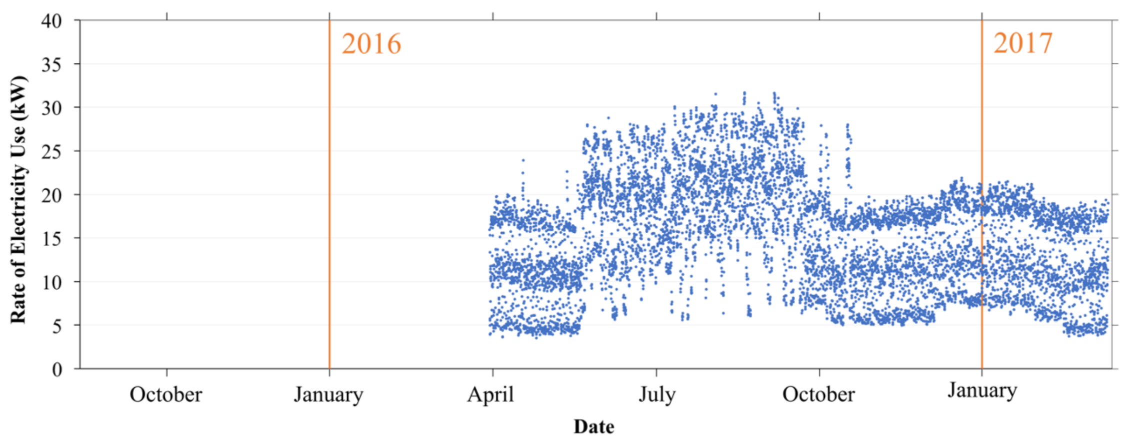

Figure 3.3: Electricity Usage – Annual – Store A

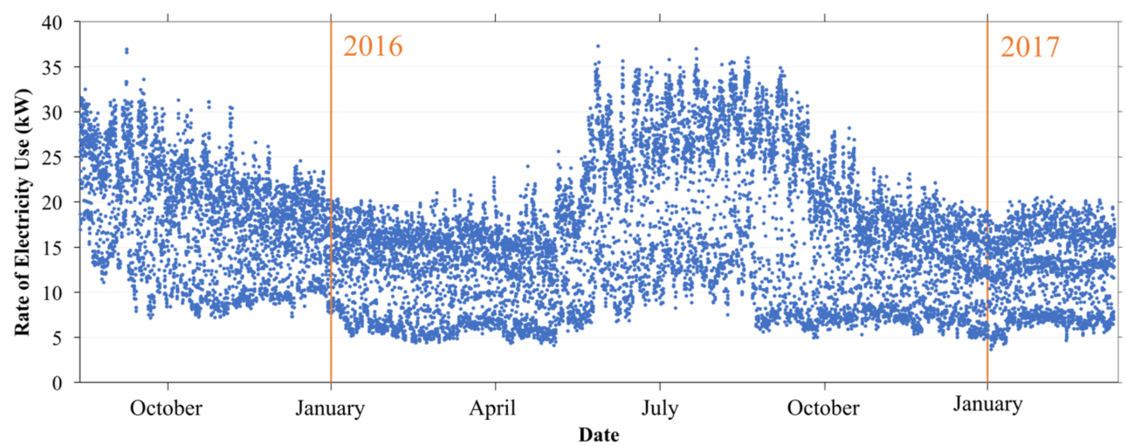

Figure 3.4: Electricity Usage – Annual – Store B

By observing the total electricity use during the winter, or all of the non-cooling months, it is clear that the daily variation in electricity use is consistent on a day to day basis, for both stores. Both stores fluctuate between a minimum demand of approximately 5 kW during the night, and a maximum demand of approximately 20 kW during peak business hours. The increase in demand during the summer months can be attributed to the air conditioning system, which roughly increases demand by 10 kW and 15 kW, for Store A and Store B respectively. The discussion of the additional electricity required for air conditioning will be left to Section 4.7 on model validation, and the case study of Chapter 5.

The focus of this section is on the heat generated by the use of electricity within the building envelope, and its impact on the building energy balance. For model validation in Section 4.7, the heat generated by the use of electricity was determined from the exact electricity usage from the specific day under consideration. For the case study of Chapter 5, the average heat generated by electricity consumption was determined from the average electricity usage over twenty-four winter days. For both cases, the heat generated was discerned from the total electricity usage by subtracting the known electrical loads that did not contribute to the HVAC energy balance of the building.

Two separate loads were removed from this section of the model. The first was the electrical power consumption of the ventilation exhaust blowers (in this case, driven by two 1.12 kW motors), which were used to ventilate the fryer and oven exhaust canopies. Since the blowers were located outside of the building envelope on the roof, the heat they generated was lost to the environment and their electrical power draw did not add to the heating of the building. Secondly, the majority of the electrical energy required to heat the domestic hot water, except to account for a 0.10 kW thermal energy loss from the tank, was also removed from the total electricity usage. It was assumed that the remaining electrical input energy stored in the hot water tank exited the building through the drainage system as the water was used, and did not impose a load on the HVAC system. The method of determining the hot water demand is discussed in detail in the experimental facility sections of Chapter 4, for the given context, it is only important to introduce how this measurement was used in the building HVAC energy balance. Figure 3.5 and Figure 3.6 below display the average heat generated by the use of electricity for both Store A and Store B, split into one hour time intervals.

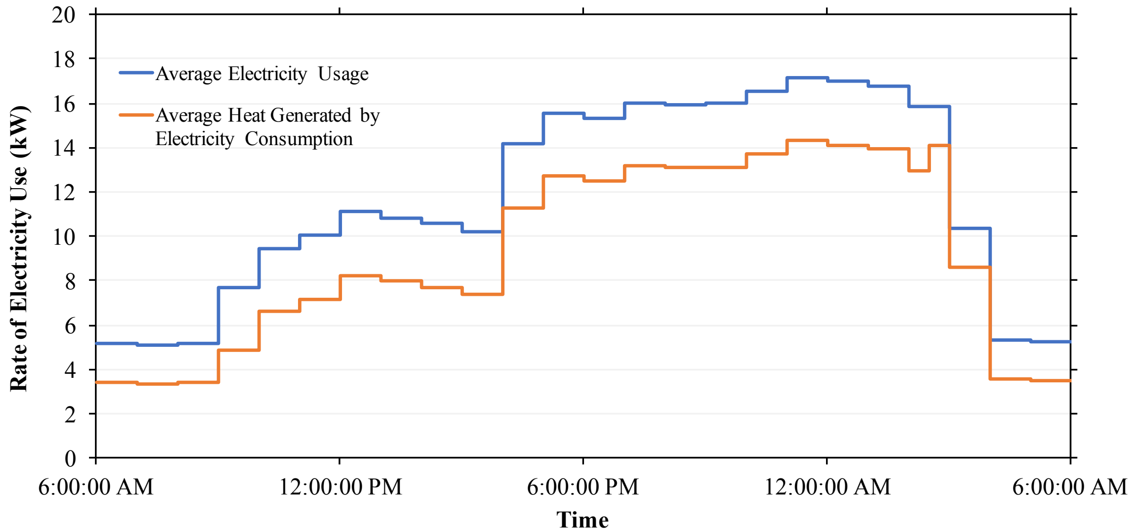

Figure 3.5: Average Heat Generated by Electricity Consumption – Store A

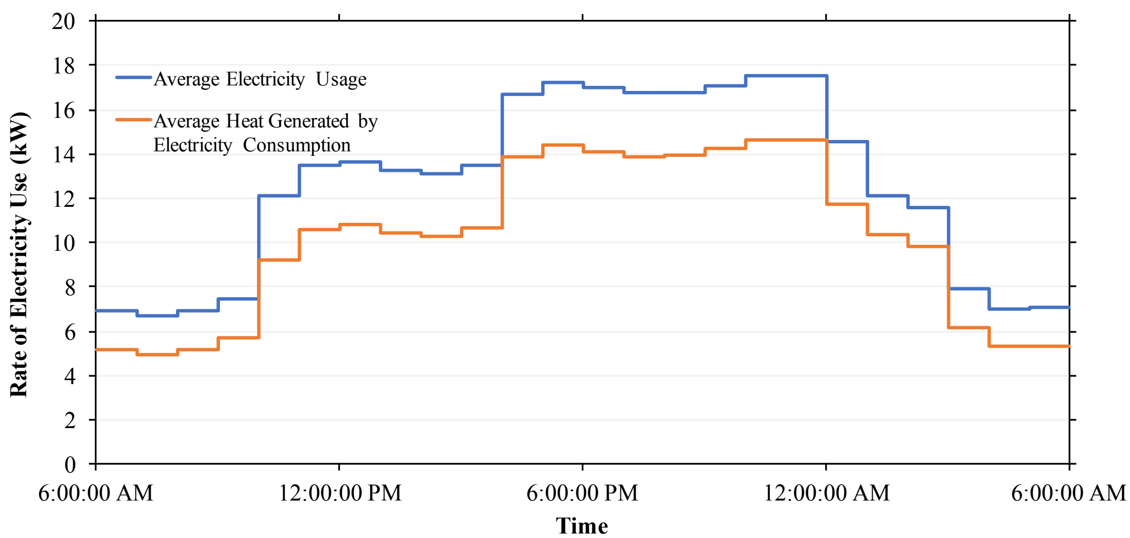

Figure 3.6: Average Heat Generated by Electricity Consumption – Store B

3.2.5 Solar Heat Gains

The solar heat gain of both buildings was modeled independently in EnergyPlus, using the Design Builder graphical user interface. The calculation procedure used in the EnergyPlus simulation engine is similar to the calculation procedure specified in Chapters 14 and 15 of the ASHRAE Fundamentals Handbook [30]. This section briefly summarizes the calculation procedure used to determine the solar heat gain, and how this value was incorporate into the building energy model.

3.2.5.1 Calculation Procedure

The rate of solar energy transfer through a window is dependent on the magnitude of the incident shortwave radiation, also known as global radiation, on the surface. The global radiation can be broken into two components: the direct normal radiation component measured perpendicular to the sun's rays, and the diffuse component which has been scattered by water vapour and air particulates [40]. Both components can be modeled separately, and the rate of heat transfer through a window, via transmitted and absorbed solar radiation, can be calculated as the sum of equations (3.16) and (3.17).

$$\dot{q}_b = E_{DN} \cdot cos\theta \cdot SHGC(\theta) \tag{3.16}$$

$$\dot{q}_d = E_d \cdot \langle SHGC \rangle_D \tag{3.17}$$

Where:

$\dot{q}_b$: direct normal (or beam) solar energy flux [W/m^2]

E_{DN}: direct normal solar irradiance [W/m^2]

The clear-sky direct normal solar irradiance can be calculated with knowledge of the sun position, which is a function of longitude, latitude, date and solar time. However, the typical meteorological year (TMY) weather file obtained from the Simcoe Weather Station (World

Meteorological Organization ID: 715270) provided actual measurements of the direct normal and diffuse irradiance in the area.

θ: incident angle [degrees]

"The angle between the line normal to the irradiated surface and the earth-sun line [30]." Calculated in EnergyPlus as a function of the sun position and surface azimuth angle.

$SHGC(\theta)$: solar heat gain coefficient

The percentage of the direct solar irradiance, $E_D = E_{DN} \cdot cos\theta$, that is transmitted and absorbed through the window as a function of the incident angle.

$\dot{q}_d$: diffuse solar energy flux [W/m^2]

E_d: diffuse solar irradiance [W/m^2]

The clear-sky diffuse solar irradiance was also obtained from the TMY weather file the Simcoe Weather Station.

$\langle SHGC \rangle_D$: hemispherically averaged solar heat gain coefficient

The percentage of the diffuse solar irradiance that is transmitted and absorbed through the window.

The EnergyPlus database contains data on the solar heat gain coefficients for various types of windows. The restaurants had double glazed, clear glass windows, with an assumed standard 13 mm air gap separating the two panes. A constant value of the solar heat gain coefficient of 0.687 was actually used. Details of the modeling approach are presented in Chapter 15 of the ASHRAE Fundamentals Handbook on Fenestration, with additional information regarding the calculation of the solar heat gain coefficient [30].

Lastly, EnergyPlus was able to account for the effect of roof overhangs, by calculating the shaded portion of the glazing at each time step.

3.2.5.2 Model Integration

An EnergyPlus simulation was run for the duration of a full year, where the total rate of solar energy transfer to the building was calculated at each fifteen-minute time step. This value was held constant at each time step, and the data was integrated to calculate the total solar gain for each day. Figure 3.7 and Figure 3.8 below display the total solar gain from all windows of Store A and Store B respectively, obtained from the EnergyPlus simulation, for each day of the year.

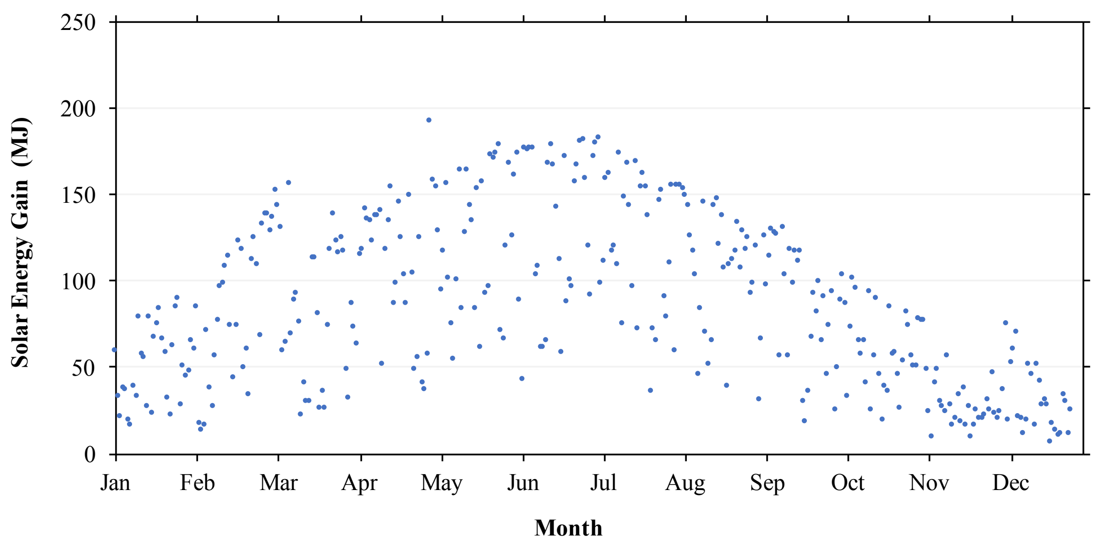

Figure 3.7: Total Solar Energy Gain per Day – Store A

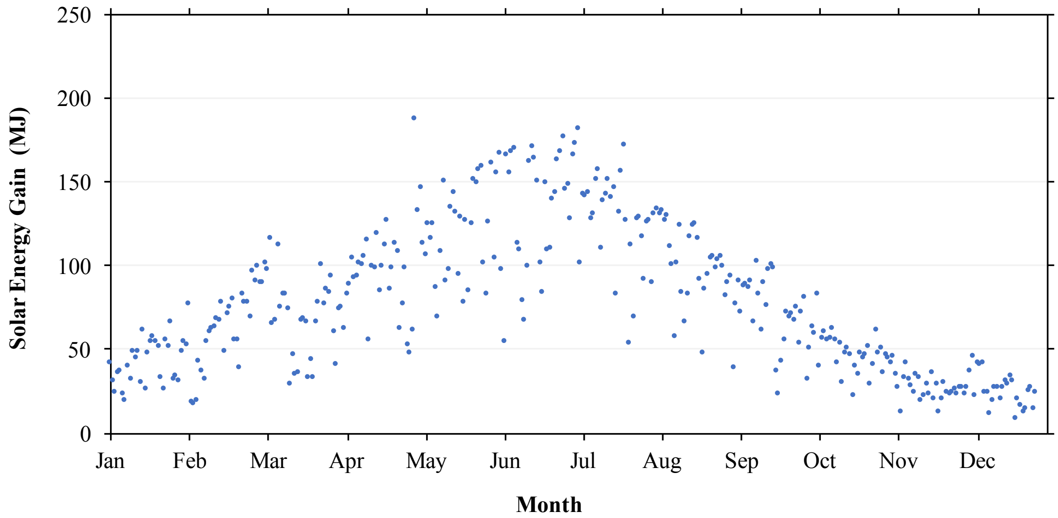

Figure 3.8: Total Solar Energy Gain per Day – Store B

The scattered nature of the data occurs because the total energy gain was calculated using actual weather data, where the magnitude of the incident beam and diffuse radiation was dependent on the cloud cover overhead. As a result, the maximum points in each time interval correspond to clear sky days, while the minimum points in each interval correspond to mostly cloudy days. The average rate of solar energy transfer was then determined, assuming that the total solar energy gain occurred uniformly between the hours of 8:00 am and 5:00 pm. Figure 3.9 and Figure 3.10 plots average rates of solar energy transfer for each day of the year for each store.

The rate of solar energy transfer was incorporated in the model in two separate ways. During model validation in Section 4.7, the maximum rate of solar energy transfer was selected for the model, and care was taken to select empirical data from days that had a fully clear sky for accurate comparison. For the case study of Chapter 5, the monthly median rate of solar energy transfer, displayed as the black line, was selected.

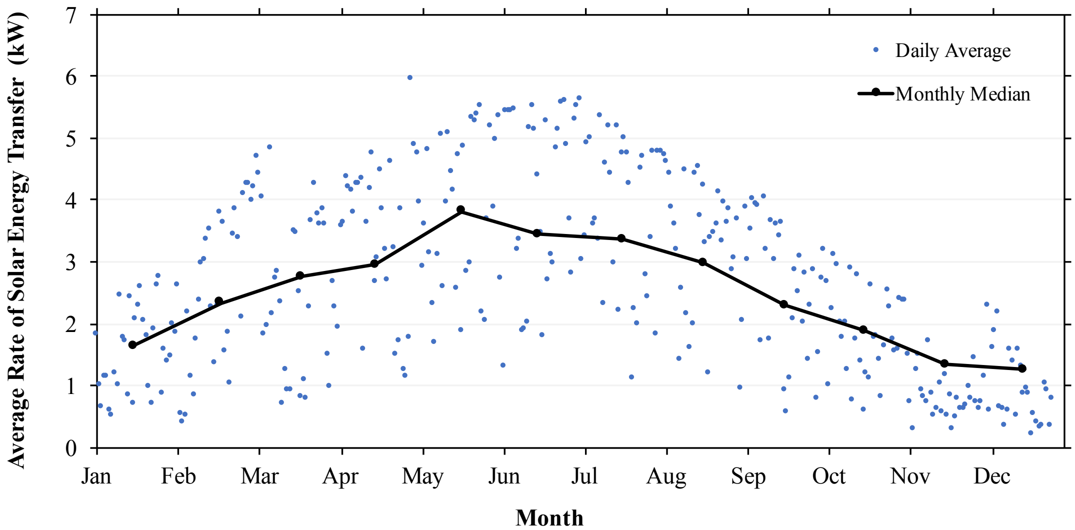

Figure 3.9: Average Rate of Solar Energy Transfer – Store A

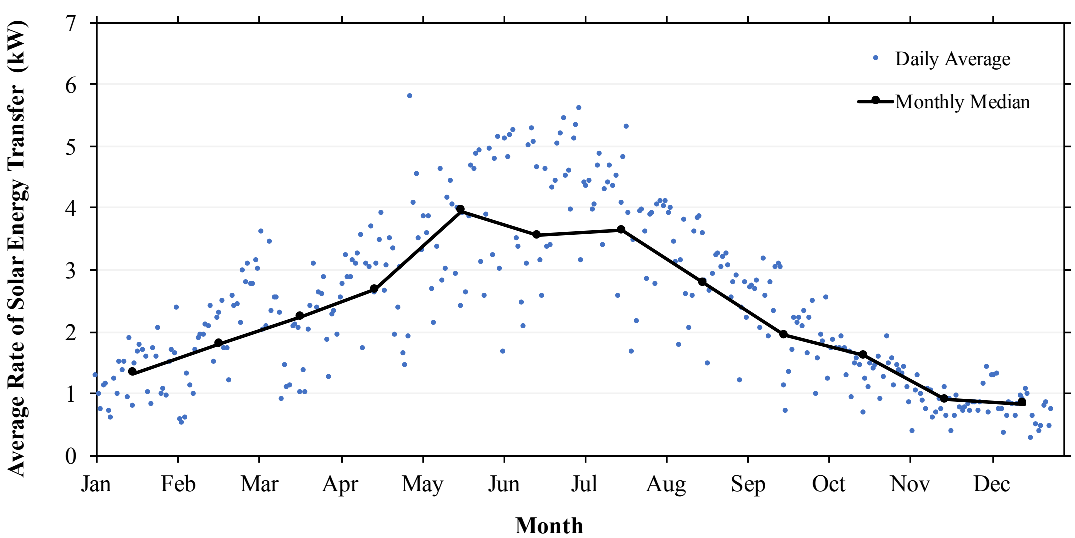

Figure 3.10: Average Rate of Solar Energy Transfer – Store B

3.2.6 Space Heating and Oven Preheating

The effect of space heating provided by the TEG POWER system was also considered in the building energy balance. Firstly, the rate of thermal energy extraction from the exhaust stream during oven operation at 288°C (550°F), described in Section 4.8, was proven to be:

$$\dot{Q}_{recovered} = 1.95\ kW$$

The available energy was then allocated to the following loads, listed in order of priority: domestic hot water, space heating and oven preheating. The rate of energy transfer required to meet the domestic hot water load was calculated using equation (3.18) below:

$$\dot{Q}_{DHW} = \frac{Q_{DHW,Electricity(avg)}}{t_{oven\ operation}} \tag{3.18}$$

Where:

$Q_{DHW,Electricity(avg)}$: measured electrical energy input to the hot water tank [kJ]

$t_{oven\ operation}$: length of time the oven was operating at 288°C (550°F) [s]

Due to the random nature of the hot water consumption, the calculation assumed that the water in the tank was heated at a constant rate, entirely during the time period when the oven was operational.

After the rate of thermal energy transfer to the water tank was deducted, the remaining energy was allocated to space heating and oven preheating, based on the demand for space heating. This was accomplished by solving the building energy balance at each half hour time step to determine the building heating requirement. If the building heating requirement exceeded the rate that thermal energy could be provided through space heating, then the available energy was simply allocated to space heating. However, if the building did not require heating, then the available energy was allocated to preheating the oven intake air, which directly lowered the natural gas consumption of the appliance.

Chapter 4
Experimental Methodology and Model Validation

4.1 Introduction

Four separate experimental facilities were used to provide inputs to the building energy model, as well as to provide a means of model validation.

The first experimental facility was Store A; standalone restaurant that ventilated ovens using exhaust canopies. The second experimental facility, Store B, was another standalone restaurant, which ventilated ovens using a combined exhaust system with chimneys and exhaust canopies. The two separate restaurants with differing exhaust configurations were purposefully selected to investigate the impact of exhaust system configuration on building energy performance. The third experimental facility consisted of a single oven located in the McMaster TMRL, which was used to accurately measure the rate of heat loss from the oven during door opening. Lastly, the fourth experimental facility encompassed the same oven within the TMRL, with the addition of the TEG POWER system to recover and repurpose a portion of the energy from the exhaust. Tests were conducted in this configuration to determine the rate of thermal energy extraction from the oven, which was used as a model input for the amount of space heating or oven preheating available.

A section on model validation has been included, where the building HVAC energy model described in Chapter 3 was compared against the experimental data collected from Store A and Store B. Chapter 4 also explains how external measurements from the McMaster Weather Station were used in the analysis, and includes an uncertainty analysis of measured variables.

4.2 Store A – Exhaust Canopy Venting

Store A was the first restaurant observed in the investigation, and was chosen for both its close proximity to the McMaster University campus, and its distinctive exhaust canopy ventilation method.

4.2.1 The Building

Store A was a standalone building, whose significant dimensions are identified in Table 4.1 below.

Table 4.1: Significant Dimensions – Store A

Component	Area (m^2)
Floor	139
Roof	139
Walls	153
Windows	37

The building was equipped with one single package air conditioner and heating unit (York Predator, Model Number: DM090N15N2AAA3). This unit had the following performance characteristics specified in the manufacturer's technical guide [41]:

$$AFUE = 80\%$$

$$COP = 2.64$$

4.2.2 Cooking Equipment and Occupant Behavior

The store contained six deck style ovens (Blodgett 1048-C series and Blodgett 1000 ovens), of which only two were operated consistently. The ovens were organized in the double stacked configuration, and ventilated with three exhaust canopies, connected to a single exhaust blower (Canarm BI-RM Series Belt Drive Utility Blower) on the roof. The ovens, and exhaust system, were operated continuously on a 24/7 scheduled, at a set-point temperature of 288°C (550°F). A single Canarm Green Series 700DD Filtered Fresh Air Supply Unit was also present on the roof which was designed to act as a source of makeup air.

The only other major cooking appliance was a single natural gas deep fryer, which was ventilated with its own separate ventilation blower (Canarm BI-RM Series Belt Drive Utility Blower). The operation of the fryer and its associated ventilation system was typically during the buildings occupied hours, from 9:00 am until close (Sunday–Wednesday: 2:00 am, Thursday–Saturday: 3:00 am).

4.2.3 Instrumentation

The store was outfitted with sensors to monitor different aspects of building's operation. The placement of the following sensors is depicted in Figure 4.1.

Four wall mounted thermocouple sensors (Omega EWS-TC-T) were used to measure the air temperature inside the building, with three dispersed throughout the customer dining area, and one in the stockroom hallway. The kitchen temperature and relative humidity were measured with a dual solid state temperature sensor and thin film temperature compensated polymer capacitor sensor respectively (Omega EWS-RH). The temperature and relative humidity measurements provided input to calculate the rate of heat transfer from the exhaust system.

Three thermocouples (Omega TMQSS-125U-6) were evenly spaced in the exhaust stream of each of the two main ovens, while one thermocouple was placed in the center of the exhaust duct of the third stack of ovens. Only one thermocouple was used on the third stack, since they were essentially never operated. The temperature measurements indicated oven operating schedules, and identified the degree of mixing that occurred between the hot exhaust gases from the top oven which was operational, and the cool air from the bottom oven which was not. The cumulative natural gas consumed by each of the two main ovens was also measured, using two positive displacement diaphragm flow meters (Elster American Meter ACM-250).

Building depressurization was measured with a low-pressure laboratory transmitter (Omega PX655-0.25BDI). Pressure measurements indicated when the fryer blower was operational.

The volume, and thermal energy content of the hot water delivered to the store was measured using two thermocouples (Omega TMQSS-125U-6) located in the cold-water inlet and hot-water exit lines of the tank, and a turbine flow meter (Omega FTB-4605) in cold water inlet line. The electrical power input to the tank was also measured using an AC power transducer (CR Magnetics CR6210-250-20), as a means of estimating the thermal energy loss.

Lastly, the operation of the HVAC system was monitored to provide a means of model validation. The cumulative natural gas consumption was measured with another positive displacement diaphragm flow meter (Elster American Meter ACM-250) located on the roof, and the electrical current flow to the unit was measured with an rms current transducer (CR9580-20-M) attached to one of the three phase wires in the electrical breaker box. The rms current measurement was used to calculate the power consumption of the air conditioning system for model validation.

For a balanced three phase circuit, the total real power is equivalent to three times the real power measured in one phase, as shown in equation (4.1) and (4.2):

$$P_{total} = 3 \cdot P_{phase} \tag{4.1}$$

$$P_{phase} = V_{phase}\, I_{phase}\, Cos\theta \tag{4.2}$$

Where:

P_{total}: total real power [W]

P_{phase}: real power measured in a single phase [W]

V_{phase}: phase voltage

$$V_{phase} = 120\ V$$

I_{phase}: phase current [A]

measured with current sensor

θ: power factor

$$\theta = 1$$

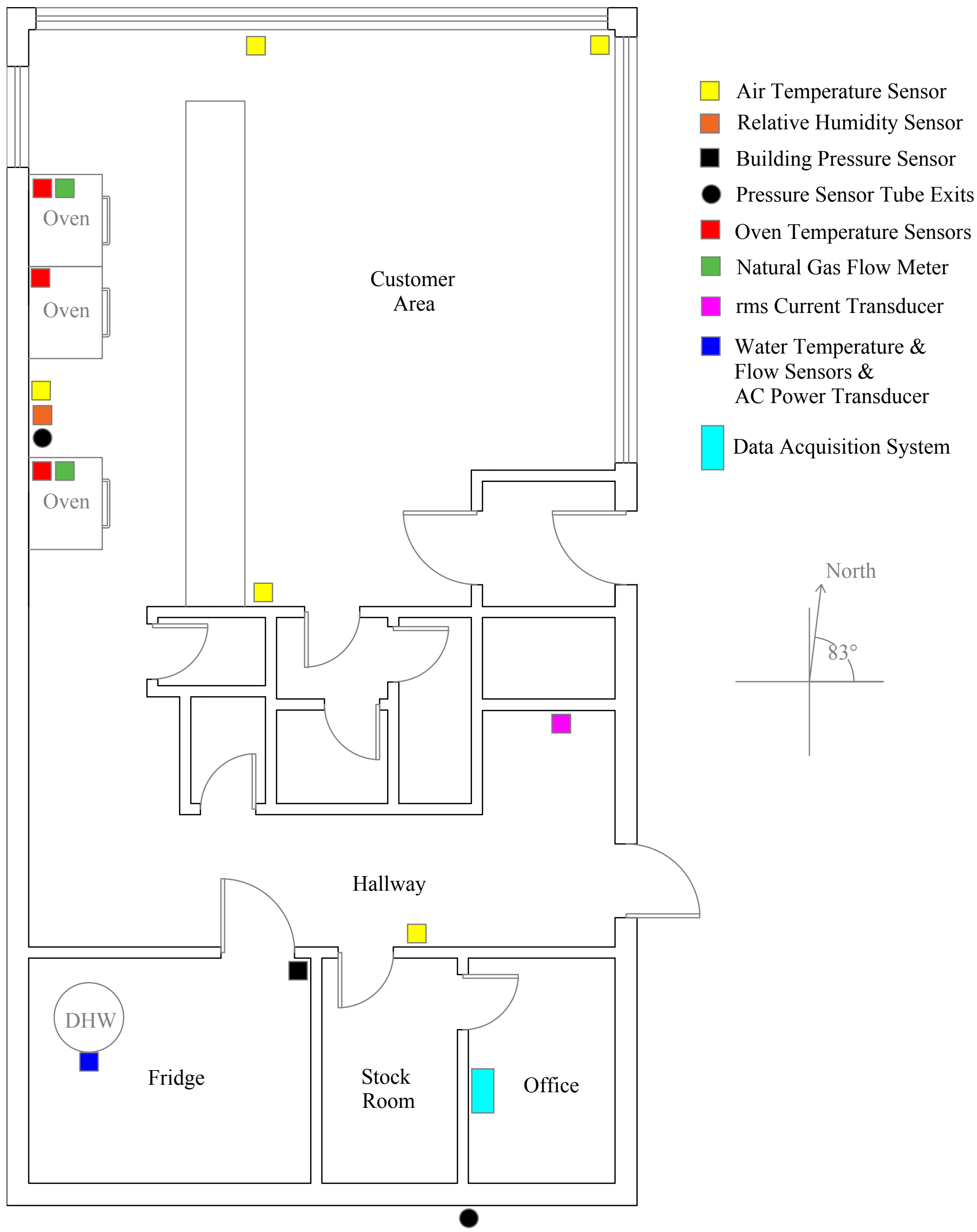

Figure 4.1: Building Floor Plan and Instrumentation Schematic – Store A

4.2.4 Data Acquisition System

The sensors were connected to a National Instruments 4 slot USB CompactDAQ Chassis (cDAQ-9174) with the following modules:

- 16-Channel C Series Temperature Input Module (NI-9213) (75S/s 24-Bit)
- 16-Channel C Series Voltage and Current Input Module (NI-9207) (500S/s 24-Bit)
- 4-Channel Sinking/Sourcing Digital Input Module (NI-9435) (delay time 2.8ms)

The Data Acquisition System (DAQ) was connected to a laptop (Lenovo), which interfaced with the data acquisition hardware through National Instruments LabVIEW 14 software. The data was sampled every minute and saved in text files on the hour. The text files were automatically uploaded to a Dropbox cloud storage system for remote data access.

4.2.5 Experimental Procedure and Data Analysis

The oven operation was conducted entirely by the operators of the individual restaurant, to capture real world scenarios. The DAQ was left to continuously monitor the restaurant's normal operation.

The experimental data was processed using the Python 2.7 programing language, in the Scientific Python Development EnviRonment (SPYDER) [42].

4.2.6 Additional Measurements – Exhaust Volume Flow Rate

The oven and fryer ventilation flow rates were determined by measuring the velocity at equally spaced points across the duct with a pitot-static tube connected to a differential pressure transducer (Fluke 922 Airflow Meter). The differential pressure readings were converted to velocities using Bernoulli's principle for flow along a streamline, as shown in equation (4.3).

$$\vec{v} = \sqrt{\frac{2(p_0 - p)}{\rho}} \tag{4.3}$$

Where:

$p_0 - p$: dynamic pressure (differential pressure measurement)

ρ: density of air at 22.5°C [43]

$$\rho = 1.20\ kg/m^3$$

The volume flow rate was then calculated by taking the integral of the velocity profile over the cross-sectional area of the duct, as shown in equation (4.4). The integral was approximated by multiplying each velocity measurement by its associated segment area, with the total volume flow rate being the sum of the segment volume flow rates.

$$\dot{V} = \int \vec{v}\, dA = \sum_{i=0}^{n} \vec{v}_i \cdot A_i \tag{4.4}$$

Figure 4.2 below displays the velocity profile across the 14 by 12-inch rectangular oven exhaust duct.

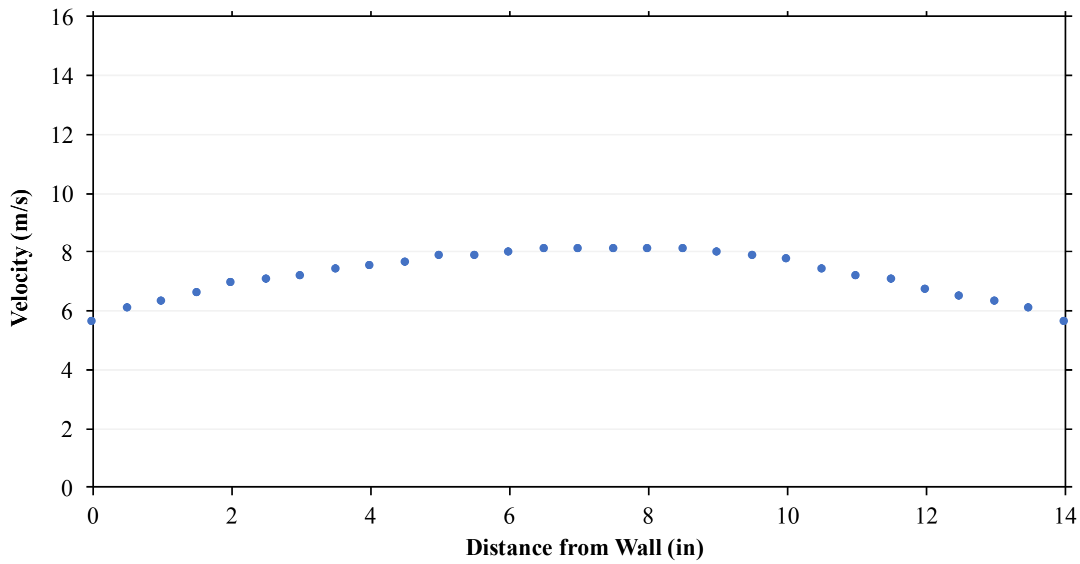

Figure 4.2: Velocity Profile – Oven Exhaust Duct – Store A

The following volume flow rate was calculated from the nearly fully developed turbulent velocity profile:

$$\dot{V}_{StoreA,\ Oven\ Exhaust} = 1555\ CFM$$

Measurement error was reduced by taking the measurements at least 10 and 5.5 hydraulic diameters away from the nearest upstream and downstream disturbance respectively. ASHRAE recommendations were followed, which states that flow rate measurements in ducts be taken at least 7.5 and 3 hydraulic diameters from the nearest upstream and downstream disturbances respectively [30].

Figure 4.3 below displays the velocity profile across the 12-inch diameter circular fryer exhaust duct. In this case, it was not possible to take the measurements at a cross section where the flow was fully developed, due to geometrical constraints in the exhaust network. The measurements were taken 3.50 hydraulic diameters upstream of the fan, and 1.75 hydraulic diameters downstream of a 90° miter bend in the plane of symmetry.

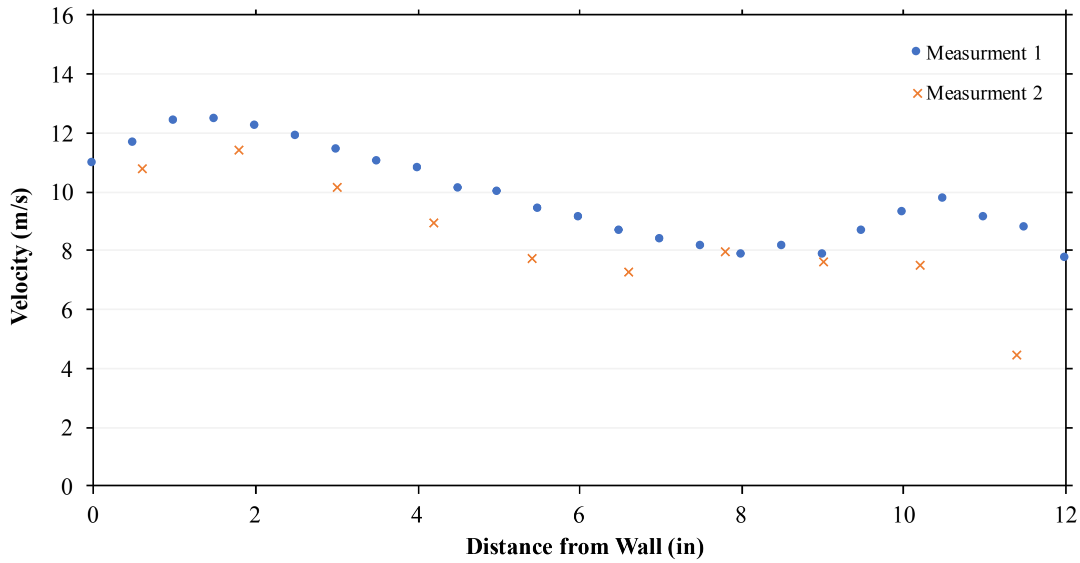

Figure 4.3: Velocity Profile – Fryer Exhaust Duct – Store A

Due to the swirling effect created by the downstream fan, and the flow acceleration and vortices created by the upstream bend, the velocity profile was clearly not fully developed. However, the shape of the velocity profile is qualitatively similar to the axial velocity profiles in the plane of symmetry observed by Austin and Seader [44] and numerically modeled by Patankar [45], where the highest velocity occurs near the outer wall of the bend, decreasing towards the inner wall, and increasing slightly before the boundary layer effects of the of the inner wall of the bend retard the flow. Due to the complex flow structure, computing the volume flow rate simply by multiplying each velocity by the segmented flow area would introduce error, since the areas of constant velocity are irregularly cashew shaped [46]. Breaking the cross-section into smaller area segments, and taking more velocity measurements would have improved measurement accuracy, however since these measurements were taken in the field as opposed to a controlled laboratory setting, increasing the number of measurement points would have been unrealistic, and caused undue damage to commercial equipment. Instead, an approximation for the volume flow rate was made, by multiplying the cross-sectional area by a simple average of the velocity measurements. The resulting volume flow rate was:

$$\dot{V}_{StoreA,\ \ Fryer\ Exhaust} = 1410\ CFM$$

It should be noted that the swirling effect would also introduce a source of experimental error, which would cause the streamlines to not be perfectly perpendicular to the traverse plane.

The measured volume flow rates were converted to mass flow rates assuming the following density of air at 22.5°C [43]:

$$\rho = 1.20\ kg/m^3$$

4.2.7 Hot Water Analysis

The quantity of hot water used on a typical day, and an estimate of the average thermal energy losses from the tank were also considered. Figure 4.4 below displays a histogram of the daily hot water use from Store A, which conforms to a normal distribution.

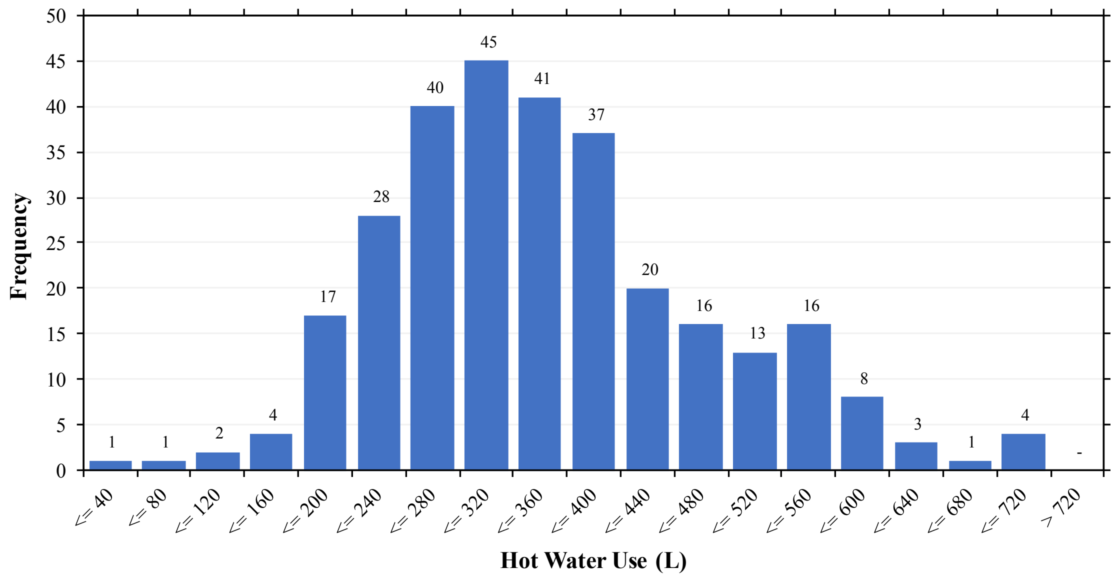

Figure 4.4: Hot Water Use – Store A

The experimental hot water data was input into the model in two separate ways. For model validation in Section 4.7, the exact amount of water used on each specific day was considered. However, for the case study presented in Chapter 5, the following average water draw was used:

$$V_{water\,(avg)} = 345\ L$$

The resulting rate of thermal energy consumption, and the electrical power input to the tank averaged over a 24-hour time window was:

$$\dot{Q}_{water,thermal\,(avg)} = 0.61\ kW$$

$$\dot{Q}_{water,electrical\,(avg)} = 0.71\ kW$$

The average rate of heat loss from the water tank was computed by taking the difference between the electrical input energy and the thermal energy content of the water:

$$\dot{Q}_{water,loss\ (avg)} = 0.10\ kW$$

The losses remained relatively constant regardless of the quantity of water used each day.

4.2.8 Estimating Fryer Gas Consumption

The gas consumption of the fryer was briefly studied, in order to produce a complete picture of the full building energy balance.

Since every natural gas consuming appliance was sub-metered, aside from the fryer, the average daily gas consumption of the fryer was calculated based on the difference between the average daily gas consumption from the utility bills, and the average daily gas consumption from the oven and HVAC sub-meters.

$$\dot{V}_{Fryer} = 5.40\ m^3/day$$

4.3 Store B - Combined Exhaust Venting System

The second restaurant observed was selected for its significantly different method of exhaust ventilation, with both exhaust canopies and chimneys ventilating the ovens.

4.3.1 The Building

Store B was also a standalone building, whose significant dimensions are identified in Figure 4.3 below.

Table 4.2: Significant Dimensions – Store B

Component	Area (m^2)
Floor	288
Roof	288
Walls	247
Windows	29

The building was equipped with three single package air conditioner and heating units (York Sunline 2000, Model Number: D7CG060N09958A). The units had the following performance characteristics specified in the manufacturer's technical guide [47]:

$$AFUE = 80\%$$

$$COP = 2.67$$

4.3.2 Cooking Equipment and Occupant Behavior

The store contained seven deck style ovens (Blodgett 1048B). Six of the ovens were organized into three sets of double stacked ovens in the kitchen. Each stack was ventilated through its own dedicated chimney; however, three exhaust canopies were also present overhead, connected to a single ventilation blower (Canarm BI-RM Series Belt

Drive Utility Blower) on the roof. The seventh oven was located behind the sales counter in the customer area, to exclusively reheat instore sales, and was ventilated with a chimney and was not equipped with an exhaust canopy. Of the seven ovens, only the oven behind the customer service counter and one cooking oven in the kitchen were operated continuously. A second cooking oven was operated occasionally based on demand. The ovens, and exhaust system, were operated continuously on a 24/7 scheduled, at a cooking set-point temperature of 288°C (550°F) and an overnight standby temperature of 149°C (300°F) to reduce oven settling time in the morning. A single Canarm 9200 Inline Duct Blower was also present on the roof which was designed to act as a source of makeup air.

The only other major cooking appliance was a single natural gas deep fryer, which was ventilated with its own separate exhaust blower (Canarm BI-RM Series Belt Drive Utility Blower). The operation of the fryer and its associated ventilation system was mostly limited to the buildings occupied hours, from 10:00 am until close (Sunday–Thursday: 12:00 am, Friday–Saturday: 3:00 am). The continuous operation of the exhaust canopy fans, combined with the lack of sufficient makeup air, caused all chimneys to reverse their direction of flow occasionally which was then vented through the canopy.

4.3.3 Instrumentation

Six wall mounted thermocouple sensors (Omega EWS-TC-T) were used to measure the air temperature inside the building, with two located in the customer area, one in the foyer, one behind the service counter, one in the kitchen and one in the stock room.

Three high temperature thermocouple probes with a braided fiberglass-insulated lead wire (Omega TJ60-CPSS-18U-6-CC) were evenly spaced in the exhaust stream of each of the two main ovens. The cumulative natural gas consumed by each of the two main ovens was also measured, using two positive displacement diaphragm flow meters (Elster American Meter ACM-250).

Building depressurization was measured with a low-pressure laboratory transmitter (Omega PX653-0.1D5V).

Lastly, the natural gas consumption of the three rooftop heating units was measured with a larger positive displacement diaphragm flow meter (Elster American Meter ALM-425) located on the roof.

Figure 4.5 presents a schematic diagram of the instrumentation placement within the restaurant.

4.3.4 Data Acquisition System

The sensors were connected to a National Instruments 4-slot USB CompactDAQ Chassis (cDAQ-9174) with the following modules:

- Two 16-Channel C Series Temperature Input Modules (NI-9213) (75S/s 24-Bit)
- 8-Channel C Series Voltage Input Module (NI-9201) (500kS/s 12-Bit)
- 4-Channel C Series Digital Module (NI-9421) (delay time 100 μs)

The DAQ was connected to a laptop (Lenovo), which interfaced with the data acquisition hardware through National Instruments LabVIEW 14 software. The data was sampled every minute and saved in text files on the hour. The text files were automatically uploaded to a Dropbox cloud storage system for remote data access.

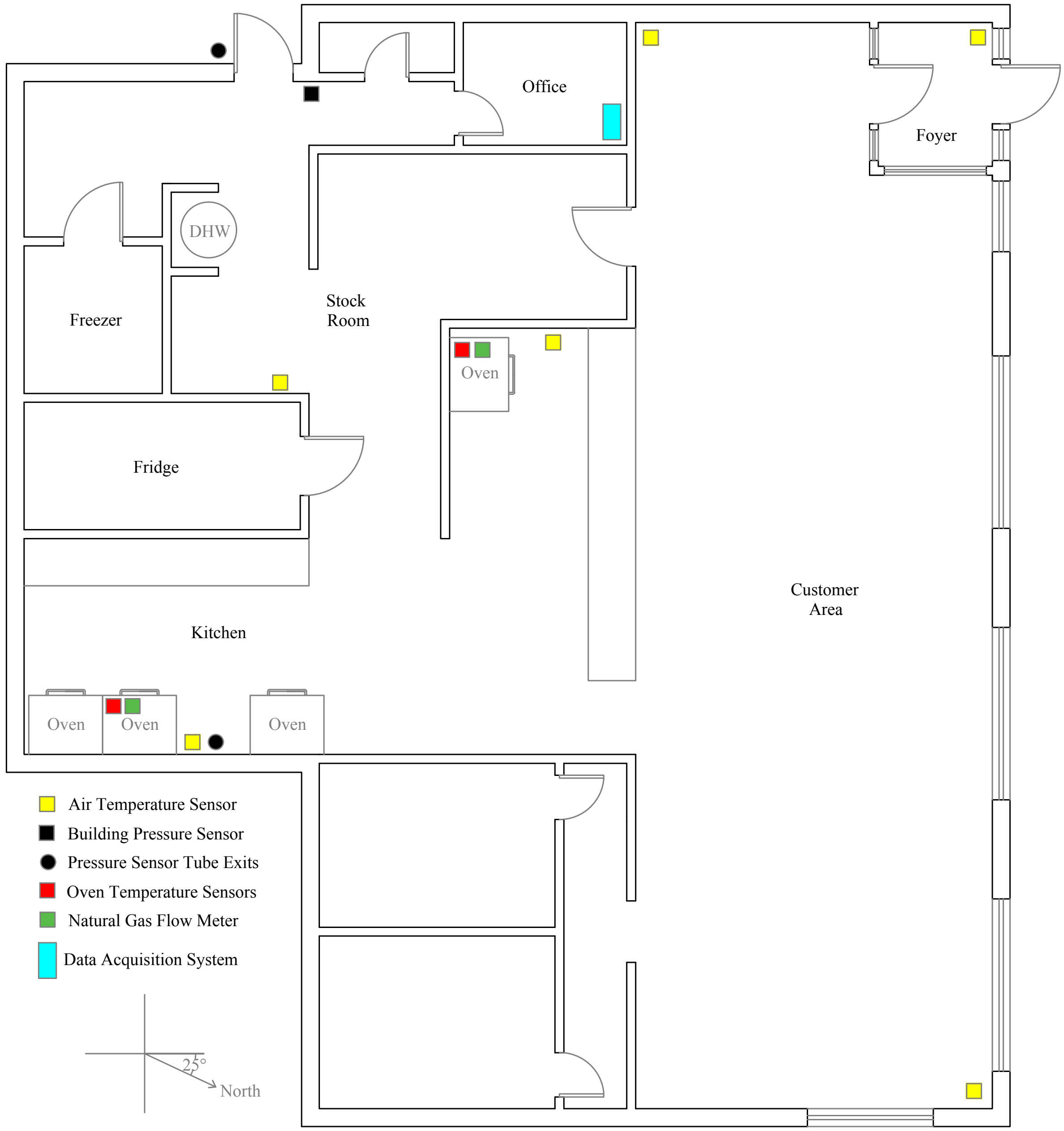

Figure 4.5: Building Floor Plan and Instrumentation Schematic – Store B

4.3.5 Experimental Procedure and Data Analysis

The experimental procedures for Store A and Store B were nearly identical, except for one test where the oven exhaust blower was turned off from 2016/12/20 to 2017/01/11, to collect store operating data when the chimneys were ventilating the ovens and flowing in the correct direction. Data analysis was conducted with the exact same Python program, modified for the different inputs.

Since measurement equipment was not available to monitor the domestic hot water system, it was assumed that the average water use characteristics of Store A were also applicable at Store B.

4.3.6 Additional Measurements – Exhaust Volume Flow Rate

The oven and fryer ventilation flow rates were determined using the same experimental procedure outlined in Section 4.2.6. Similar errors were involved since the traverse plane was located directly between the blower and a 90° square bend, and the volume flow rate was approximated by multiplying the cross-sectional area by a simple average of the velocity measurements. Figure 4.6 and Figure 4.7 below display the velocity profiles across the 15.75-inch diameter oven exhaust duct and the 14-inch diameter fryer exhaust duct respectively.

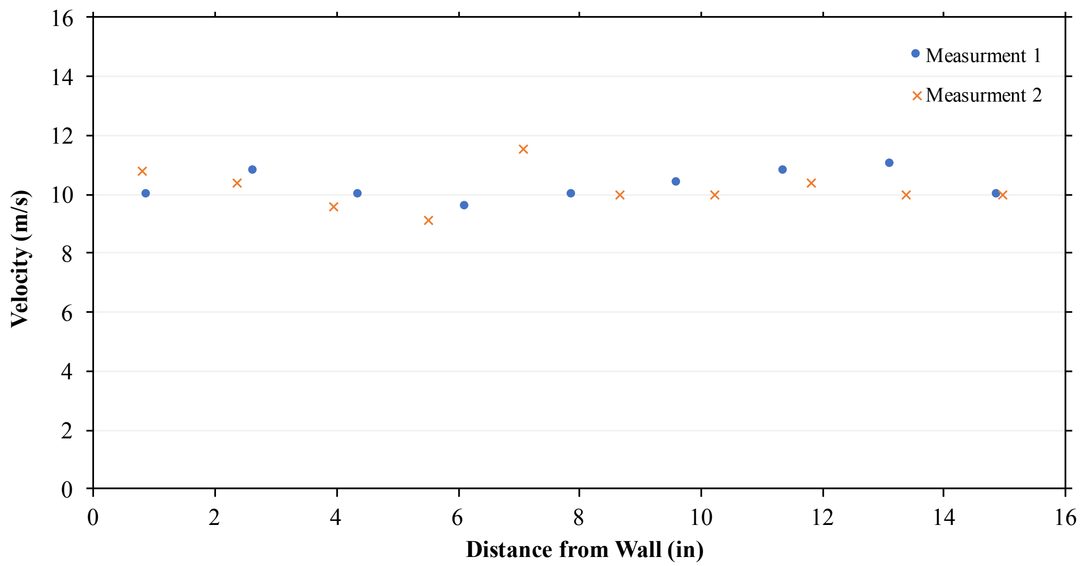

Figure 4.6: Velocity Profile – Oven Exhaust Duct – Store B

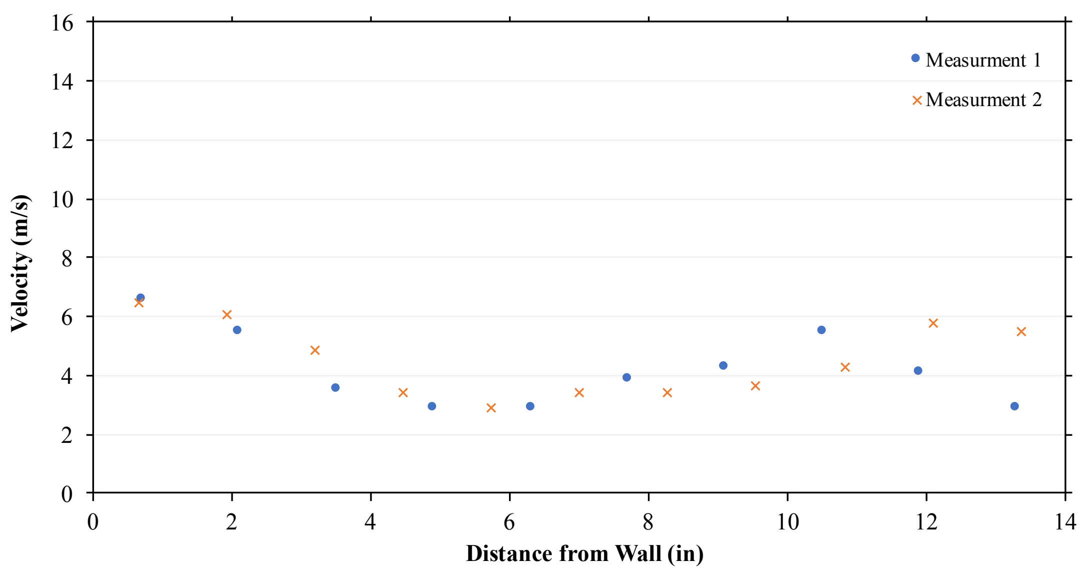

Figure 4.7: Velocity Profile – Fryer Exhaust Duct – Store B

The resulting volume flow rates were:

$$\dot{V}_{StoreB,\ Oven\ Exhaust} = 2727\ CFM$$

$$\dot{V}_{StoreB,\ Fryer\ Exhaust} = 917\ CFM$$

4.4 Experimental Facility 3 – Laboratory Oven Testing

The Blodgett 1048B oven at the McMaster Thermal Management Research Laboratory was used to measure the rate of heat loss from the oven during door opening, as well as the energy loss from continuous door exfiltration.

4.4.1 Instrumentation and Data Acquisition System

An internally compensated laminar flow meter (Alicat M-50SLMP-D) was used to measure the volumetric flow rate of natural gas to the oven. The temperature of the oven was measured with a single thermocouple (Omega EMQSS-125U-24) placed beside the oven thermostat temperature sensor.

The thermocouple sensor was connected to a National Instruments 4-slot USB CompactDAQ Chassis (cDAQ-9174) with the following module:

- 16-Channel C Series Temperature Input Module (NI-9213) (75S/s 24-Bit)

The laminar flow meter was connected to a multifunctional USB DAQ (NI USB 6009) with the following inputs:

- 4 differential analog voltage inputs (48kS/s 14 Bits)
- 2 analog outputs (12 Bits)
- 12 TTL/CMOS digital I/O lines
- One 32-bit, 5 MHz counter

The DAQ was connected to a computer which interfaced with the data acquisition hardware through National Instruments LabVIEW 14 software. The data was sampled every second and saved in a single text file.

4.4.2 Experimental Procedure and Data Analysis – Oven Door Opening

Experiments began 2.5 hours after the oven was started, when the oven natural gas flow rate fell within 2% of its steady state value. The tests were conducted by opening the oven door for seven seconds, the average time required to insert a product, and recording the natural gas flow rate as it returned to its steady state value. The three tests were performed successively, waiting at least 20 minutes between each door opening. Figure 4.8 below superimposes the three natural gas profiles for comparison. Each point on the graph represents the average natural gas flow rate over a five second interval for clarity.

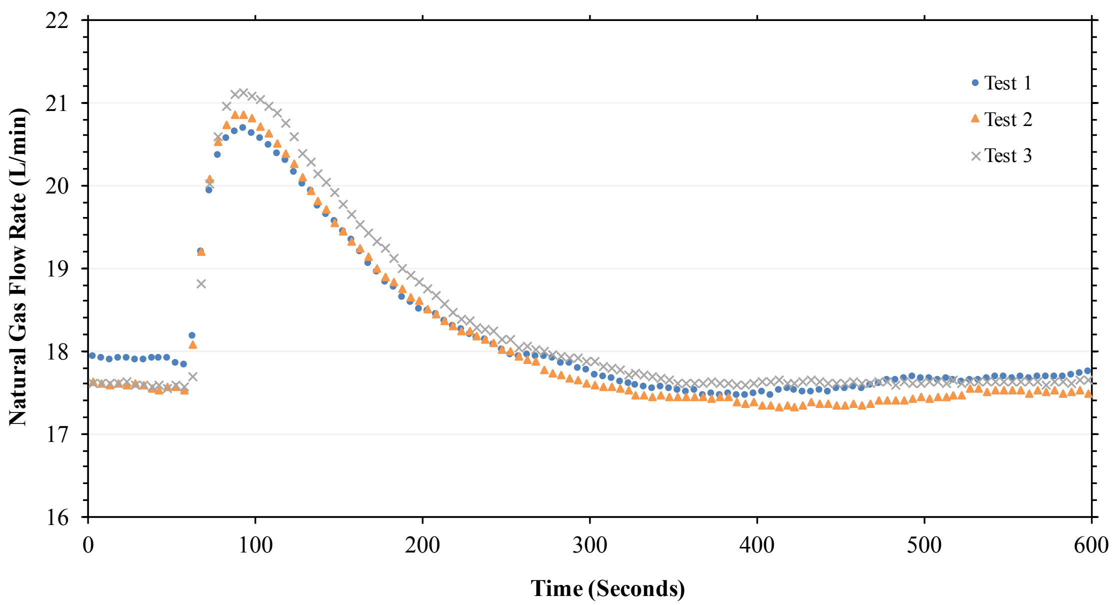

Figure 4.8: Oven Door Opening - Effect on Oven Gas Flow Rate

The total increase in the natural gas input was determined by calculating the volume of gas that was used above the initial steady state conditions over a seven-minute time period. Measuring the total increase in the natural gas input was an indirect method of measuring the energy losses through mass transfer and radiation that occurred during the seven second door opening. The total heat loss of the oven for each door opening test is shown below in Table 4.3.

Table 4.3: Oven Door Opening – Total Heat Loss

Test #	Energy (kJ)
1	122
2	187
3	246
Average	185
Standard Deviation	62

The average energy lost from each door opening was 185 kJ, and over a seven second time interval, corresponds to a total rate of energy loss of 26.4 kW.

The relative contributions of mass transfer and radiation to the total energy loss from a single door opening were estimated, by calculating the net rate of energy transfer by thermal radiation between two surfaces, using equation (4.5).

$$\dot{Q}_{oven,door\ (rad)} = \varepsilon\sigma A_{door}(T_b^4 - T_s^4) \tag{4.5}$$

Where:

ε: emissivity of oven interior

(assuming baking stone and weathered steel are perfect emitters)

$$\varepsilon = 1$$

σ: Stefan-Boltzmann constant

$$\sigma = 5.67 * 10^{-8} \frac{W}{m^2K^4}$$

A_{door}: area of door (10 x 45-inch opening)

$$A_{door} = 1.143\ m^2$$

T_b: average oven surface temperature

$$T_b = 288°C = 561K$$

T_s: temperature of surroundings

$$T_s = 21°C = 294K$$

Therefore, the rate of heat transfer from the oven to the room through radiation was:

$$\dot{Q}_{oven,door\ (radiation)} = 5.9\ kW \quad \text{(22.4\% of total)}$$

or

$$Q_{oven,door\ (radiation)} = 41\ kJ$$

And the rate of heat transfer from the oven through mass transfer was:

$$\dot{Q}_{oven,door\ (mass\ transfer)} = 20.5\ kW \quad \text{(77.6\% of total)}$$

or

$$Q_{oven,door\ (mass\ transfer)} = 144\ kJ$$

4.4.3 Experimental Procedure and Data Analysis – Continuous Door Exfiltration

The rate of energy loss from continuous door exfiltration was measured by fully sealing the oven door once the oven had reached a steady operating state, and measuring the change in the average natural gas flow rate. Figure 4.9 presents the results of the oven door sealing experiment, where the oven was operated at a set-point temperature of 288°C (550°F).

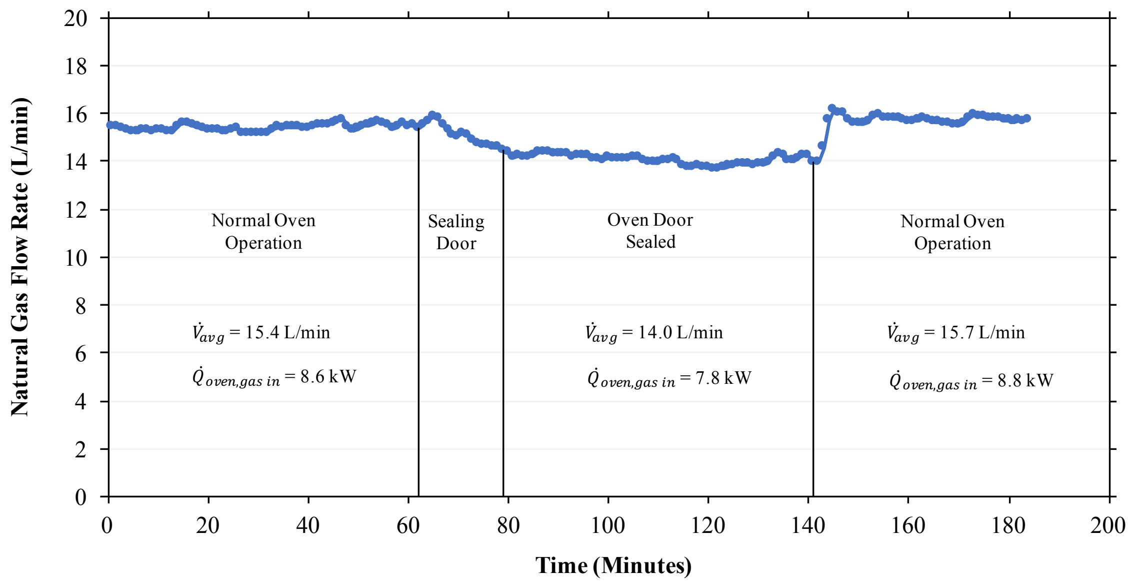

Figure 4.9: Effect of Oven Door Sealing on the Steady State Natural Gas Flow Rate

The experimental results show that fully sealing the oven door had the effect of reducing the appliance natural gas flow rate by 1.5 L/min. Therefore, the rate of energy loss through continuous door exfiltration was:

$$\dot{Q}_{oven,leakage} = 0.9\ kW$$

Using equation (3.15), the mass flow rate of continuous door exfiltration was determined to be:

$$\dot{m}_{oven,leakage} = 0.003\ kg/s$$

4.5 External Measurements

Data from the McMaster Weather Station provided external temperature, relative humidity and downward shortwave radiation measurements that were used in the model validation.

4.6 Uncertainty Analysis

An uncertainty analysis of the measured variables may be viewed in Appendix C.

4.7 Model Validation

The model validation is shown below in the following subsections. In all cases, exact measurements from either the experimental facilities or the McMaster Weather Station were used as inputs to the model for each specific day under consideration. The only exception was for the solar gains, which were implemented using two separate methods, which will be explained at their time of use.

4.7.1 Model Validation: Heating and Cooling Energy Requirements

A detailed comparison of the model outputs against the experimental data for Store A, with exhaust canopies was conducted, to validate the model's ability to accurately predict the heating and cooling energy requirements of the building, during the different operating seasons. The comparison days were selected specifically based on two factors. Firstly, the test days were selected in order to minimize the temperature fluctuations of both the inside and outside air, to achieve conditions that were as close to steady state as possible. Secondly, only clear sky days were selected, so that the maximum value of the solar gain at the specific date could be used in the calculation with minimal error. Clear sky days were identified by observing the shortwave downward radiation measurements from the McMaster Weather Station, and only days with an uninterrupted parabolic profile were selected.

The results of each validation case are summarized in the form of an energy flow diagram, showing the rates of energy transfer averaged over twenty-four hours. Three different colours were used to represent the different flows of energy, with red indicating paths of energy loss, green representing energy transferred into the building, and blue denoting energy flows that do not have an impact on the HVAC system. The accuracy of the model in each case was evaluated by comparing the percentage difference between the sum of the energy inflows and the sum of the energy outflows, which are theoretically identical assuming the quantity of energy stored in the building remains constant.

4.7.1.1 Case 1: Coldest Day of the Year

Case 1 was used to validate the model's ability to predict the natural gas required to heat the building on the coldest day of the year, which also happened to have a fully clear sky.

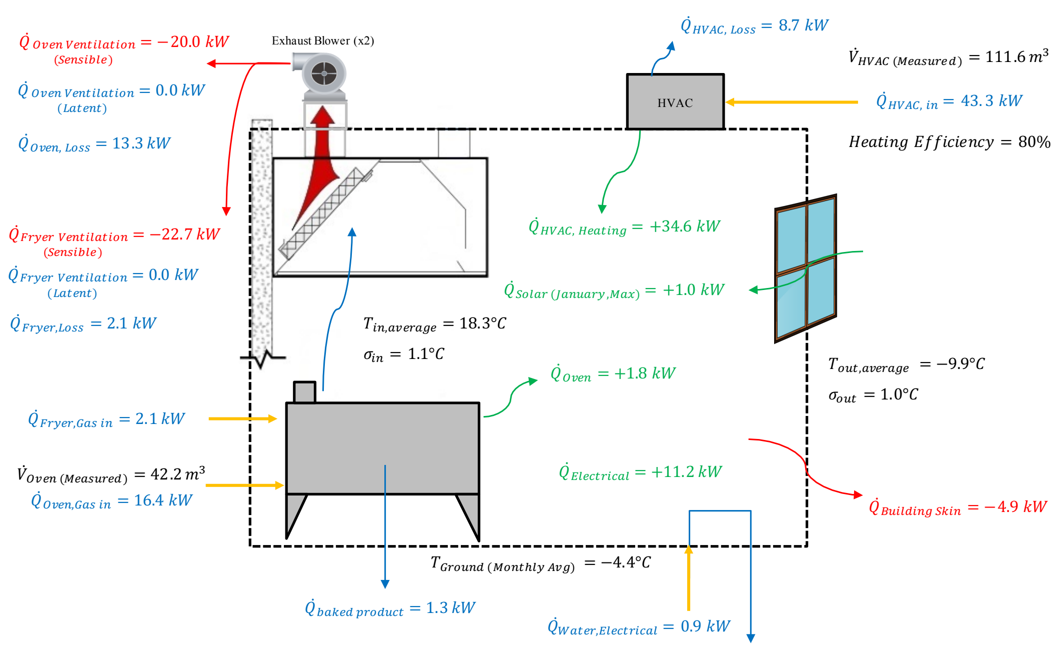

Figure 4.10: Model Validation – Coldest Day of the Year – January 8, 2017

Figure 4.10 above illustrates the discrepancy between the different energy inflows and outflows, which are summarized as follows:

$$\dot{E}_{in} = 48.6\ kW$$

$$\dot{E}_{out} = 47.6\ kW$$

$$\%\ difference = 2.0\%$$

4.7.1.2 Case 2: Hottest Day of the Year

Case 2 was used to validate the model's ability to predict the electricity required to cool the building on the hottest day of the year.

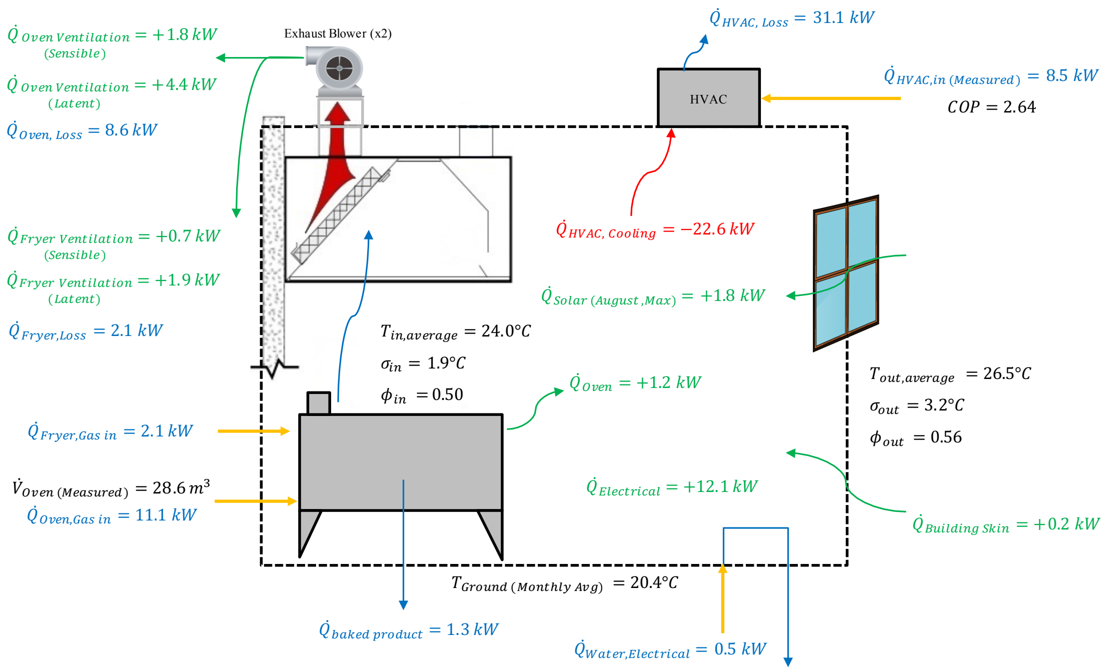

Figure 4.11: Model Validation – Hottest Day of the Year – August 4, 2016

Figure 4.11 above illustrates the discrepancy between the different energy inflows and outflows, which are summarized as follows:

$$\dot{E}_{in} = 24.1\ kW$$

$$\dot{E}_{out} = 22.6\ kW$$

$$\%\ difference = 7.1\%$$

4.7.1.3 Case 3: Building Temperature Equivalent to Outside Temperature

Case 3 was used to validate the model's ability to predict the cooling energy requirements on a day where the outside temperature was equivalent to the building temperature.

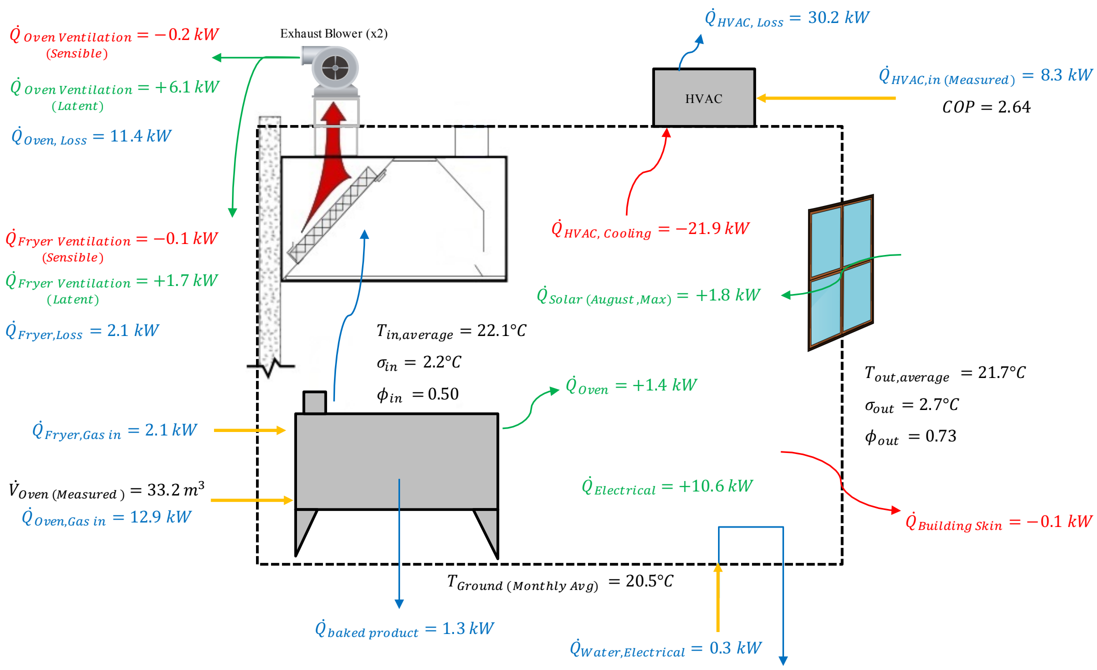

Figure 4.12: Model Validation – Building and Outdoor Temperature Equivalent – August 1, 2016

Figure 4.12 above illustrates the discrepancy between the different energy inflows and outflows, which are summarized as follows:

$$\dot{E}_{in} = 21.6\ kW$$

$$\dot{E}_{out} = 22.3\ kW$$

$$\%\ difference = 4.0\%$$

4.7.1.4 Case 4: No heating or Cooling Required

Case 4 was used to compare the energy balance on a day where no heating or cooling was required.

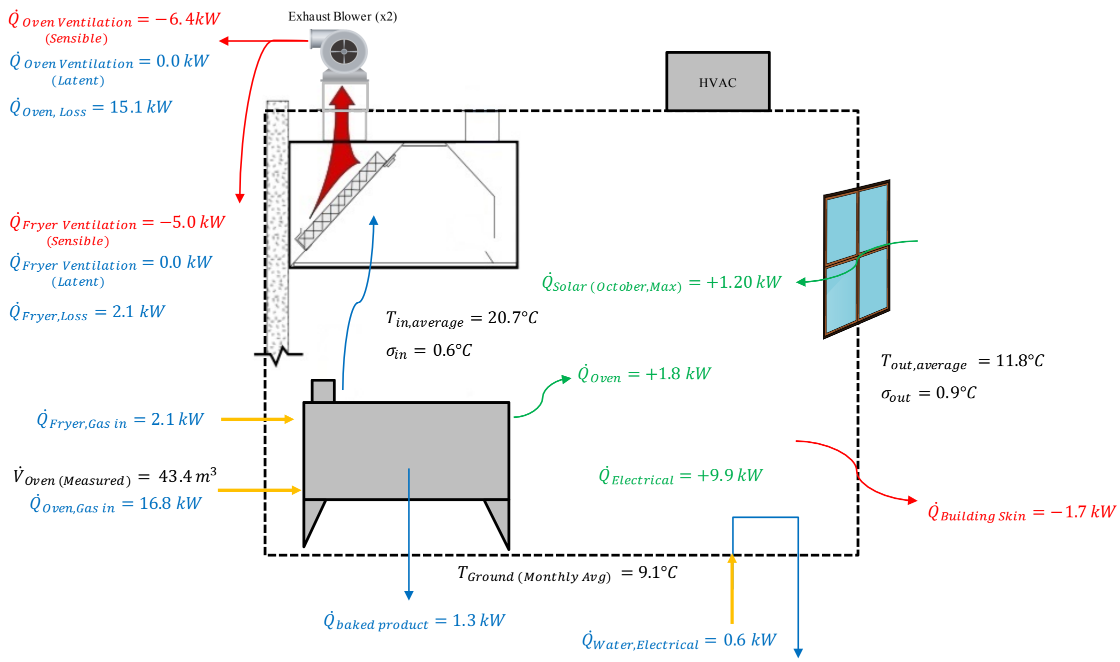

Figure 4.13: Model Validation – No Heating or Cooling Required – October 20, 2016

Figure 4.13 above illustrates the discrepancy between the different energy inflows and outflows, which are summarized as follows:

$$\dot{E}_{in} = 12.9\ kW$$

$$\dot{E}_{out} = 13.1\ kW$$

$$\%\ difference = 2.0\ \%$$

4.7.2 Model Validation: Different Operating Configurations

Several other validation studies were conducted to show congruence between the model and the entire experimental data set. The purpose of this comparison was to validate the model's ability to accurately represent restaurants with different exhaust configurations. These three ventilation configurations were:

1) Exhaust Canopies
2) A Combined Exhaust System with both Canopies and Chimneys
3) Chimneys

During these tests, an effort was not made to select only clear sky days, but instead, test days were chosen that covered the full range of outside temperatures. For this reason, the solar gains were included as error bars showing the maximum amount of energy that could have been added to the store via solar radiation.

Figure 4.14, Figure 4.15 and Figure 4.16 display the natural gas required by the HVAC system to heat the building for one day, plotted against the associated number of heating degree days. The heating degree days were calculated from the air temperature measurements from the McMaster Weather Station using equation (4.6), with a base temperature of 21°C.

$$HDD = \frac{\sum_{t=1}^{n}\left(21°\text{C} - T_{out}(t)\right)}{n} \tag{4.6}$$

In the following plots, the blue diamonds represent the model outputs, while the orange dots represent the corresponding measurements. The comparisons have been superimposed on the entire experimental data set, marked by the grey crosses, to visualize the true spread of the data.

The plots show the model data following the makeup air adjustments, which estimated the flow rate of makeup air by minimizing the sum of squared errors between the model outputs and corresponding measurements. The amount of makeup air introduced was:

$$\dot{V}_{makeup,Store\ A} = 310\ CFM$$

$$\dot{V}_{makeup,Store\ B-Canopy} = 680\ CFM$$

$$\dot{V}_{makeup,Store\ B-Chimney} = 0\ CFM$$

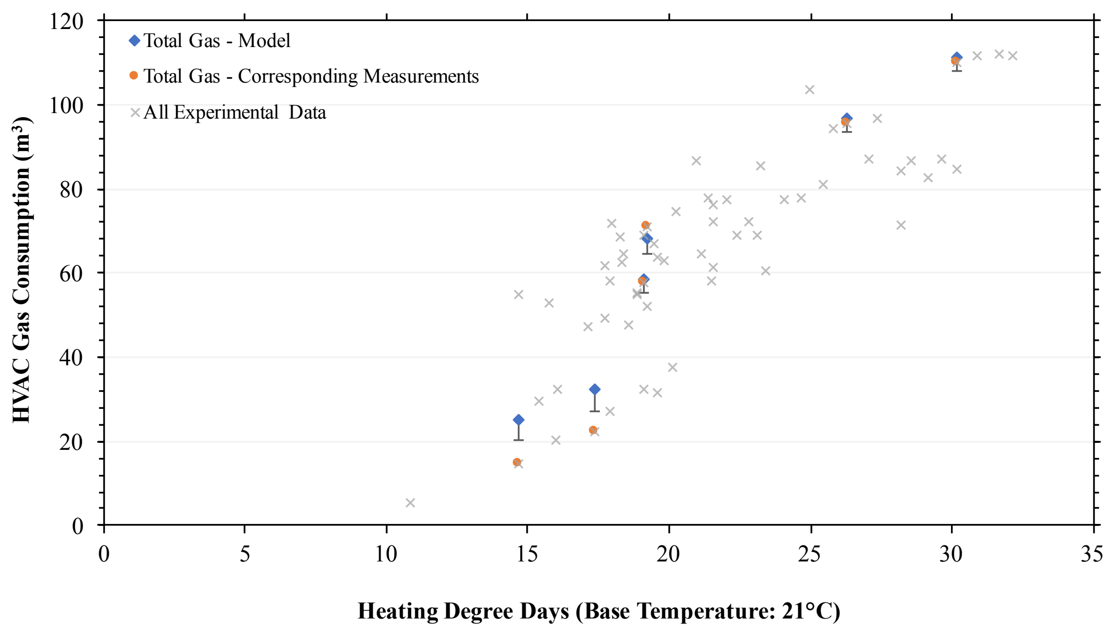

Figure 4.14: Model Validation – HVAC Gas Consumption – Store A – Exhaust Canopy Ventilation

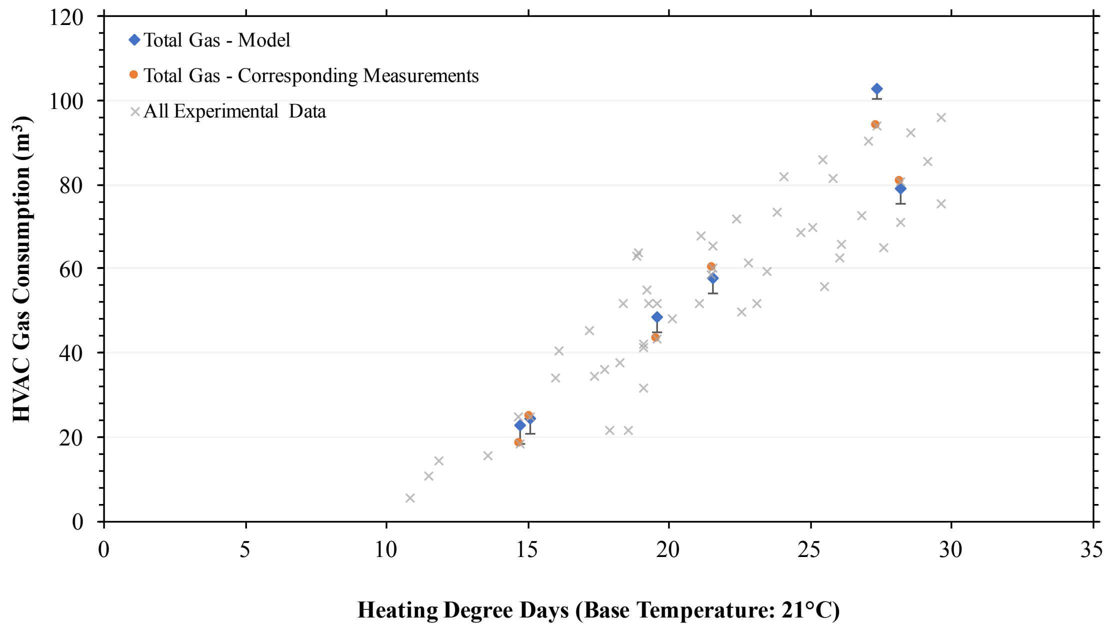

Figure 4.15: Model Validation – HVAC Gas Consumption – Store B – Combined Exhaust System

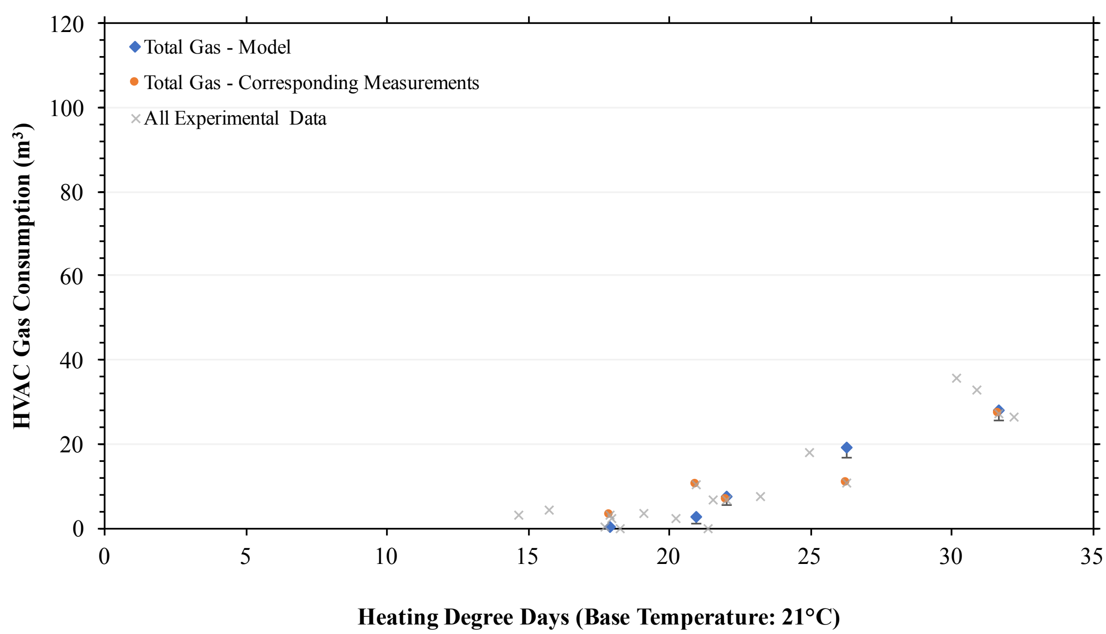

Figure 4.16: Model Validation – HVAC Gas Consumption – Store B – Chimney Ventilation

The validation study shows that the energy model developed is capable of predicting the natural gas heating requirement of the building, with an average absolute error of 4.0 m^3, with a standard deviation of 2.7 m^3. The associated average relative error was 19%, with a standard deviation of 26%, excluding a single outlier from the calculation which skewed the average relative error.

4.8 Experimental Facility 4 – TEG POWER System

Experiments were conducted on the TEG POWER system, to characterize its performance, and to provide inputs to the building energy model related to energy harvesting. Several tests were conducted on the completed TEG POWER prototype, to experimentally measure the amount of thermal energy that would be available; to provide hot water, space heating and oven preheating.

4.8.1 Instrumentation and Data Acquisition System

Experiments were conducted on the Blodgett 1048B oven at the McMaster TMRL, equipped with the TEG POWER exhaust gas energy recovery device installed in the exhaust stream, before the draft hood. The coolant water side of the exhaust gas heat exchanger was connected to a combined solar thermal water tank and louvered fin heat exchanger, which were assembled in parallel, to form a thermodynamic cycle. A fan, equipped with a temperature controller, was mounted on the louvered fin heat exchanger to maintain quasi-steady state operation, with the coolant water temperature below 80°C.

Several measurement instruments were identical to Experimental Facility 3, including the laminar flow meter (Alicat M-50SLMP-D) and the single oven temperature sensing thermocouple (Omega EMQSS-125U-24). Two additional thermocouples (Omega TMQSS-125U-6), one in the coolant water inlet and one in the coolant water outlet of the heat exchanger, were included. The thermocouples were used to measure the temperature difference of the coolant water as it passed through the heat exchanger. Lastly, a Coriolis flowmeter (Endress+Hauser Promass 80E) was connected in series, to measure the volume flow rate of the coolant water. A more detailed description of this experimental facility can be found in [48].

The measurement equipment was connected to the same data acquisition system detailed in Experimental Facility 3, with data sampled and recorded at one minute intervals.

4.8.2 Experimental Procedure and Data Analysis

Experimental data was collected once the oven reached quasi-steady state operating conditions at 288°C (550°F). The rate of heat transfer to the coolant water was calculated using equation (4.7) as follows:

$$\dot{Q}_{recovered} = (\dot{V}_{coolant\ water} \cdot \rho_{water}) C_{p_{water}} (T_{outlet,avg} - T_{inlet,avg}) \tag{4.7}$$

Where:

$\dot{V}_{coolant\ water}$: volume flow rate of coolant water through heat exchanger

$$\dot{V}_{coolant\ water} = 5.8\ L/min$$

ρ_{water}: density of coolant water, kg/m^3 [34]

$C_{p_{water}}$: specific heat capacity of coolant water, $kJ/kg \cdot K$ [49]

Density and specific heat capacity were taken at the average of the bulk fluid temperatures at the inlet and exit of the heat exchanger.

A sample of the experimental data from one specific test is shown in Figure 4.17.

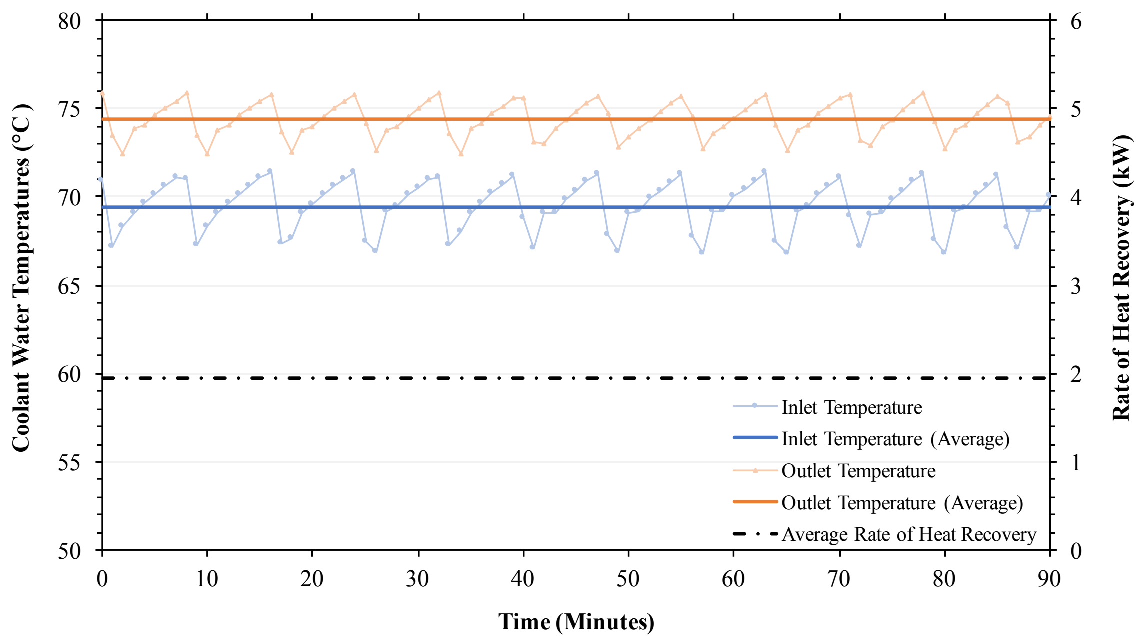

Figure 4.17: Rate of Heat Recovery from a Single Oven Operating at 288°C (550°F)

The noise observed in the inlet and exit temperatures occurred due to the heat exchanger fan operation, which cycled between on and off settings to maintain the coolant temperature below 80°C. The average inlet and exit temperatures were used in equation (4.7) to determine the rate of thermal energy recovery.

$$\dot{Q}_{recovered} = 1.95\ kW$$

It should be noted that the aforementioned value is a conservative estimate of the rate of thermal energy recovery, since the rate of heat transfer is inversely related to the coolant water temperature, which decreases during times when the water tank is recharging.

Chapter 5
Results and Discussion

5.1 Introduction

In this chapter, the effectiveness of the building energy model developed will be tested, for its ability to predict the energy savings from four potential energy conservation measures. The results presented in Section 5.4 through Section 5.11 are from a specific case study of Store A, however the modeling techniques used to predict energy savings may be applied to any commercial institution operating natural gas ovens. In addition, as many restaurant franchisees follow similar operating practices, these four energy conservation measures would be directly applicable at other locations. Section 5.12 highlights the results of the case study on Store B for comparison.

The operational changes and technology developments are all a part of the ideal TEG POWER Solution, and are presented sequentially. The solutions have been structured as four incremental changes; where the additional energy savings can be attributed solely to the current change, while the total energy savings assumes that prior changes have already been implemented. The first conservation measure, is to substitute exhaust canopies with chimneys for oven ventilation. The second, is to seal and insulate all ovens, to mitigate the increased heat loss side effects that arise from chimney based oven ventilation. The third, is to turn off all ovens at night with the introduction of an automated startup functionality. The fourth, and final technological innovation, is the inclusion of energy harvesting, to recover a portion of the waste heat from the exhaust stream, and to repurpose it for space heating in the winter, and oven preheating in the summer.

An alternative technology roadmap is also presented, where an exhaust gas energy harvesting system is commissioned on an oven operating with exhaust canopy ventilation. The purpose is to contrast the maximum energy savings that may be achieved with the ideal TEG POWER Solution, against the solution that is permitted by current regulations.

Each section begins by solving the building HVAC energy balance (described in detail in Chapter 3) for the specific restaurant operating configuration, to determine the heating and cooling energy requirements for a typical year, in cubic meters of natural gas and kilowatt-hours of electricity respectively. Considering that the different energy flows within a building are highly interdependent, the results of the HVAC energy balance were then analyzed in the context of the full building energy balance, to show the relative contributions of the HVAC system, internal electrical loads, domestic hot water, exhaust blowers, and oven and fryer gas use, to the total restaurant energy use. Since the building is supplied with two different primary sources of energy, electricity and natural gas, the common unit of gigajoules was used to make meaningful comparisons between the total building energy consumption of each operational configuration.

5.2 Weather Data Inputs

In order to accurately simulate the energy requirements and fuel consumption of the building for the duration of a full year, weather data inputs that were representative of the local climate were selected. Since the stores under consideration in this study were located in Southern Ontario near McMaster University (ASHRAE Climate Zone 5), the Hamilton Airport Weather Station (World Meteorological Organization ID: 71263) was selected as the source of the measured climate data. This latest Climate Normal data set, comprised of a three-decade average of meteorological variables from 1981 to 2010, was obtained from the Canadian Governments Department of Environment and Natural Resources data archives [50]. The monthly average temperature and relative humidity, Figure 5.1, was used in the model and held constant while simulating each of the operational changes.

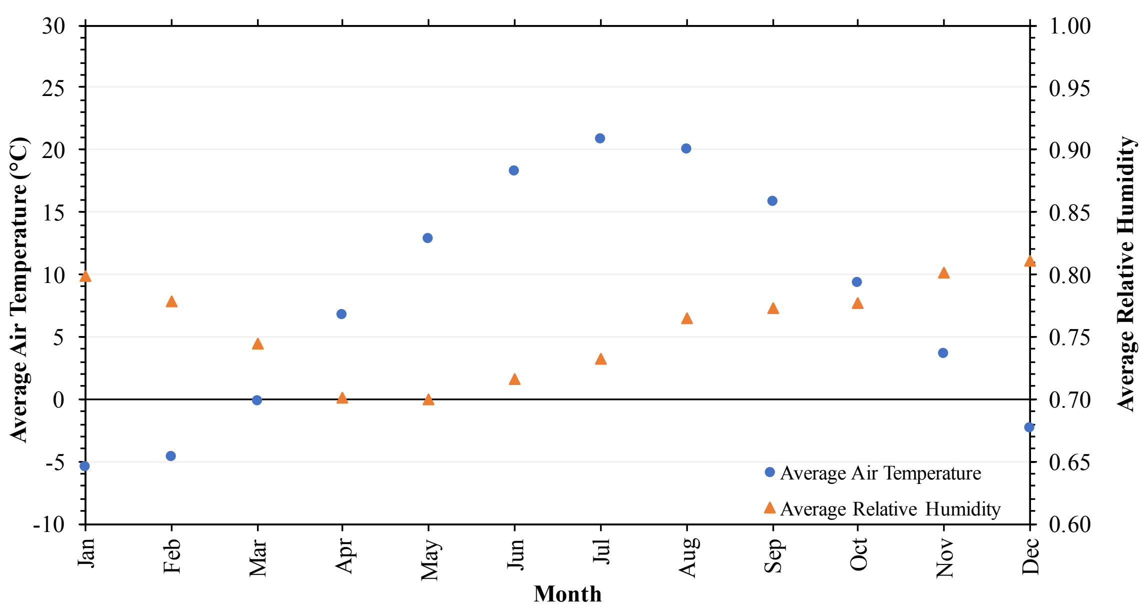

Figure 5.1: Energy Model Weather Inputs – Average Outdoor Temperature and Relative Humidity [50]

5.3 Utility Data Comparison

The actual natural gas and electricity use of both Store A and Store B was obtained from a singles years' worth of utility bills collected from Union Gas and Alectra Utilities (Formerly Horizon Utilities). The data, summarized in Appendix D, was used in comparing the results of the full year simulations to the actual building performance data.

5.4 Common Assumptions – Store A

Several common assumptions were made in each of the simulations. They are listed below:

- The restaurant is a single zone building, and the air in the zone is perfectly mixed
- The store is operating two ovens
- The inside air temperature remains at 21°C (the typical building set-point temperature), with a relative humidity of 50% during the cooling season (average of the measured values). The total energy required was calculated assuming that the HVAC system does not have a fixed capacity, and can provide the required heating or cooling in all situations. In reality, the HVAC system would reach its maximum heating capacity of 42.2 kW and cooling capacity of 26.9 kW [41].
- Every day follows the same operational schedule, with employees arriving to the store at 9:00 am, at which time the fryer and associated ventilation system is switched on, and leaving at 2:30 am the next day, when the fryer and associated ventilation system is switched off. The weighted average closing

time of 2:30 am was used to account for the differing hours of operation between weekends and weekdays. The 10 statutory holidays observed in Ontario were not considered.

- Cooking begins at 9:30 am, an hour and a half before the store opens
- 200 baked products are cooked every day
- The restaurant uses 345 L of domestic hot water every day

5.5 Baseline Model

Store A was first simulated with inputs designed to represent the baseline operating conditions, where the kitchen was equipped with an exhaust canopy to ventilate the ovens. Two separate exhaust blowers were required for this configuration, with one operating continuously to ventilate the oven combustion gases, and the other operating during occupied hours to ventilate the fryer.

The modeling tool was used to establish the buildings baseline energy performance, which potential retrofits could be compared against to determine their effectiveness. Figure 5.2 below illustrates an energy flow diagram of the store, showing the rates of energy transfer averaged over a single operating day, during the month of January.

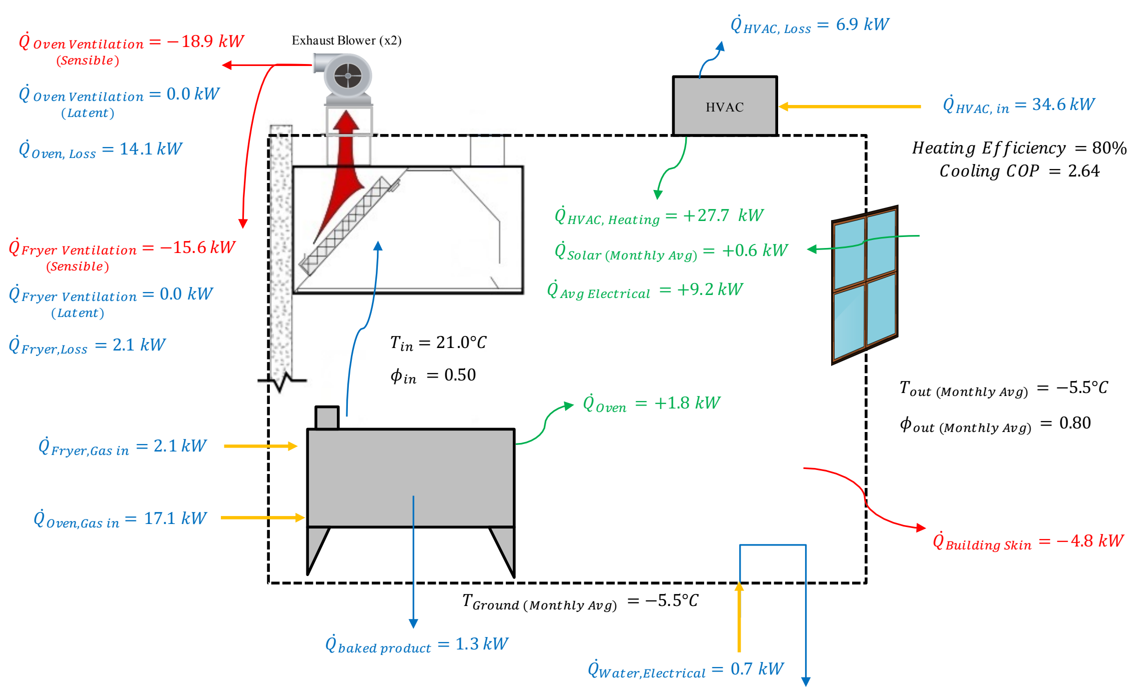

Figure 5.2: Building Energy Flow Diagram – Store A – Baseline Conditions

The oven and fryer blowers were the greatest contributors to building energy loses, via mass transfer, with ventilation losses of 18.9 kW and 15.6 kW respectively, during the winter months.

The two ovens, operated continuously on a 24/7 schedule at a set-point temperature of 288°C (550°F), required a constant natural gas input of 17.1 kW of thermal energy. The ovens have the potential to provide a portion of this heat to offset the losses from ventilation, albeit only 1.3 kW (7.5%) and 1.8 kW (10.2%) was transferred to the baked products and to the room respectively, and the remaining 14.1 kW (82.3%) exited with the oven ventilation air, and is essentially lost to the outdoors. The resulting oven thermodynamic efficiency was 17.7%. The thermodynamic efficiency in the summer would be even lower, since the only useful output would be the energy input to the baked product, while the oven heat losses to the room impose a negative impact on the HVAC system. Therefore, the oven thermodynamic efficiency during the summer would be less than 7.5%.

In the base case, the single largest energy input to the building was the electrical loads, which contributed 9.2 kW, compared to the addition of 27.7 kW from the HVAC system to maintain the building in equilibrium. The upcoming case studies presented in Sections 5.6 through 5.9 will identify methods of reducing the major energy losses from the ventilation system, and introduce strategies to capture and repurpose the wasted heat from the ovens.

The results of the full year simulation are presented below in Figure 5.3 in the form of an HVAC energy balance, broken into twelve different components based on the months of the year. In each column, the building skin, fryer and oven sensible ventilation losses are shown additively below the x-axis, and the electrical, oven, solar, fryer and oven latent ventilation gains are shown additively above the x-axis. The net heating or cooling energy requirements, the difference between the total gain and loss columns, are represented as the independent black line.

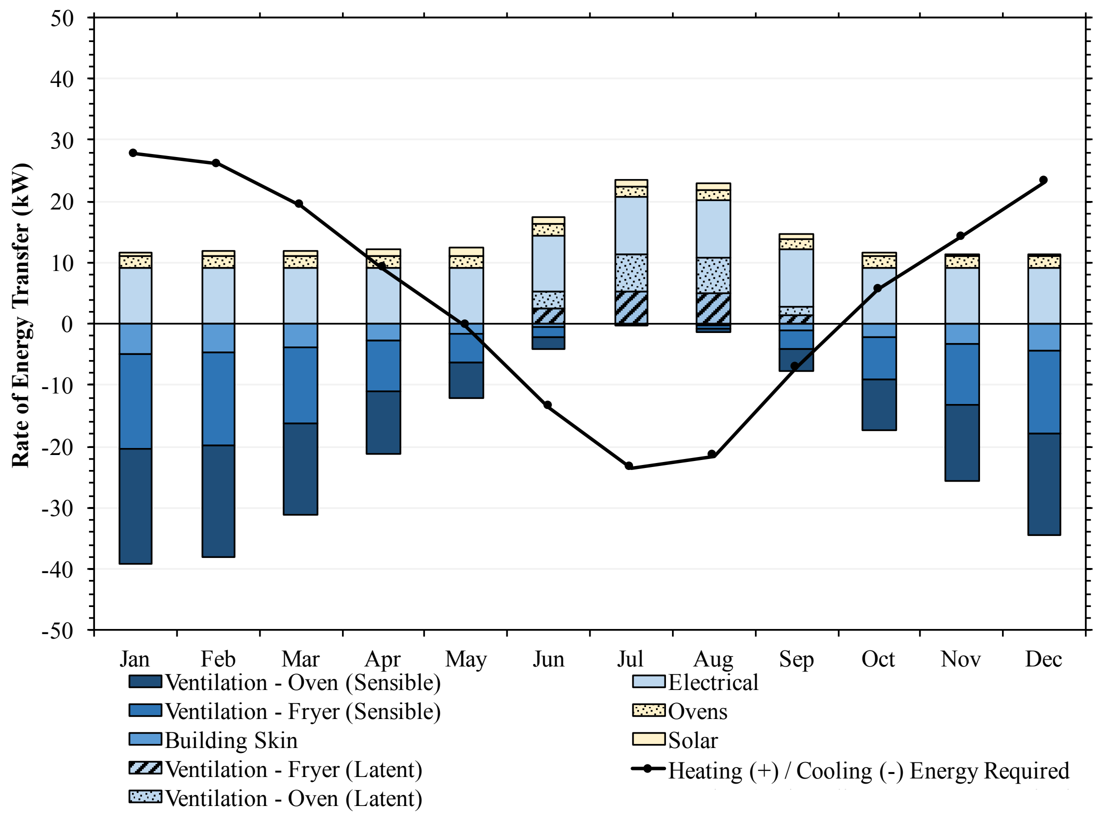

Figure 5.3: Building HVAC Energy Balance – Store A – Baseline Conditions

Under the current store operations, a total of 326 GJ was required to heat the building during in the winter, and a total of 175 GJ of thermal energy needed to be removed from the building during the cooling season. The resulting primary energy requirements were 12,194 m^3 of natural gas, and 18,570 kWh of electricity for the year.

The largest contribution to the heating requirements was the sensible energy necessary to heat the replacement air drawn into the building by the oven and fryer exhaust ventilation, which accounted for 88% of the total building energy losses. Looking at the hottest month of the cooling season, July, reveals that the heat gain from the oven had a relatively small contribution of 7% to the total energy gain of the building, while the largest contribution of 48% was made by the sum of the two latent components of ventilation, followed by the heat generated by electricity consumption which contributed 39%. The solar gains were included for each month of the analysis, although its impact on the building energy balance was minimal, partly due to the roof overhang which intercepted a portion of the incident radiation effectively shading the fenestration.

The total HVAC energy use derived from the HVAC energy balance was then analyzed in the context of the building energy balance. The comparison is shown below in Figure 5.4.

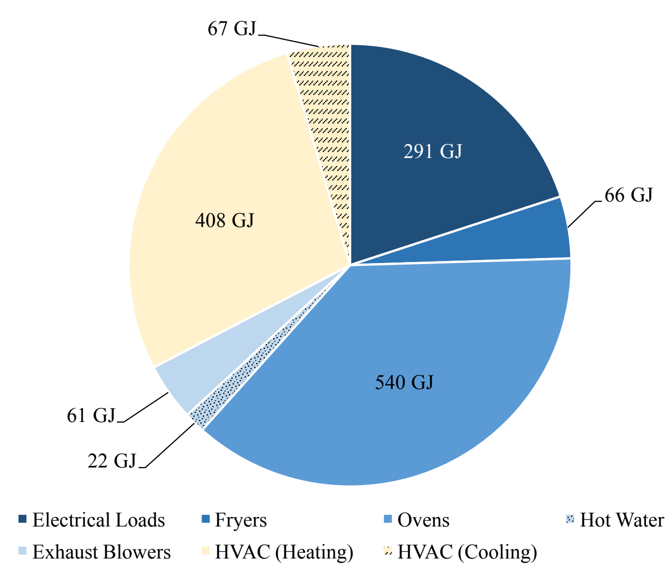

Figure 5.4: Breakdown of Building Energy Consumption by End Use – Store A – Baseline Conditions

In order to operate the building in this configuration for the duration of a full year, the total energy requirements amounted to 1,456 GJ. Of this total, the electrical loads, exhaust blowers, hot water, and cooling portion of the HVAC operation require 441 GJ (122,487 kWh) of electrical energy, while the ovens, fryers and heating portion of the HVAC operation require 1,015 GJ (30,300 m^3) of energy from natural gas.

To verify model accuracy, the calculated total electricity and natural gas requirements were compared to the corresponding utility bills from Store A. The total consumption from each separate billing period has been compiled in Appendix D, and Table 5.1 below summarizes the comparison of the model outputs against the utility measurements.

Table 5.1: Comparison of Building Energy Model to Utility Data – Store A – Baseline Conditions

Utility	Model	Utility Bills	% Error
Natural Gas (m^3)	30,300	29,276	3%
Electricity (kWh)	122,487	132,362	-7%

It is clear that the model overpredicted the natural gas use, and underpredicted the electricity use. There are several explanations for why the outputs from the simplified model differed from the empirical results. One assumption was that the two ovens were operated continuously, on a 24/7 schedule. In reality, there was approximately a two-month period, during July and August of 2016, where one of the ovens was turned off midday, or not operated at all. Considering the specific operator behavior would have reduced the natural gas use by approximately 700 m^3. There was also an approximately three-month period from December of 2016 to February of 2017, where the fryer exhaust blower was left to operate continuously, instead of following the standard shutdown procedure during non-operating hours. Operating the blower for this extended period of time would have increased the electrical consumption of the store by nearly 500 kWh, although the additional ventilation would have also resulted in a higher heating load. It is also possible that food refrigeration systems inside of the building would consume more electricity in the summer months, considering the internal temperature of the building departs from the 21°C set-point temperature specified in the model, as the HVAC system was not able to keep up with the loads that were placed on it.

As the model represents a simplification of reality, the actual operating schedules, occupant behavior and building microclimates that occurred over the billing period certainly differed from those that were assumed. However, the simplified base case model was able to produce results that were within a 10% error of the empirical test data, justifying that the assumptions employed can be used to predict the future building energy performance with reasonable credibility.

5.6 Ideal Exhaust Ventilation

The first energy conservation measure considered in the model was the implementation of an ideal exhaust ventilation method. Ideal exhaust ventilation includes both the installation of a chimney to ventilate each oven, as well as adjusting any remaining exhaust canopy flow rates to the minimum allowable values outlined in ASHRAE Standard 154-2003, Ventilation for Commercial Cooking Operations [26].

Firstly, the decision of whether to implement chimney ventilation or canopy ventilation for a greenfield project is straightforward. The installation of a Type B gas vent chimney is less complicated and capital intensive than the installation of a mechanically vented exhaust system, and requires no electricity to operate.

For the case of Store A, installing each chimney would involve: creating a hole in the building's roof and installing the chimney support structure, flashing, Type B vent ductwork, and creating two holes in the sheet metal of the existing canopy. However, this type of retrofit would produce the largest decrease in the net ventilation flow rate, since there was no original chimney acting as a source of short circuit makeup air within the canopy. For Store A, switching from canopy to chimney oven ventilation, for two ovens, would markedly reduce the net ventilation mass flow rate by 68%, from 0.71 kg/s to between 0.20 and 0.25 kg/s [7] (since chimney flow rate is inversely correlated to outside temperature). In the case of Store B, which had the combined exhaust system with both a chimney and exhaust canopy, converting to chimney exhaust ventilation would only involve deactivating the exhaust canopies. Although, assuming the fan at Store B moves the same volume of air and has the same total ventilation flow rate as the fan at Store A, the original net ventilation flow rate would be less than 0.71 kg/s, since the original chimney would have reversed direction (due to building depressurization) acting as a source of short circuit makeup air. As a result, the percent decrease in the net ventilation flow rate at Store B would be smaller than the percent decrease at Store A.

Regardless, both new installations and retrofits would require a custom engineered solution for each location, since NFPA 96 (Standard for Ventilation Control and Fire Protection of Commercial Cooking Operations) requires that the maximum depressurization in a cooking area may not exceed 4.98 Pa [23]. As the enclosure air tightness is building specific, the negative pressure created by a certain total exhaust flow rate must be limited by ensuring that an adequate source of makeup air is available.

Lastly, adhering to the recommendations of ASHRAE Standard 154-2003 for any exhaust canopies remaining in operation would also decrease the net ventilation flow rate. For Store A specifically, the fryer ventilation flow rate could be reduced by 22%, considering the current volume flow rate per linear foot of hood space was 385 CFM, while the required ventilation flow rate for an unlisted hood is 300 CFM [26].

The impact of adjusting the building exhaust flow rates was assessed by simulating the building operation with the energy modeling tool. The revised energy flows during the month of January are first shown below in Figure 5.5.

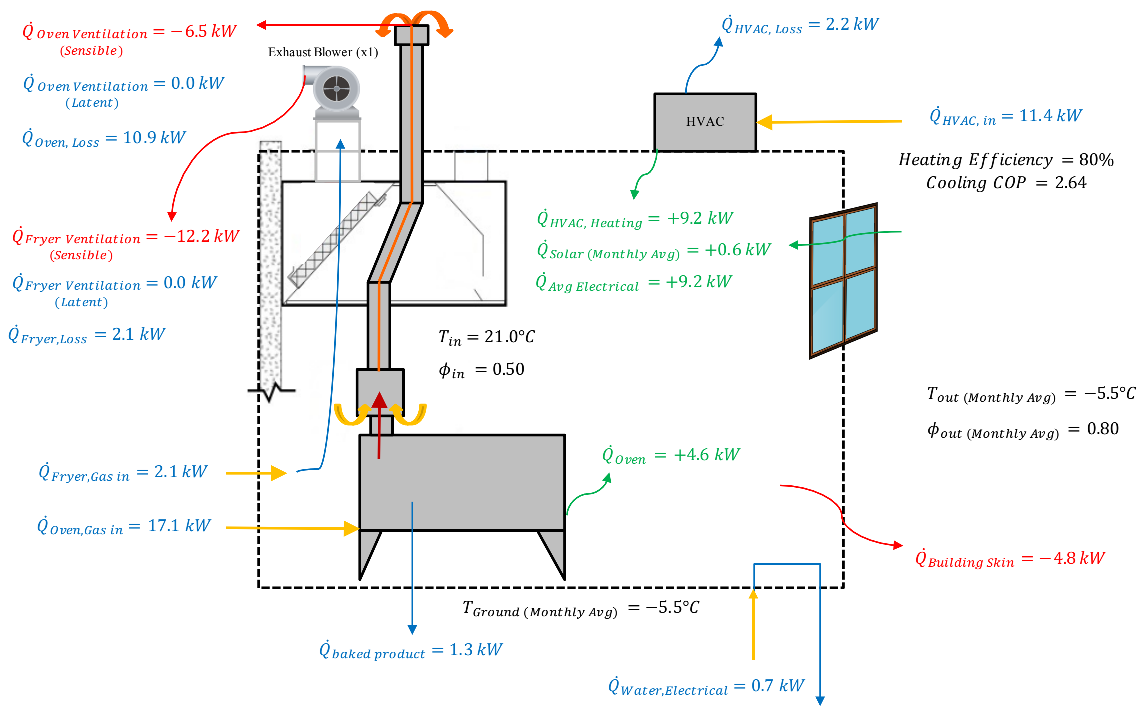

Figure 5.5: Building Energy Flow Diagram – Store A – Ideal Exhaust Ventilation

A side effect of removing the exhaust canopy is that the continuous oven door exfiltration is included as a heat gain to the room, as a part of the 4.6 kW oven gain shown above. The benefit, a decreased winter heating demand, and the cost, an increased summer cooling demand, of this side effect will be addressed in Section 5.7. The impact of this ideal exhaust ventilation system on HVAC performance, over the full year, is shown in Figure 5.6 on the following page.

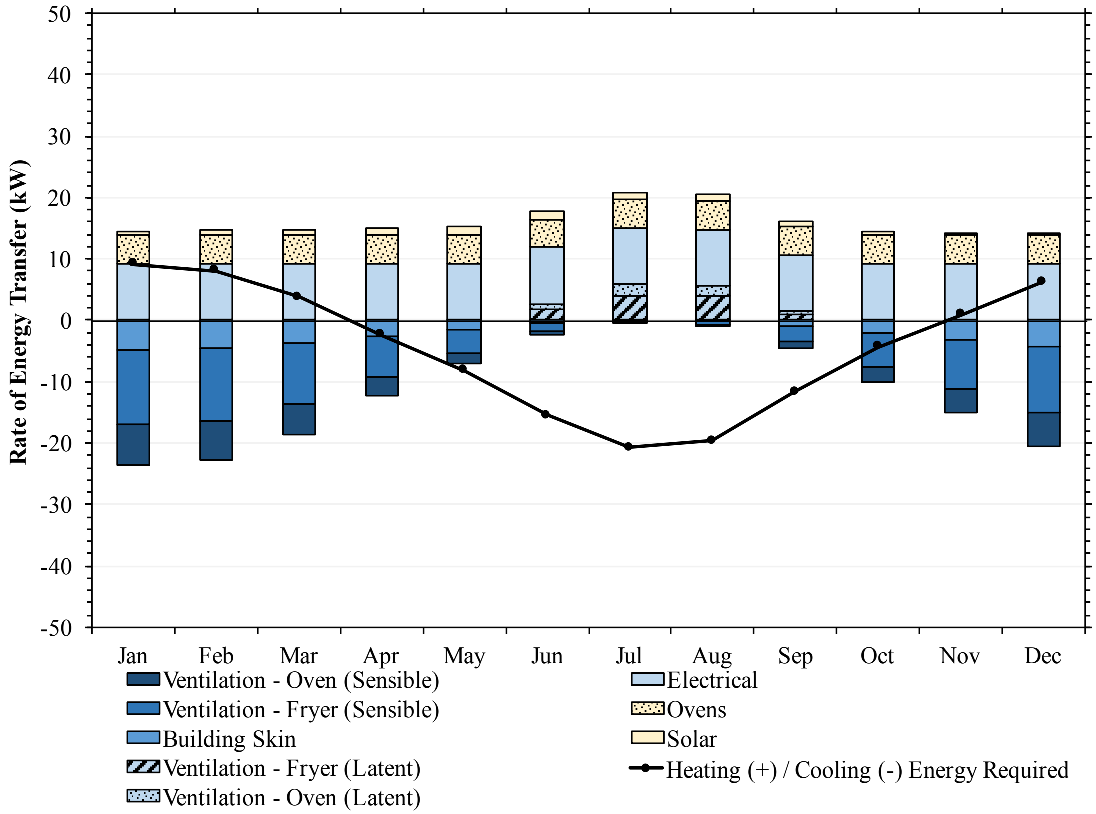

Figure 5.6: Building HVAC Energy Balance – Store A – Ideal Exhaust Ventilation

To heat and cool Store A would require 2,888 m^3 of natural gas and 23,045 kWh of electricity, resulting in a 76% reduction in the heating energy requirement, and a 24% increase in cooling energy requirement, relative to the base model. The length of the heating and cooling seasons has shifted, and the building which once required heating for seven months of the year now only requires heating for four months of the year, while the cooling season has increased from four months to seven months.

The total energy savings are shown below in Figure 5.7. The energy values have been superimposed on select column areas, to specifically identify which values have changed from one case to the next. Note that the overarching title of "TEG POWER

Solution" is only meant to indicate that the energy conservation measure is a component of the ideal TEG POWER Solution, and does not imply that exhaust gas energy recovery through the TEG POWER heat exchanger was included.

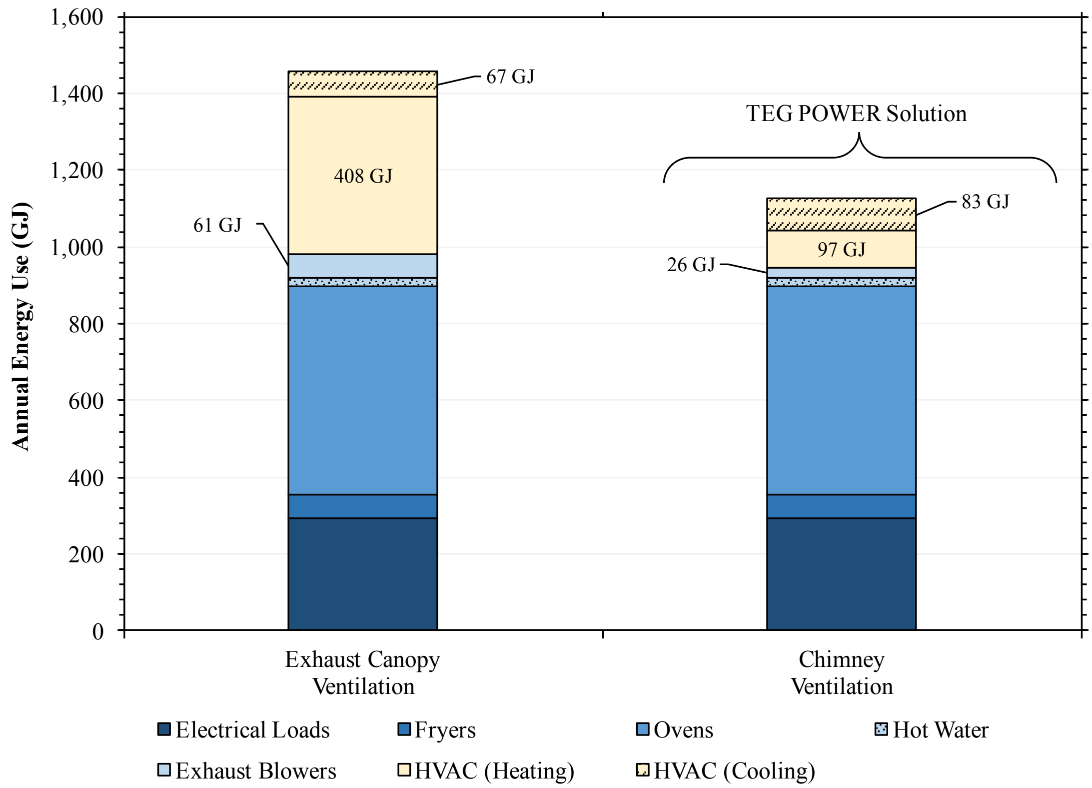

Figure 5.7: Breakdown of Building Fuel Consumption by End Use – Store A – Ideal Exhaust Ventilation

Redesigning the exhaust system could provide an annual energy savings of 22.7% (331 GJ per year). The savings would be composed of a 311 GJ (76%) and 35 GJ (57%) reduction in the HVAC heating natural gas requirement and the exhaust blower electricity requirement respectively, despite a 16 GJ (24%) increase in the electricity needed for cooling the building.

5.7 Sealing and Insulating Ovens

Sealing and insulating the ovens becomes important when stores are operated with chimneys as opposed to exhaust canopies, because there is no longer a major flow of air ventilating the space around the oven. Since the continuous oven exfiltration is allowed to vent into the room, the kitchen may reach uncomfortably high temperatures in the summer, and an extra load will be placed on the (potentially already undersized) building cooling system. A proposed method of improving the building operation to avoid this problem, is to fully seal the oven door to eliminate the exfiltration heat gain, and to surround the oven with a 2-inch fiberglass insulating cover to limit conduction heat losses through the oven walls. Through this conservation measure, the rate of energy transfer from the oven to the room would be reduced by 79%, from 4.6 kW to 1.0 kW.

These updated oven heat losses were then used as inputs in the building energy modeling tool, to evaluate the effectiveness of this energy conservation measure. Figure 5.8 displays the impact of sealing and insulating the oven on the building HVAC energy balance.

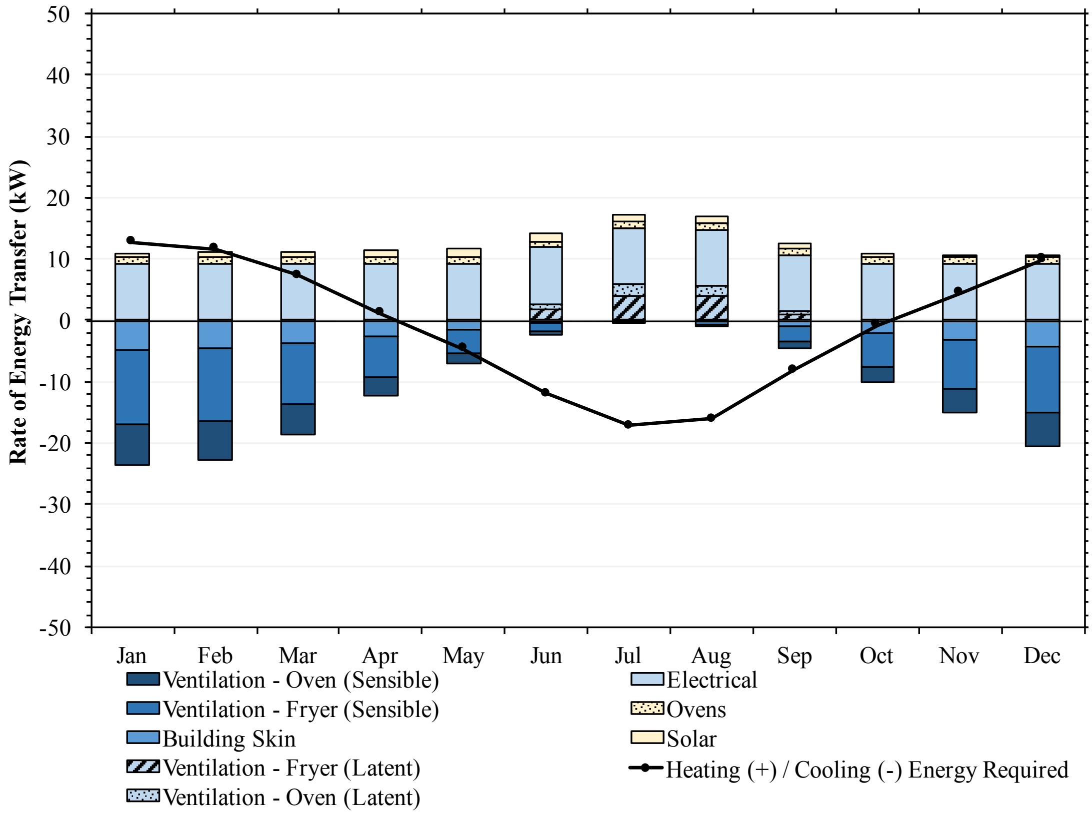

Figure 5.8: Building HVAC Energy Balance – Store A – Seal and Insulate Ovens

To heat and cool Store A, with sealed and insulated ovens, would require 4,674 m^3 of natural gas and 16,528 kWh of electricity. This equates to a 1,786 m^3 (62%) increase in the amount of natural gas needed for building heating, and a 6,518 kWh (28%) decrease in the amount of electricity required for building cooling throughout the year, relative to the ideal exhaust ventilation case.

An additional benefit of sealing and insulating the ovens is that the natural gas flow rate required to maintain the ovens at a steady state operating temperature would be reduced, dropping the thermal energy input from 17.1 kW to 13.6 kW. Over the course of a year, this amounts to a 3,377 m^3 (21%) reduction in natural gas required for oven operation.

Regardless of the relative price of electricity and natural gas, implementing this solution will always be favorable, since the reduction in oven gas consumption was more than able to offset the increased gas consumption required for heating the building during six months of the year.

Figure 5.9 displays the total energy savings that can be achieved through sealing and insulating the ovens, compared to the savings from switching to chimney based oven ventilation. Again, the energy values have been included on the chart to emphasize only the constituents that have changed.

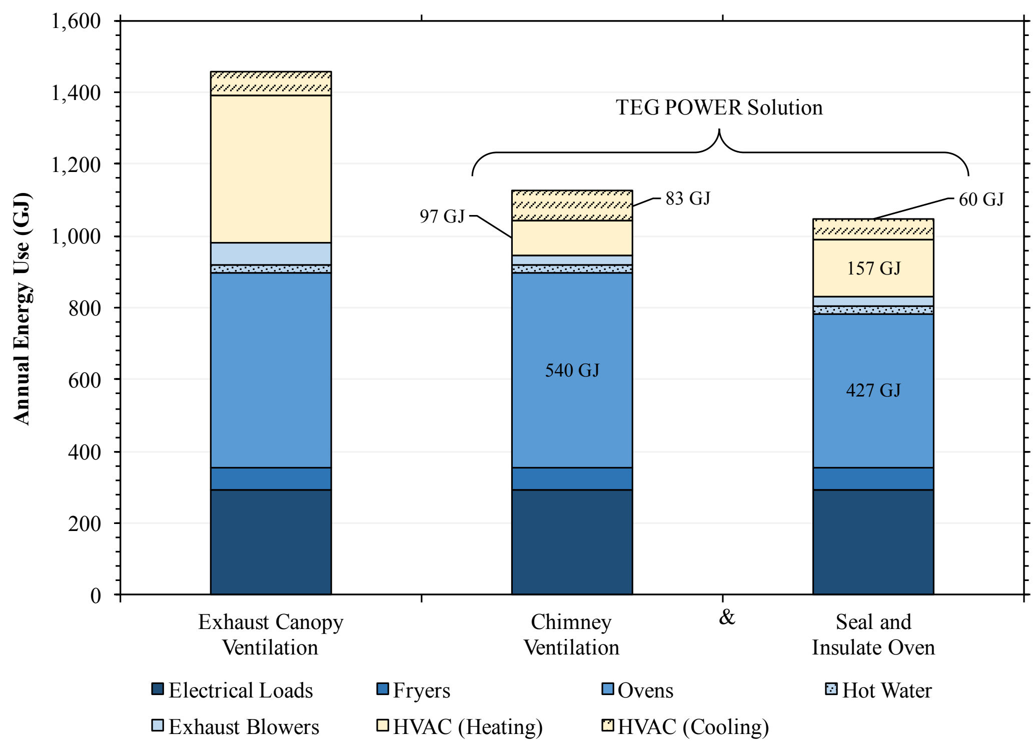

Figure 5.9: Breakdown of Building Fuel Consumption by End Use – Store A – Seal and Insulate Ovens

Limiting oven heat losses through insulation and door sealing has the potential to further reduce total energy use by 6.8% (77 GJ per year), through a 23 GJ (28%) reduction in the electricity required for building cooling and a 113 GJ (21%) reduction in natural gas required for continuous oven operation, relative to the case of chimney ventilation. Although an additional 60 GJ (62% increase) of natural gas would be necessary to heat the building in the winter, it is offset by the energy savings from oven operation. Additionally, this would create a more comfortable working environment for the restaurant staff.

5.8 Smart Oven Operation

The third operational change that can be implemented is “Smart Oven Operation”, which involves shutting all ovens off during the night, and reheating them to operating temperature in the morning before cooking commences. The main benefit of this practice would be a reduction in oven gas consumption, along with a minute reduction in the building heating and cooling energy requirements. This section quantifies these benefits using the building energy modeling tool, to simulate store operation under the new operating schedule.

Although standard operating procedures could be modified to have store personnel shut off and turn on the ovens, the large thermal mass of the baking stone creates settling times in the range of 95 to 110 minutes. Turning off the oven, and sealing the exhaust vent remotely with a mechanical damper, would limit the ovens rate of cooling overnight by eliminating heat loss via mass transfer. Since the baking stone would retain most of its thermal energy throughout the night, the settling time would be drastically reduced, and the oven could be started automatically just before cooking begins at 9:30 am. Experimental data and detailed calculations for oven settling time, transient cool down temperature profiles, and the reduction in oven natural gas consumption justifying these claims may be viewed in Appendix B, for a variety of oven arrangements and operating schedules.

The case of two independent ovens that are turned off and sealed remotely during non-operating hours was adopted, to achieve the maximum reduction in natural gas use, while still maintaining workplace ergonomics by having the two cooking decks at chest level.

Limiting the oven operation to the establishments cooking hours, therefore shortening the oven operating timespan by 29%, would not only reduce the oven natural gas consumption by 29%, but would also reduce the cost associated with conditioning the space. As the chimney would only operate in conjunction with the appliance, the oven ventilation sensible heat loss and latent heat gains would also be reduced by 29%. The impact of Smart Oven Operation on the HVAC energy balance can be seen below in Figure 5.10.

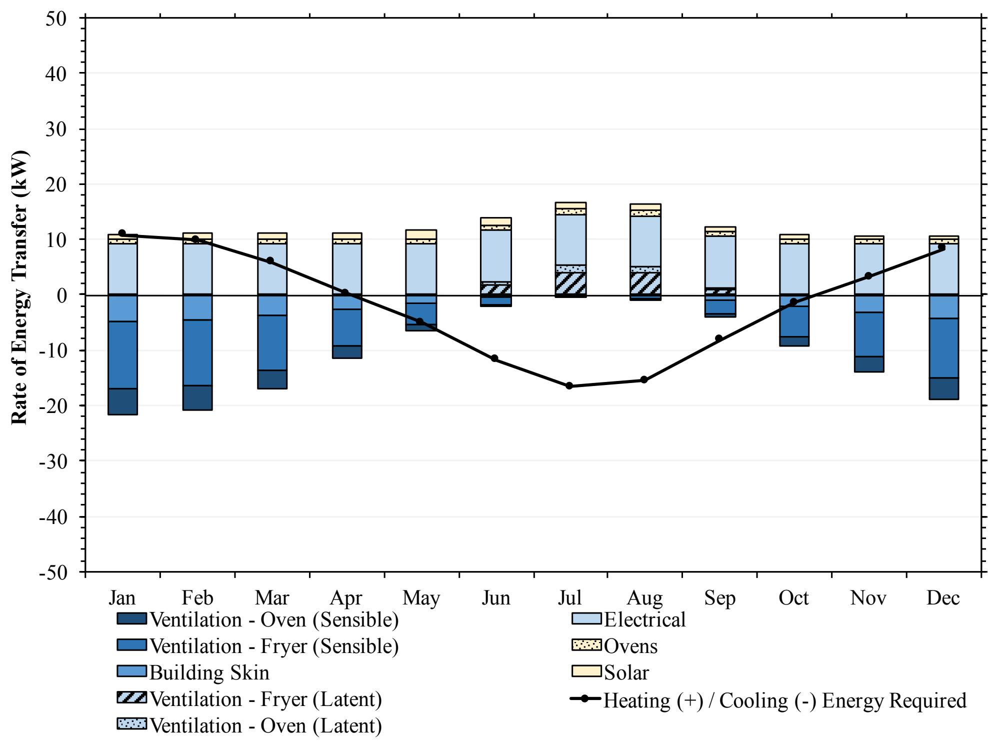

Figure 5.10: Building HVAC Energy Balance – Store A – Smart Oven Operation

Operating the HVAC system for one year would require 4,036 m^3 of natural gas and 16,526 kWh of electricity, corresponding to a 638 m^3 (14%) reduction in the amount of natural gas required for building heating, with no measureable impact on cooling, relative to case of a sealed and insulated oven. The impact of Smart Oven Operation in the context of the full building energy balance can be seen in Figure 5.11.

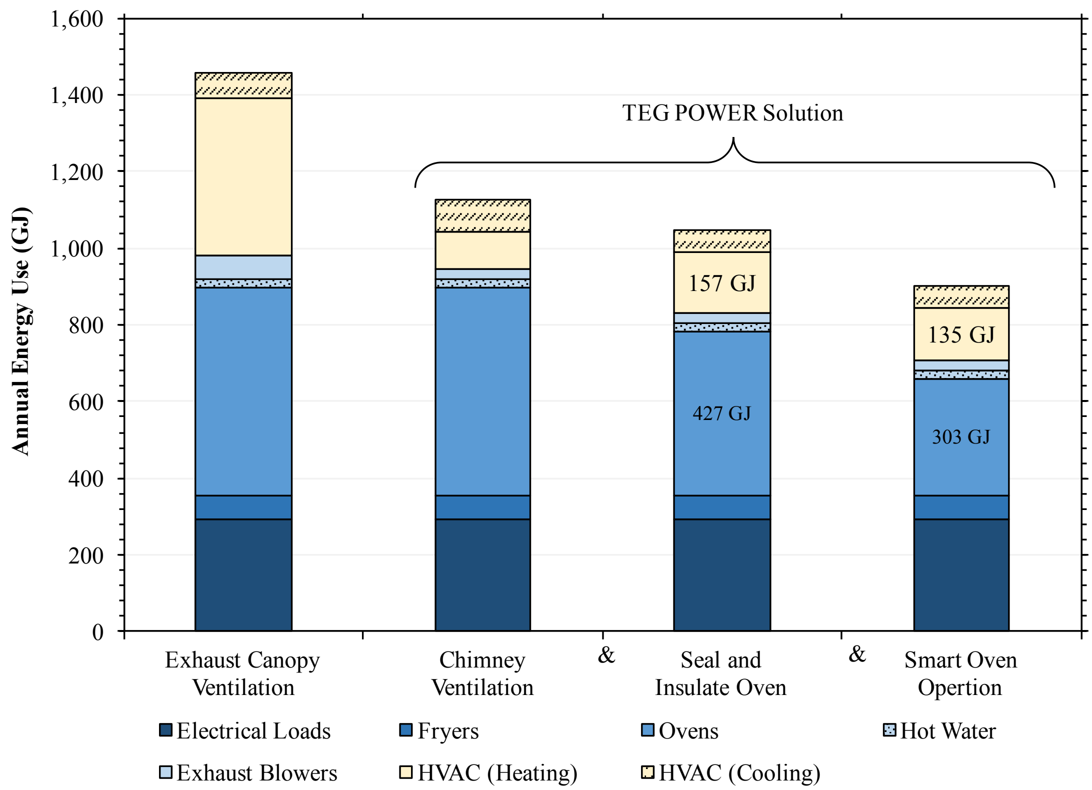

Figure 5.11: Breakdown of Building Fuel Consumption by End Use – Store A – Smart Oven Operation

Smart Oven Operation has the potential to create 146 GJ in annual energy savings (13.9%), through a 124 GJ (29%) reduction in oven operating energy and a 22 GJ (14%) reduction in the energy required to heat the building, relative to the case of sealing and insulating the ovens.

5.9 Energy Harvesting

The final, and most significant proposition, is the inclusion of energy harvesting, to recover and repurpose the thermal energy of the oven exhaust. A TEG POWER system on each oven was considered.

The TEG POWER system would impact the building energy balance in several ways. At a steady state the TEG POWER system was capable of recovering 1.95 kW per oven from the exhaust stream continuously while the oven was operating, for a total of 3.90 kW for a system on two ovens. Firstly, this energy would go towards heating the domestic hot water of the store, via the solar thermal hot water tank. Assuming the restaurant uses 345 L of water each day, equivalent to an energy input of 61 MJ, the average rate of energy use over the operating day would be 1.0 kW. The remaining 2.9 kW could then be used for space heating the store in the winter time, or preheating the intake air of the oven when space heating is not required. Prioritizing space heating over preheating essentially accomplishes both purposes, since the heated room air eventually acts as the oven intake air. The TEG POWER system has also been proven to reduce the chimney mass flow rate, through a combination of the air-to-liquid heat exchanger, flow restrictions in the dilution air path, and exhaust throttling [7]. The chimney mass flow rate can be reduced by 34% from 0.12 kg/s to 0.08 kg/s in the winter, and by 42% from 0.10 kg/s to 0.06 kg/s in the summer [7].

The energy flow diagram shown below in Figure 5.12 illustrates the impact of the energy harvesting on the building HVAC system, for a -5.5°C January day. Note that the hot water and space heating values are slightly different in the diagram than stated in the paragraph above, since the diagram displays the average rate of energy transfer over the entire day, as opposed to the rate of energy transfer over the operating hours.

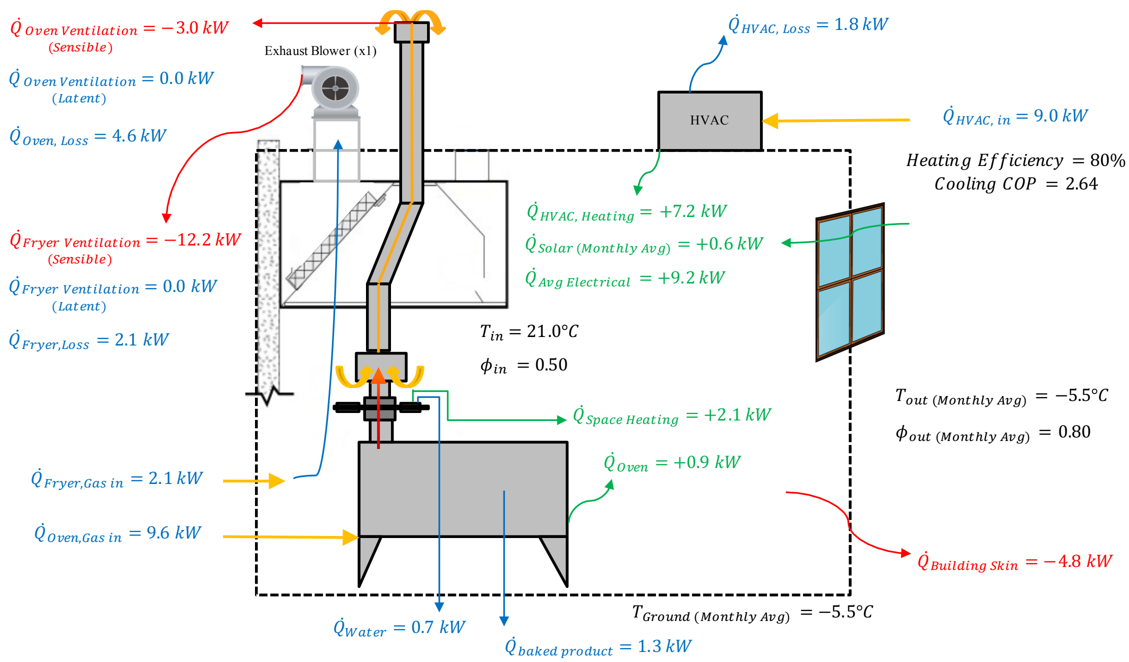

Figure 5.12: Building Energy Flow Diagram – Store A – Energy Harvesting – Space Heating

The thermodynamic efficiency of the ovens has substantially increased in comparison to the base case of Section 5.5. Recall, the two ovens originally required an input of 17.1 kW, with a resulting thermodynamic efficiency of 17.7% in the winter and 7.5% in the summer. The simulation results with energy harvesting showed that the thermodynamic efficiency of the oven during the winter would be 52%; with 13%, 7% and 31% of the input energy transferred to the baked product, hot water and room respectively. Since the TEG POWER system has the potential to switch between space heating and oven preheating based on demand, Figure 5.13 below illustrates the building energy flows for a typical 20.9°C July day.

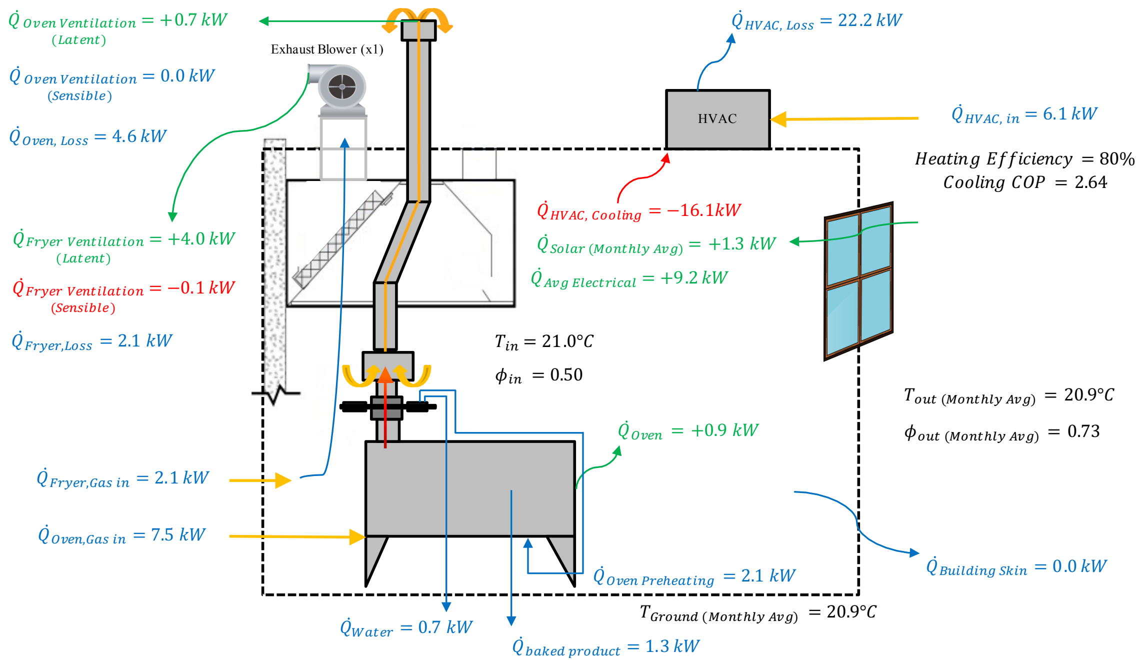

Figure 5.13: Building Energy Flow Diagram – Store A – Energy Harvesting– Oven Preheating

As a result of the TEG POWER preheating system, the two ovens only required an average input of 7.5 kW. From the natural gas input, 17% and 9% of the energy was transferred to the baked product and water respectively, leading to an oven thermodynamic efficiency of 26%.

The performance of the buildings HVAC system was once again simulated throughout the year using the building energy modeling tool. The results are shown below in Figure 5.14, with an additional white bar representing the space heating contributions of the TEG POWER system.

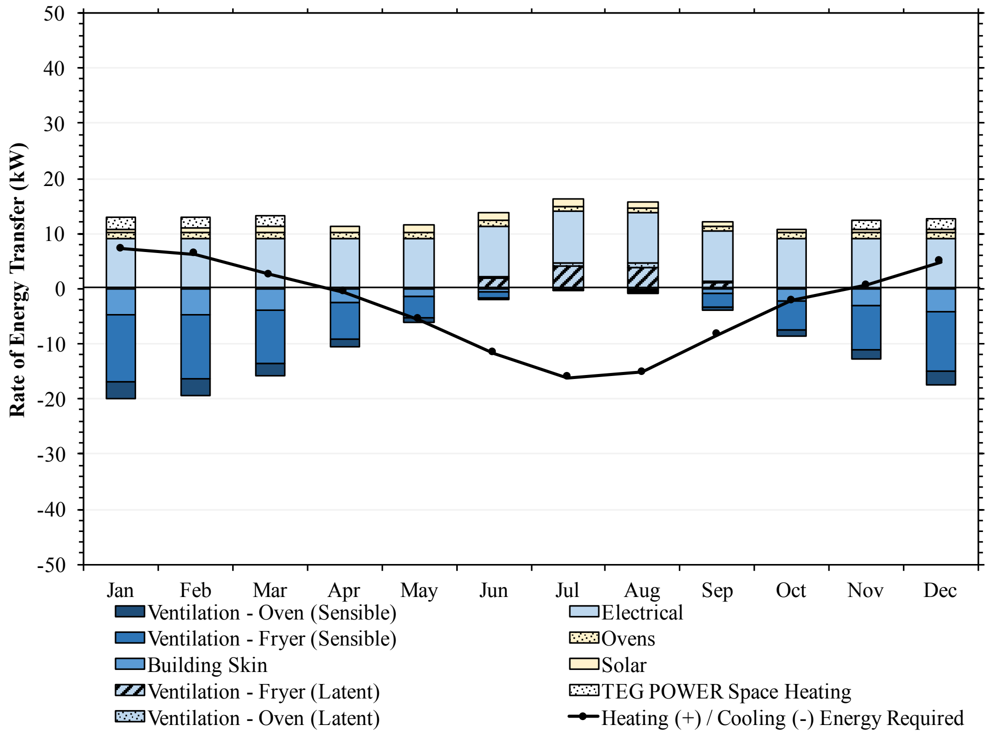

Figure 5.14: Building HVAC Energy Balance – Store A – Energy Harvesting

Operating the HVAC system for one year would require 2,305 m^3 of natural gas and 16,900 kWh of electricity, corresponding to a heating energy reduction of 1,731 m^3 (43%), and a cooling energy increase of 374 kWh (2%), relative to the case of Smart Oven Operation. The reduction in the heating requirement can be attributed to the space heating provided by the TEG POWER system, as well as the ~34% decrease in the chimney mass flow rate during the winter, which reduced the building ventilation losses via mass transfer. The increase in the cooling demand is attributed to the ~42% decrease in the chimney mass flow rate during the cooling season, coupled with the relative magnitudes of the sensible ventilation losses, and the latent heat gains. Table 5.2 helps to explain these observations, by comparing the results of Figure 5.8 and Figure 5.14 on a monthly basis. During the winter months of January, February, March, April, November and December, the heating requirements were reduced as stated previously. In the summer months of June, July and August, the cooling load was reduced by 293 kWh. During these months, the latent heat gains from ventilation were 740% greater than the ventilation sensible heat losses, therefore reducing the ventilation flow rate had the net effect of lowering the building heat gains and lowering the cooling load. In the transition seasons, encompassing April, May, September and October, the cooling load actually increased by 667 kWh. All four of these months required building cooling, however, the latent ventilation heat gains were either small to negligible in comparison to the sensible ventilation heat losses. Therefore, reducing the ventilation flow rate reduced the effect of ventilation cooling during months where cooling was required, and had a negative effect on the HVAC system performance.

Table 5.2: Effect of Energy Harvesting on the Heating and Cooling Demand

Month	Smart Oven Operation		Energy Harvesting			
	Heating (m^3 CH_4/Month)	Cooling (kWh_e/Month)	Heating (m^3 CH_4/Month)	Difference (m^3 CH_4/Month)	Cooling (kWh_e/Month)	Difference (kWh_e/Month)
Jan	1122	0	757	-364	0	0
Feb	925	0	601	-324	0	0
Mar	640	0	308	-332	0	0
Apr	107	0	0	-107	353	353
May	0	1430	0	0	1568	138
Jun	0	3211	0	0	3189	-22
Jul	0	4682	0	0	4535	-146
Aug	0	4384	0	0	4259	-125
Sep	0	2253	0	0	2302	49
Oct	0	566	0	0	693	127
Nov	372	0	113	-259	0	0
Dec	871	0	525	-345	0	0
Total Change in Heating and Cooling Demand:				-1731		374

The impact of energy harvesting in the context of the full building energy balance can be seen in Figure 5.15.

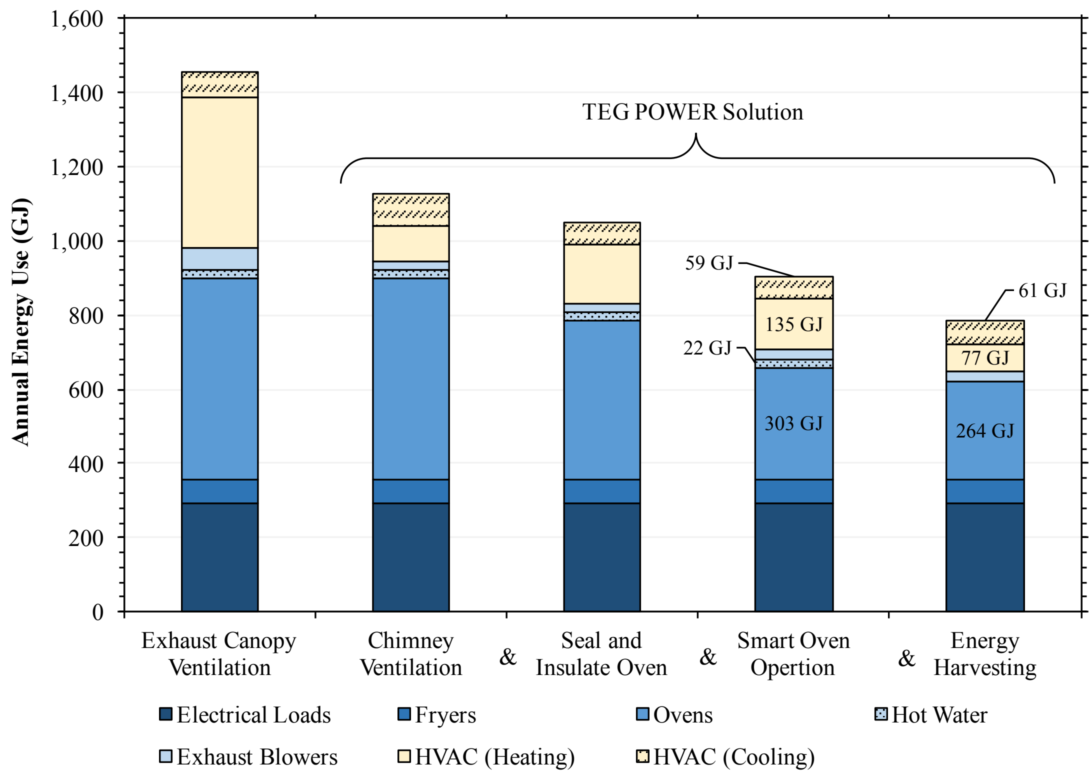

Figure 5.15: Breakdown of Building Fuel Consumption by End Use – Store A – TEG POWER Solution

Commissioning a TEG POWER system on each oven in Store A has the potential to further reduce total energy use by 118 GJ (13.1%) through a 39 GJ (13%) reduction in oven operating energy, a 56 GJ (29%) reduction in net HVAC energy, and by eliminating the 22 GJ of energy required to provide hot water.

5.10 Comparison of Store Operating Configurations

The results of Section 5.5 through Section 5.9 have been summarized in the following tables.

Table 5.3 summarizes the total energy use, in cubic meters of natural gas and in kilowatt-hours of electricity, required to operate Store A under the five different operating configurations. The equivalent CO_2 reduction has also been calculated for each operational change, based on the Ontario Planning Outlook 2016 report from the Independent Electricity System Operator (IESO) [51], and emissions statistics from the U.S. Energy Information Administration [52]. The equivalent carbon dioxide emissions from electricity production and the complete combustion of natural gas are 0.052 $kgCO_2e/kWh$ and 1.88 $kgCO_2e/m^3$ respectively [51], [52].

Finally, Table 5.4 summarizes the energy breakdown of each operational change and the associated yearly energy savings, in gigajoules, for the four operational changes considered.

In summary, the result of implementing all aspects of the TEG POWER Solution at Store A is a 14% or 17,653 kWh (64 GJ) reduction in electricity, and a 60% or 18,115 m^3 (608 GJ) reduction in natural gas, over one year. Total energy savings amount to 671 GJ, or 46% reduction, when compared to the base case.

Table 5.3: CO_2 Emissions from Different Operating Configurations – Store A

Contributors to Total Energy Use	Operating Configuration				
	Exhaust Canopy Ventilation	Chimney Ventilation	Seal and Insulate Oven	Smart Oven Operation	Energy Harvesting
Electricity (kWh)					
Electrical Loads	80,789	80,789	80,789	80,789	80,789
Building Cooling	18,570	23,045	16,528	16,526	16,900
Exhaust Blowers	16,943	7,145	7,145	7,145	7,145
Hot Water	6,185	6,185	6,185	6,185	0
Total Electricity	122,487	117,164	110,646	110,644	104,834
CO_2e Emissions (tonnes)	6.3	6.1	5.7	5.7	5.4
CO_2e Reduction (tonnes)	-	0.3	0.3	-	0.3
Natural Gas (m^3)					
Ovens	16,136	16,136	12,759	9,038	7,870
Building Heating	12,194	2,888	4,674	4,036	2,305
Fryers	1,971	1,971	1,971	1,971	1,971
Total Natural Gas	30,301	20,995	19,404	15,045	12,146
CO_2e Emissions (tonnes)	56.8	39.4	36.4	28.2	22.8
CO_2e Reduction (tonnes)	-	17.5	3.0	8.2	5.4

Table 5.4: Energy Consumption of Different Operating Configurations – Store A

Contributors to Total Energy Use	Operating Configuration				
	Exhaust Canopy Ventilation	Chimney Ventilation	Seal and Insulate Oven	Smart Oven Operation	Energy Harvesting
Electrical Loads [GJ]	291	291	291	291	291
Fryers [GJ]	66	66	66	66	66
Ovens [GJ]	540	540	427	303	264
Hot Water [GJ]	22	22	22	22	0
Exhaust Blowers [GJ]	61	26	26	26	26
HVAC (Heating) [GJ]	408	97	157	135	77
HVAC (Cooling) [GJ]	67	83	59	59	61
Total Restaurant Energy Use [GJ]	1,456	1125	1048	902	784
Additional Savings [GJ]	-	331	77	146	118
	-	22.7%	6.8%	13.9%	13.1%

5.11 Alternative Technology Implementation Plan

In this section, the energy modeling tool was used to evaluate the results of an alternative technology implementation plan, one where an exhaust gas energy harvesting system is commissioned on two ovens operating with exhaust canopy ventilation. The purpose is to contrast the maximum energy savings that may be achieved with the ideal TEG POWER Solution, against the solution that is permitted by current regulations. Current regulation does not permit chimney based oven ventilation in conjunction with waste heat recovery, nor does it permit a remotely operated exhaust damper. Figure 5.16 displays the results of the building energy balance, with the addition of space heating being the only departure from the base case.

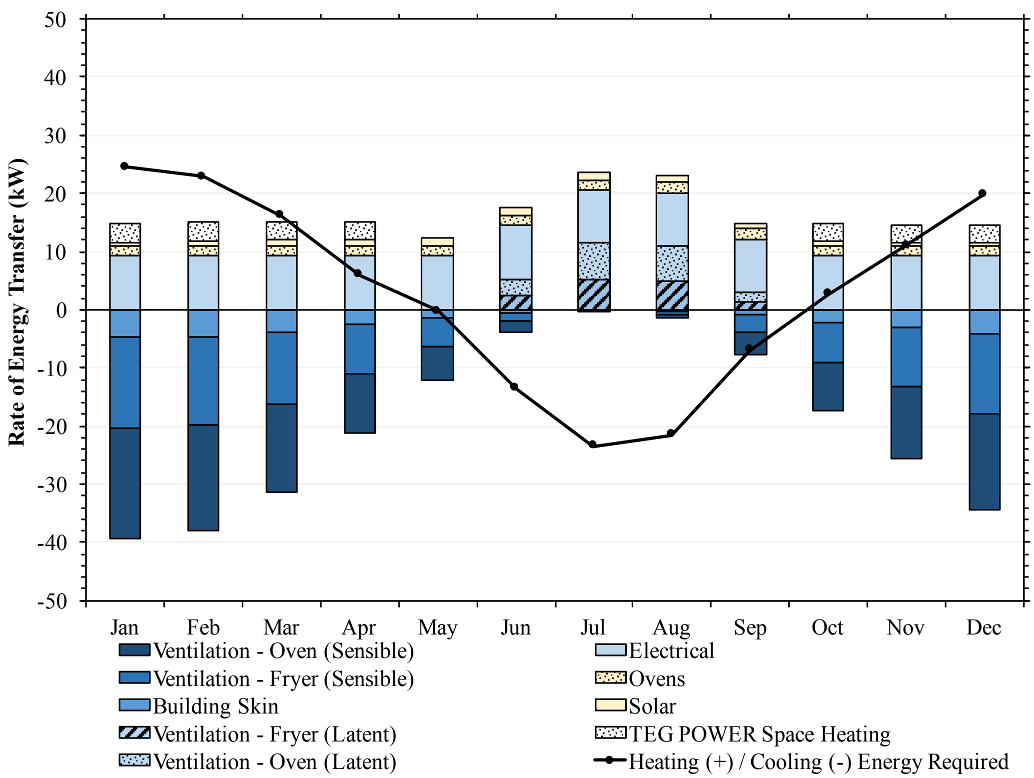

Figure 5.16: Building HVAC Energy Balance – Store A – Energy Harvesting with Canopy

Operating the HVAC system for one year would require 10,045 m^3 of natural gas and 18,570 kWh of electricity. The natural gas consumption of the HVAC system was reduced by 18% in relation to the base case due to space heating provided, while the building cooling requirements remained unchanged. The impact of energy harvesting on the full building energy balance is shown in Figure 5.17 below.

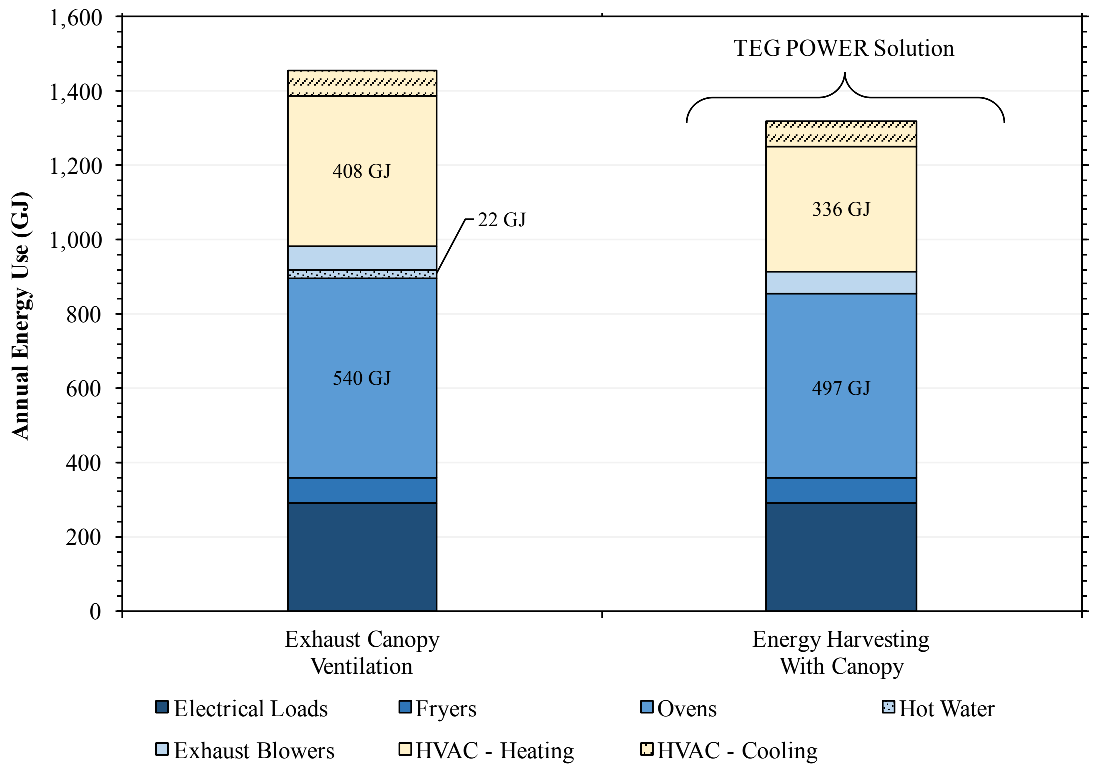

Figure 5.17: Breakdown of Building Fuel Consumption by End Use – Store A – Energy Harvesting with Canopy

In addition, Table 5.5 and Table 5.6 summarize the breakdown of the total building energy use, along with the equivalent CO_2 reduction.

Table 5.5: CO_2 Reduction – Store A – Energy Harvesting with Canopy

Contributors to Total Energy Use	Operating Configuration	
	Exhaust Canopy Ventilation	Energy Harvesting With Canopy
Electricity (kWh)		
Electrical Loads	80,789	80,789
Building Cooling	18,570	18,570
Exhaust Blowers	16,943	16,943
Hot Water	6,185	0
Total Electricity	122,487	116,302
CO_2e Emissions (tonnes)	6.3	6.0
CO_2e Reduction (tonnes)	-	0.3
Natural Gas (m^3)		
Ovens	16,136	14,848
Building Heating	12,194	10,045
Fryers	1,971	1,971
Total Natural Gas	30,301	26,864
CO_2e Emissions (tonnes)	56.8	50.4
CO_2e Reduction (tonnes)	-	6.4

Table 5.6: Energy Reduction – Store A – Energy Harvesting with Canopy

Contributors to Total Energy Use	Operating Configuration	
	Exhaust Canopy Ventilation	Energy Harvesting With Canopy
Electrical Loads [GJ]	291	291
Fryers [GJ]	66	66
Ovens [GJ]	540	497
Hot Water [GJ]	22	0
Exhaust Blowers [GJ]	61	61
HVAC (Heating) [GJ]	408	336
HVAC (Cooling) [GJ]	67	67
Total Restaurant Energy Use [GJ]	1,456	1,318
Additional Savings [GJ]	-	137
	-	9.4%

Only implementing the energy harvesting component of the TEG POWER Solution at Store A has the potential to reduce electricity and natural gas consumption by 5% (6,185 kWh) and 11% (3,437 m^3) respectively. This is equivalent to a 137 GJ, or 9.4%, reduction in total energy consumption, when compared against the base case model.

Without changes made to current regulations to keep pace with technology advancements, only 20% of the total energy savings potential may be realized.

5.12 Store B Case Study

This section concisely presents the results of the case study on Store B, showing the effect of the same four energy conservation measures.

Several of the common assumptions differed for the case of Store B. They are listed below:

- The HVAC system maximum heating and cooling capacity was 87.0 kW and 51.9 kW respectively [47]
- Every day follows the same operational schedule, with employees arriving to the store at 10:00 am, at which time the oven is set to operating temperature (288°C, 550°F), and the fryer and associated ventilation system is switched on. The employees leave the restaurant at 1:00 am the next day, and the oven is set to standby temperature (149°C, 300°F), and the fryer and associated ventilation system is switched off. The weighted average closing time of 1:00 am was used to account for the differing hours of operation between weekends and weekdays. The 10 statutory holidays observed in Ontario were not considered.
- Cooking begins at 10:00 am, one hour before the store opens
- 150 baked products are cooked every day
- The restaurant uses 345 L of domestic hot water every day (The same as Store A)

Figure 5.18 and Figure 5.19 on the following page present the impact of the complete TEG POWER Solution on the HVAC energy balance of Store B.

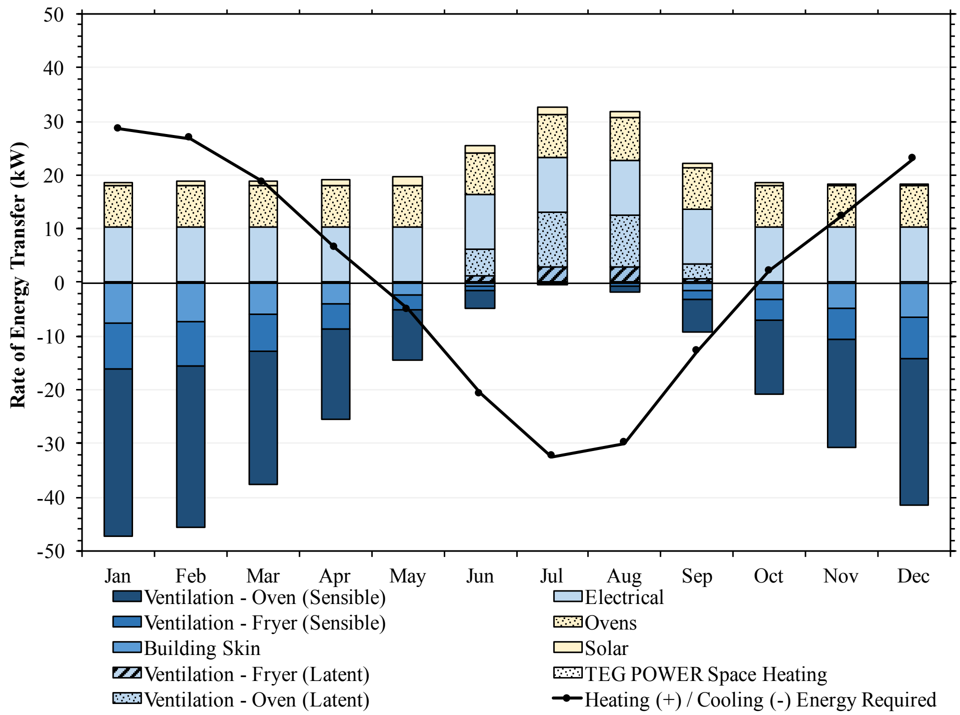

Figure 5.18: Building HVAC Energy Balance – Store B – Baseline Conditions

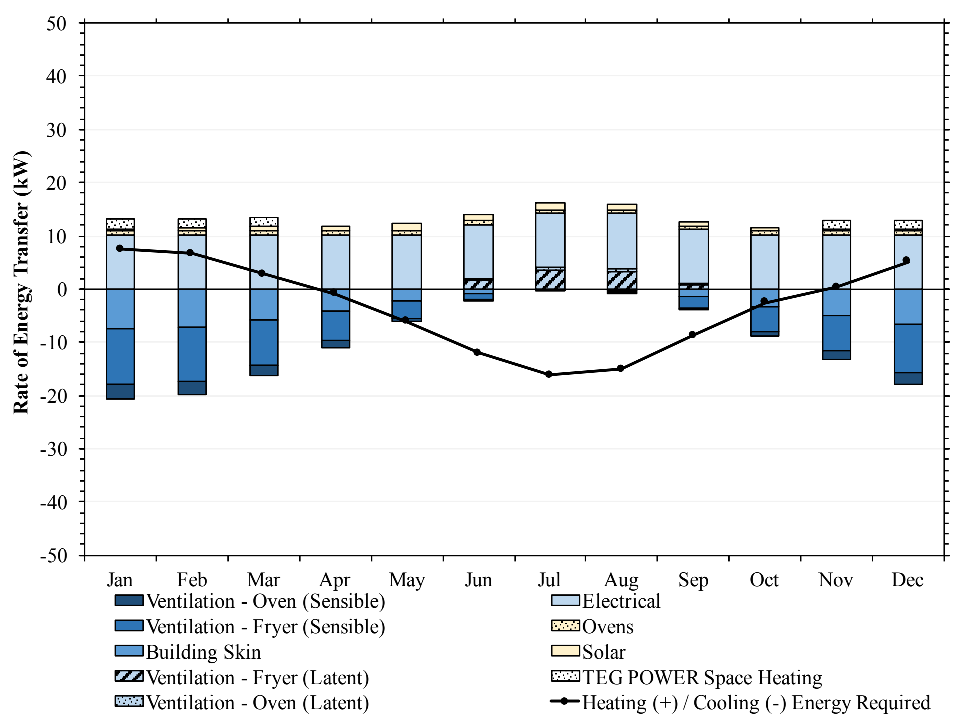

Figure 5.19: Building HVAC Energy Balance – Store B – Energy Harvesting

With the complete TEG POWER Solution in place, operating the HVAC system for one year would require 2,363 m^3 of natural gas and 17,111 kWh of electricity. This corresponds to a 9,126 m^3 (79%) reduction in natural gas and a 10,802 kWh (39%) reduction in electricity for heating and cooling the building respectively, when compared to the base case.

The results of the base case model were also verified against the corresponding utility bills collected from Store B. Table 5.7 below summarizes the comparison of the model outputs against the utility measurements. The model was able to predict the base case natural gas and electricity consumption with a ± 7% error.

Table 5.7: Comparison of Building Energy Model to Utility Data – Store B – Baseline Conditions

Utility	Model	Utility Bills	% Error
Natural Gas (m^3)	26,872	25,194	7%
Electricity (kWh)	139,596	142,429	-2%

Table 5.8 and Table 5.9 on the following pages report the energy savings from each separate operational change independently. Figure 5.20 on page 130 presents a graphical depiction of these total energy savings.

Table 5.8: Energy Consumption of Different Operating Configurations – Store B

Contributors to Total Energy Use	Operating Configuration				
	Exhaust Canopy Ventilation	Chimney Ventilation	Seal and Insulate Oven	Smart Oven Operation	Energy Harvesting
Electricity (kWh)					
Electrical Loads	89,575	89,575	89,575	89,575	89,575
Building Cooling	27,913	21,911	16,615	17,022	17,111
Exhaust Blowers	15,923	6,124	6,124	6,124	6,124
Hot Water	6,185	6,185	6,185	6,185	0
Total Electricity	139,596	123,796	118,499	118,907	112,810
CO_2e Emissions (tonnes)	7.2	6.4	6.1	6.2	5.8
CO_2e Reduction (tonnes)	-	0.8	0.3	-	0.3
Natural Gas (m^3)					
Ovens	13,412	13,412	10,694	7,974	7,017
Building Heating	11,489	3,079	4,575	3,789	2,363
Fryers	1,971	1,971	1,971	1,971	1,971
Total Natural Gas	26,872	18,462	17,240	13,734	11,350
CO_2e Emissions (tonnes)	50.4	34.6	32.3	25.8	21.3
CO_2e Reduction (tonnes)	-	15.8	2.3	6.6	4.5

Table 5.9: CO_2 Emissions from Different Operating Configurations – Store B

Contributors to Total Energy Use	Operating Configuration				
	Exhaust Canopy Ventilation	Chimney Ventilation	Seal and Insulate Oven	Smart Oven Operation	Energy Harvesting
Electrical Loads [GJ]	322	322	322	322	322
Fryers [GJ]	66	66	66	66	66
Ovens [GJ]	449	449	358	267	235
Hot Water [GJ]	22	22	22	22	0
Exhaust Blowers [GJ]	57	22	22	22	22
HVAC (Heating) [GJ]	385	103	153	127	79
HVAC (Cooling) [GJ]	100	79	60	61	62
Total Restaurant Energy Cost [GJ]	1,403	1,064	1,004	888	786
Additional Savings [GJ]	-	339	60	116	102
	-	24.1%	5.6%	11.5%	11.5%

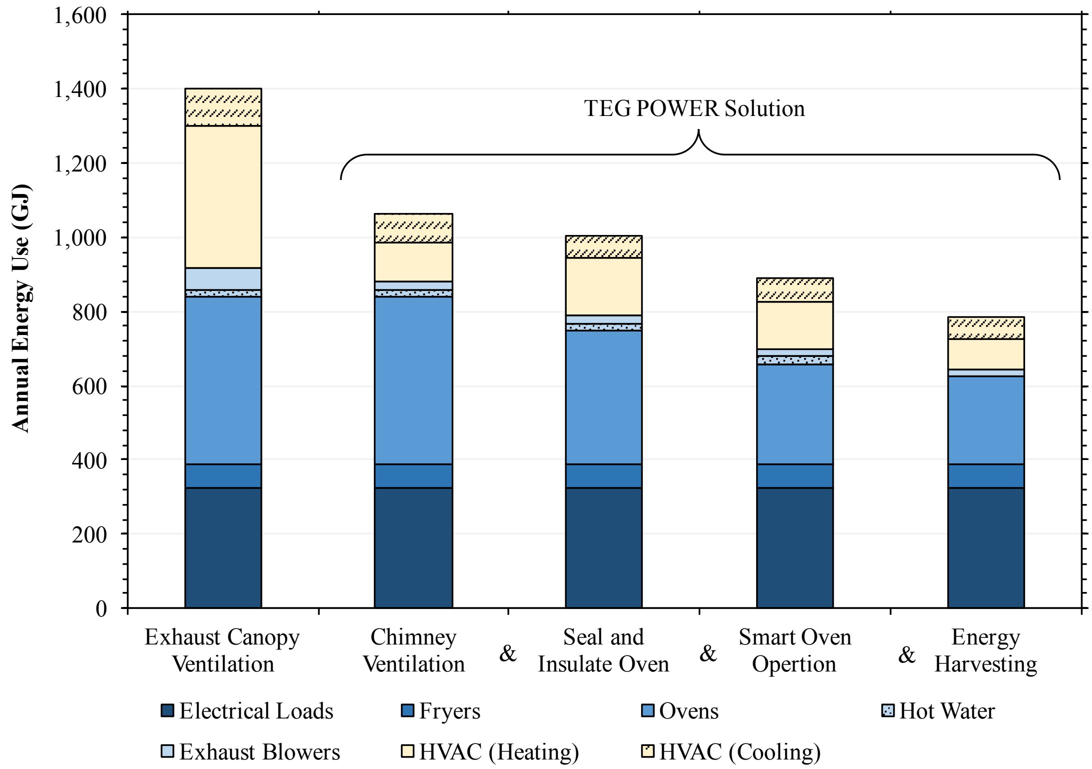

Figure 5.20: Breakdown of Building Fuel Consumption by End Use – Store B – TEG POWER Solution

Implementing the TEG POWER Solution at Store B will create a 19% or 26,785 kWh (96 GJ) reduction in electricity, and a 58% or 15,521 m^3 (520 GJ) reduction in natural gas, over one year. Total energy savings amount to 616 GJ, or 44% reduction, when compared to the base case.

Chapter 6
Conclusions and Recommendations

6.1 Conclusions

In this study, a mathematical modeling tool was developed that is capable of predicting the energy consumption of a building HVAC system. The tool provides a simple and rapid means of determining the total annual energy savings that can be realized by a commercial building, that is subject to operational changes and energy conservation measures. The need for such a tool was evident, based on the initial investigation of commercial baking operations, in order to identify and evaluate methods of reconciling the excessive energy demand and the wasted energy supply.

The analysis tool developed was based on a first principles modeling approach using the fundamentals of thermodynamics, heat and mass transfer. The building was modeled using a quasi-steady state energy balance, incorporating the effects of heat transfer through the building skin, ventilation, oven heat gains, heat generated by electricity consumption, solar energy transfer and space heating provided through exhaust gas energy recovery from the appliances.

Four separate experimental facilities were used, for the purpose of providing inputs to the building energy model case studies, and for a means of model validation.

Two separate commercial baking operations were monitored, in order to investigate the effects of different appliance ventilation methods on the building energy balance. The oven located at the McMaster TMRL was also used to experimentally quantify two specific inputs to the energy model; the rate of heat loss from oven door opening, and the rate of energy recovery from the appliance exhaust stream. The validation cases of Store A, which illustrated the building energy flows for the full range of outside temperatures, showed that the energy balance had an average error of 3.8%, with a maximum error 7.1% observed for the case of maximum building cooling. The model was also evaluated for the ability to predict HVAC energy requirements for buildings with different appliance exhaust configurations. When the building heating data sets, for the chimney, the exhaust canopy and the combined exhaust system cases were compared against the associated model outputs, the average absolute error was 4.0 m^3 of natural gas, with a standard deviation of 2.7 m^3. This translated to an average relative error of 19%, with a standard deviation of 26%. The validation proved that the model was in good agreement with experimental results.

A case study of Store A and Store B was presented, showcasing the modeling tools ability to quantify the effects of implementing four potential energy conservation measures:

- A base case model of Store A was first established, which was able to predict the buildings total annual natural gas and electricity requirements with a 3% and 7% error respectively.

- Secondly, methods of ideal exhaust ventilation were investigated, and were shown to decrease the annual natural gas heating requirement by 311 GJ (76%) and decrease ventilation system electricity requirement by 35 GJ (57%), despite increasing the electricity required for cooling by 16 GJ (24%), relative to the base case.
- Thirdly, the act of sealing the oven door and insulating the oven structure was shown to decrease the cooling electricity requirement by 23 GJ (28%), decrease the natural gas required for continuous oven operation by 113 GJ (21%), while increasing the building heating requirement by 60 GJ (62%), relative to the case of ideal exhaust ventilation.
- Next, the possibility of fully sealing the exhaust vent and turning off the oven at night proved to decrease the natural gas consumption of the oven and HVAC system by 124 GJ (29%) and 22 GJ (14%) respectively, relative to the sealed and insulated case.
- Lastly, the inclusion of exhaust gas energy harvesting showed potential to reduce the energy required for oven operation by 39 GJ (13%), reduce net HVAC energy by 56 GJ (29%), and eliminate the 22 GJ of energy required to provide hot water.

Overall, implementing all four energy conservation measures at Store A would create a 14% or 17,653 kWh (64 GJ) reduction in electricity, and a 60% or 18,155 m^3 (608 GJ) reduction in natural gas, over one year.

The modeling tool was also used to complete the exact same simulation for Store B. The base case showed excellent agreement with the annual natural gas and electricity measurements made by the utility providers, with only a 7% error. Implementing the same four energy conservation measures would create a 19% or 26,785 kWh (96 GJ) reduction in electricity, and a 58% or 15,521 m^3 (520 GJ) reduction in natural gas annually.

Assuming the results of this study are implemented at 2,000 similar establishments across Ontario, there is a potential to reduce electricity consumption by 44.4 million kWh, natural gas consumption by 33.7 million cubic meters and CO_2 emissions by 65,500 metric tonnes per year.

6.2 Recommendations for Future Work

The simplified building energy modeling tool presented in this thesis, was originally developed as a means of predicting the total energy savings that could be achieved by commissioning the TEG POWER system at a restaurant. Although the modeling methodologies can most certainly be applied to predict and analyze the energy consumption of any commercial building, the code was built in Microsoft Excel, to specifically produce the outputs required to complete the case studies of the two restaurants. Future work could be done to translate the energy modeling code to an object-oriented programing language, to increase the turnaround time and flexibility of modeling new buildings.

Several features could also be added to the model to increase its generality, so that it could be applied to wider range of problems.

- The analysis could be extended into the time domain, to model the thermal capacitance of the structure. Although the thermal capacitance of the building was not significant in this specific study, since the building was operated at a constant set-point temperature due to its extended operating hours, the ability to specify a reduced setback temperature during unoccupied hours could be useful.
- A module for calculating the solar gains, based on the analysis procedure described in Chapter 3, was created during the model development phase of this project. However, it was not integrated into the building energy model, since solar gains proved to be insignificant in relation to the other modes of energy transfer. For other applications, having a simplified model capable of quickly calculating the rate of solar radiation transfer through a window could be useful, to avoid the need to learn and use an additional software package.

Additional energy conservation measures could also be analyzed to expand the case studies presented in Chapter 5. An example would be simulating the switch from a compact fluorescent to an LED lighting system.

Appendices

Appendix A
Energy Balance of the Cooking Process

The total energy transferred from an oven to a baked product during a cooking process was experimentally quantified. Tests were conducted at a local "Training Center" in Southern Ontario, using a deck style oven (Blodgett 1048B). The flow rate of natural gas to the appliance was measured with a thermal dispersion flow meter (McMillan 50D-13). In this test, the baked product under consideration was a single pizza, with an average mass of 1.9 kg.

Experiments began once the oven reached a steady state, at a set-point temperature of 288°C (550°F). The tests were conducted by opening the oven door for seven seconds (the average time required to insert a product), inserting the baked product into the oven, waiting seven minutes for the product to fully cook, and opening the oven door for seven seconds to remove the finished product. During the test, the natural gas flow rate to the oven was recorded every ten seconds. The data from one of the cooking tests is shown below in Figure A.1.

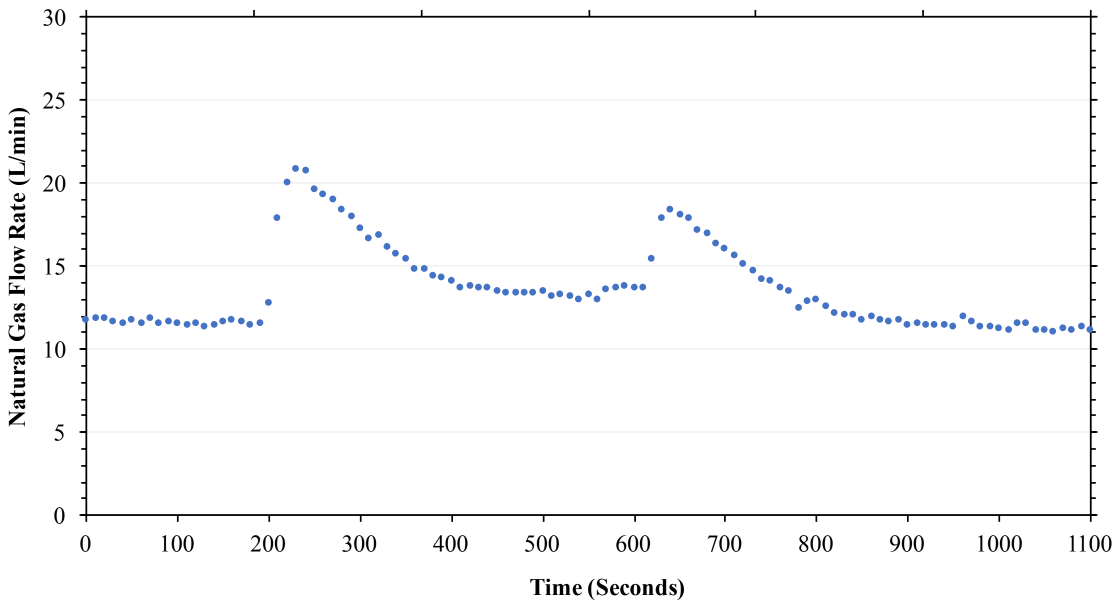

Figure A.1: Single Pizza Cooking – Effect on Oven Gas Flow Rate

The total energy transferred to the baked product was measured indirectly as follows:

- The total energy that was transferred to the baked product and lost through the two door openings, was equivalent to the energy content of the additional natural gas used above the baseline natural gas flow rate.

$$Increase\ in\ Energy\ During\ Cooking\ Process = 924\ KJ$$

- The total energy transferred to the baked product was then discerned, by subtracting the energy lost through each of the two oven door openings, as determined in Section 4.4.

$$Energy\ Lost\ from\ One\ Door\ Opening = 185\ KJ$$

$$Energy\ Transferred\ to\ Baked\ Product = 554\ KJ$$

Appendix B
The Effect of Oven Selection and Operating Schedules on Oven Gas Consumption

Oven operating schedules and arrangements can measurably impact the natural gas consumption of the appliance over a single day. This appendix presents a compilation of the oven operating characteristics of the six, deck style, ovens (Blodgett) that were monitored throughout the duration of this study. The results presented identify the absolute and percent reduction in energy required for oven operation that may be achieved, as well as provide inputs required to complete the building energy balance.

Firstly, the steady state natural gas flow rates of the six restaurant ovens were measured. The two ovens from Store A, two ovens from Store B, and the set of double stacked ovens from the test kitchen, described in Appendix A, were considered. The steady state natural gas flow rates, at cooking temperature (288°C, 550°F) and the reduced standby temperature (149°C, 300°F), are shown below in Table B.1.

Table B.1: Measured Oven Gas Flow Rates

Oven	Gas Flow Rate (L/min)	
	Cooking Temperature 288°C (550°F)	Reduced Standby Temperature 149°C (300°F)
Store A - Oven 1	15.40	-
Store A - Oven 2	13.51	-
Store B - Oven 1	16.55	9.08
Store B - Oven 2	15.93	8.02
Test Kitchen - Bottom Oven	15.35	-
Test Kitchen - Top Oven	10.95	-

Several elements of the table must be explained. The gas flow rate of the top oven at the test kitchen was 28.7% lower than that of the bottom oven. The gas flow rate was lower, because the intake air to the top oven was preheated as it passed through the 3-inch gap that separated the two ovens. By this observation, it was assumed that a top oven operating in a double stack, where both ovens are operational, would have a gas flow rate that is 28.7% less than the gas flow rate of the bottom oven.

It was also observed that the gas flow rate at 149°C (300°F) was 45% and 50% lower than the flow rate at 288°C (550°F), for Store B – Oven 1 and Store B – Oven 2 respectively. The change can be explained by examining the steady state energy balance of the oven, which requires the energy content of the natural gas input to equal the heat losses from all sources, which can be modeled with equation (B.1).

$$\dot{Q}_{Natural\ Gas} = \dot{m}_{exhaust} C_p \Delta T + (UA)_{Oven} \Delta T \tag{B.1}$$

Assuming that the exhaust mass flow rate remains constant as the oven set-point temperature changes, as proven in [7], then the steady state gas flow rate is solely a function of the difference between the oven set-point temperature and the temperature of the surroundings. Therefore, assuming that the surroundings remain at a constant temperature of 21°C (70°F), a set-point temperature reduction from 288°C (550°F) to 149°C (300°F), constitutes a 52% reduction in the temperature difference, which in turn constitutes a 52% reduction in the natural gas flow rate. The experimental observations are consistent with this reasoning based on the first law of thermodynamics, and the slight differences are likely due to the ovens uncalibrated open loop temperature control system. Moving forwards, it was assumed that the natural gas flow rate would decrease by 52%, when the oven set-point temperature is reduced from 288°C (550°F) to 149°C (300°F).

From these measurements, ovens were generalized into two distinct operational arrangements:

1) Operated Independently - or - Bottom Oven in a Double Stack

2) Top Oven in a Double Stack (With both Ovens Operating)

The average gas flow rates, for each operational arrangement and set-point temperature, carried forward in the analysis are shown below in Table B.2.

Table B.2: Generalized Oven Gas Flow Rates

Operating Arrangement	Temperature	Gas Flow Rate (L/min)
Operated Independently - or - Bottom Oven in a Double Stack	High 288°C (550°F)	15.35 (average of the first 5 ovens)
	Low 149°C (300°F)	7.37 (52% reduction from high value)
Top Oven in a Double Stack (With both ovens operating)	High 288°C (550°F)	10.95 (28.7% reduction due to preheating)
	Low 149°C (300°F)	5.26 (52% reduction from high value)

The oven gas consumption during startup and shutdown processes was also considered, by measuring the gas flow rate profiles using the laboratory oven described in Experimental Facility 3. This oven was used to measure the transient flow rates, since the internally compensated laminar flow meter (Alicat M-50SLMP-D) was able to measure the instantaneous volume flow rate with a maximum error of 0.3 L/min [53]. Four different step changes were tested including: 149°C to 288°C, 288°C to 149°C, 21°C to 288°C, and 288°C to 21°C. A relationship was then derived between the average natural gas flow rate during startup, and the difference between the initial and final steady state gas flow rates. A similar relationship was derived for the shutdown process. The results of the startup and shutdown tests are shown below in Figure B.1 through Figure B.3.

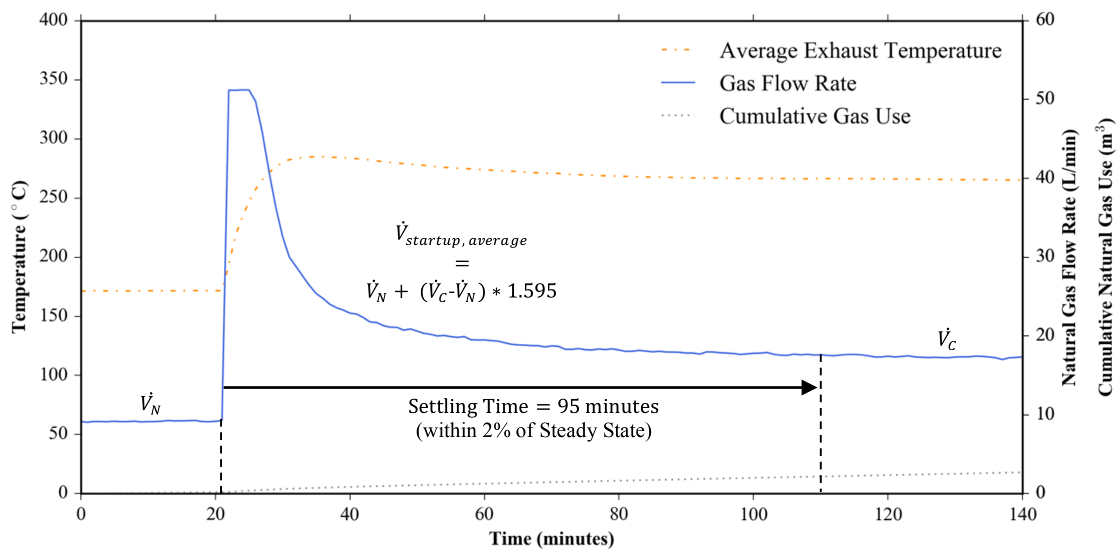

Figure B.1: Oven Startup Test (149°C to 288°C)

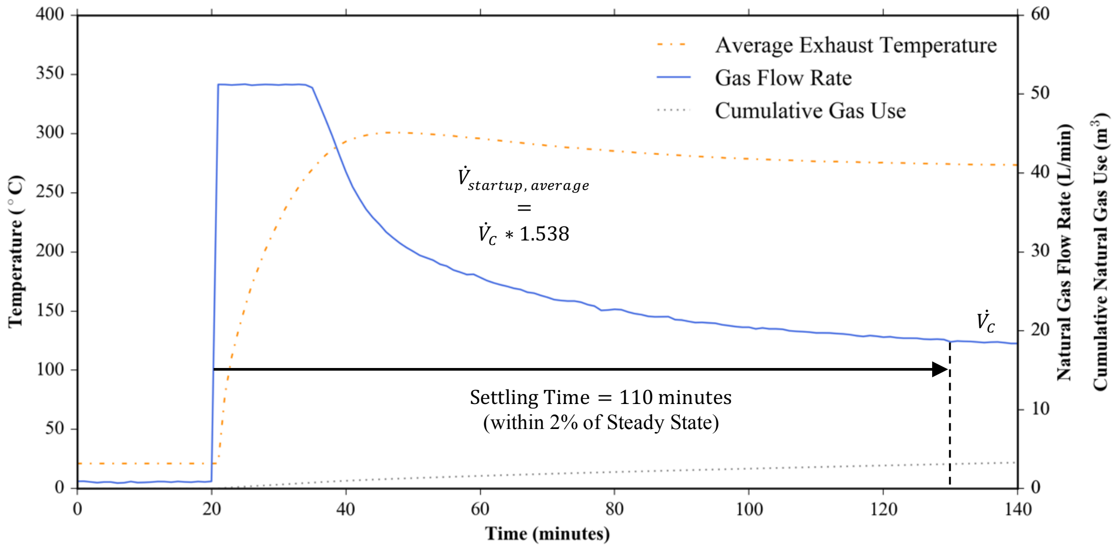

Figure B.2: Oven Startup Test (21°C to 288°C)

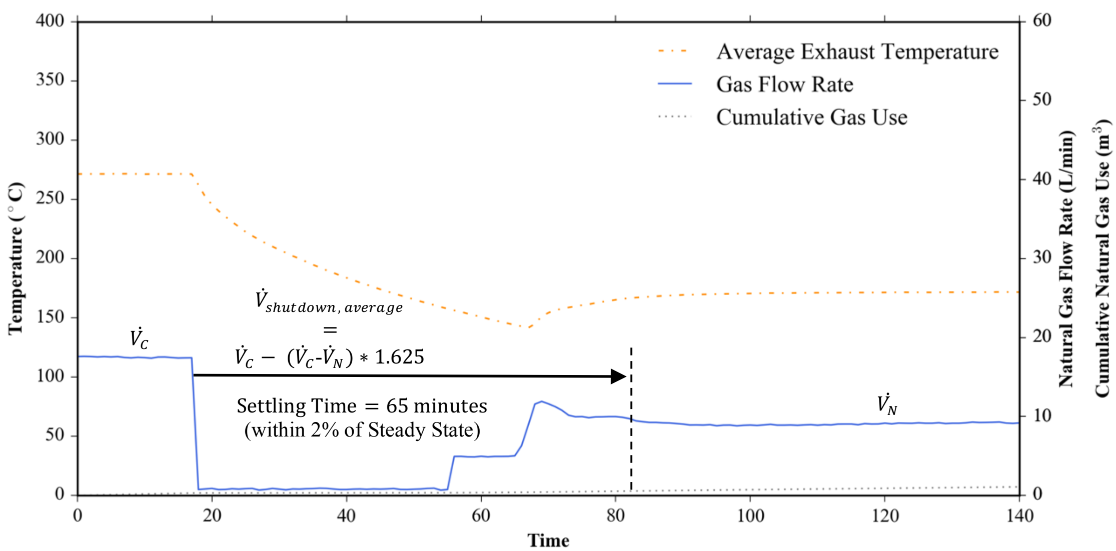

Figure B.3: Oven Shutdown Test (288°C to 149°C)

Before presenting an operating schedule, the starting time of the oven was determined, taking the settling time of the two step changes into account. In order to not adversely affect the quality of the product, the design constraints required the oven to be at steady state operating conditions before the first products of the morning were cooked.

Although this time may vary on a day to day basis, it was assumed that cooking begins at 9:30 am, an hour and a half before the store is opened at 11:00 am. In the case where the ovens are turned down to 149°C (300°F) at night, the settling time during oven startup was 95 minutes, which would require the ovens to be turned on at roughly 8:00 am. In the case where the ovens are fully turned off at night, the settling time during oven startup was 110 minutes, which would require the ovens to be turned on at approximately 7:30 am.

Figure B.4 and Figure B.5 below display the natural gas flow rates, and temperatures, that would be seen at a single oven assuming the startup process begins at 8:00 am when the oven is set to 149°C (300°F) at night, and at 7:30 am when the oven is turned off at night. The oven was set to standby mode, or turned off, at a typical weighted average closing time of 2:30 am the next day.

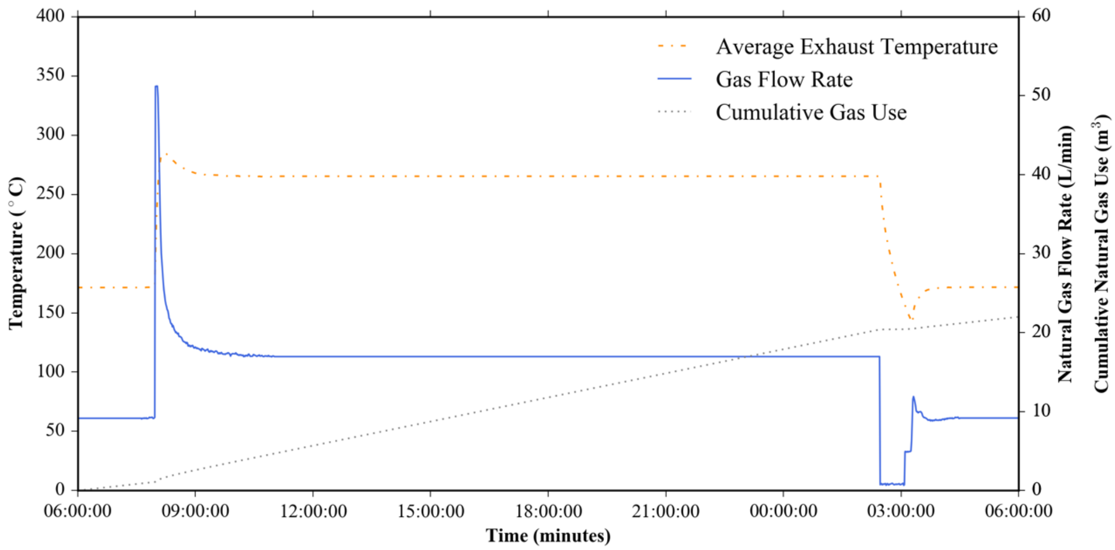

Figure B.4: Oven Gas Flow Rate and Temperature Profile for a Typical Day (149°C – 288°C – 149°C)

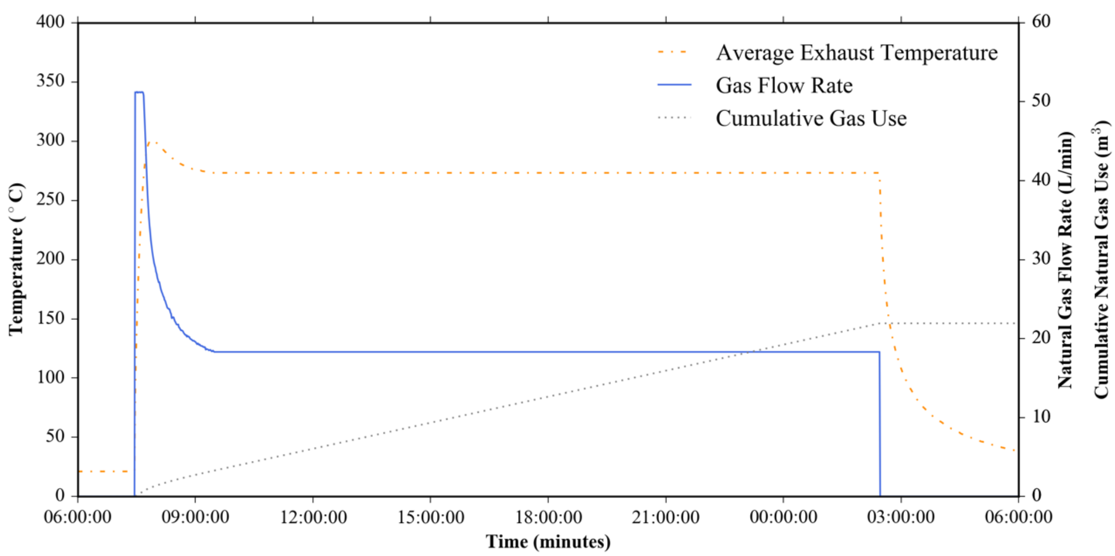

Figure B.5: Oven Gas Flow Rate and Temperature Profiles for a Typical Day (21°C – 288°C – 21°C)

Finally, the total amount of gas required to operate two ovens for a single day was inferred, by applying the steady state natural gas flow rates summarized in Table B.2, to the profiles illustrated in Figure B.4 and Figure B.5. The amount of natural gas required to operate the two ovens for a single day is shown below in Table B.3.

Table B.3: Summary of Natural Gas Requirements for Different Oven Schedules and Arrangements

Operating Setup	Overnight Oven Temperature					
	550°F		300°F		Off	
	Operating Cost	Savings	Operating Cost	Savings	Operating Cost	Savings
Two Independent Ovens	44.2 m^3/day 16,136 m^3/year	-	39.2 m^3/day 14,306 m^3/year	5.0 m^3/day 1,830 m^3/year 11.3%	36.8 m^3/day 13,437 m^3/year	7.4 m^3/day 2,699 m^3/year 16.7%
Two Ovens in a Double Stack	37.9 m^3/day 13,823 m^3/year	6.3 m^3/day 2,313 m^3/year 14.3%	33.6 m^3/day 12,256 m^3/year	10.6 m^3/day 3,880 m^3/year 24.0%	31.5 m^3/day 11,512 m^3/year	12.7 m^3/day 4,624 m^3/year 28.7%

Oven operating characteristics in two additional cases were also considered. The first was the sealed and insulated case, the topic of Section 5.7 where the oven door was fully sealed to eliminate exfiltration, and the oven was surrounded with a 2-inch fiberglass insulating cover to limit conduction heat losses through the oven walls. The second case was where the oven exhaust vent was fully sealed during the night, the topic of Section 5.8, by remotely closing the exhaust damper.

For both cases, a transient cool down analysis was conducted, to determine the rate of oven cooling throughout the night. It was important to determine the starting temperature of the oven in the morning, so that an appropriate startup time could be selected. Given the value of the oven overall heat transfer coefficient, the lumped capacitance energy balance could be solved, and fit to the experimental cool down tests conducted in the restaurants. The model was then used to calculate the transient temperature profiles that would occur for the two oven setups.

The governing equation for conservation of energy assuming that the oven can be modeled as a lumped system was proposed by Girard [7], and is shown in equation (B.2).

$$\left(mC_p\right)_{oven}\frac{dT}{dt} = -\left(\dot{m}C_p\right)_{air}\left(T_{oven} - T_{room}\right) - (UA)_{oven}\left(T_{oven} - T_{room}\right) \quad \text{(B.2)}$$

Where:

m_{oven}: mass of cordierite baking stone [7]

$$m_{oven} = 85\ kg$$

$C_{p_{oven}}$: specific heat capacity of cordierite baking stone [55]

$$C_{p_{oven}} = 1464\ \frac{J}{kg\ \cdot K}$$

$\dot{m}_{air}$: average mass flow rate of air through the oven, which was assumed to be constant. This value was determined by regression analysis [kg/s]

$C_{p_{air}}$: specific heat capacity of air at 20°C [33]

$$C_{p_{air}} = 1005\ \frac{J}{kg \cdot K}$$

T_{room}: temperature of the surrounding air [$°C$]

$(UA)_{oven}$: overall heat transfer coefficient of the oven [7]

$$(UA)_{oven,uninsulated} = 3.71\frac{W}{K} \qquad (UA)_{oven,insulated} = 0.20\ \frac{W}{K}$$

This first order, linear, homogeneous, ordinary differential equation can be solved by integration using separation of variables to yield the solution:

$$\frac{T_{oven} - T_{room}}{T_{oven,initial} - T_{room}} = \exp\left(-\left[\frac{\left(\dot{m}C_p\right)_{air} + (UA)_{oven}}{\left(mC_p\right)_{oven}}\right]t\right) \tag{B.3}$$

First, the solution of equation (B.3) was fit to the experimental oven cool down data collected from Oven 2 at Store B on March 19, 2017 to determine the average mass flow rate of air through the oven during shutdown. $\dot{m}_{air}$ was determined by minimizing the error sum of squares using equation (B.4):

$$\min_{\dot{m}_{air}} \sum_{t=1}^{N_p} \left[T_{oven_{(experimental)}}(t) - T_{oven_{(model)}}(t)\right]^2 \tag{B.4}$$

The resulting model and experimental data from the test are shown below in Figure B.6.

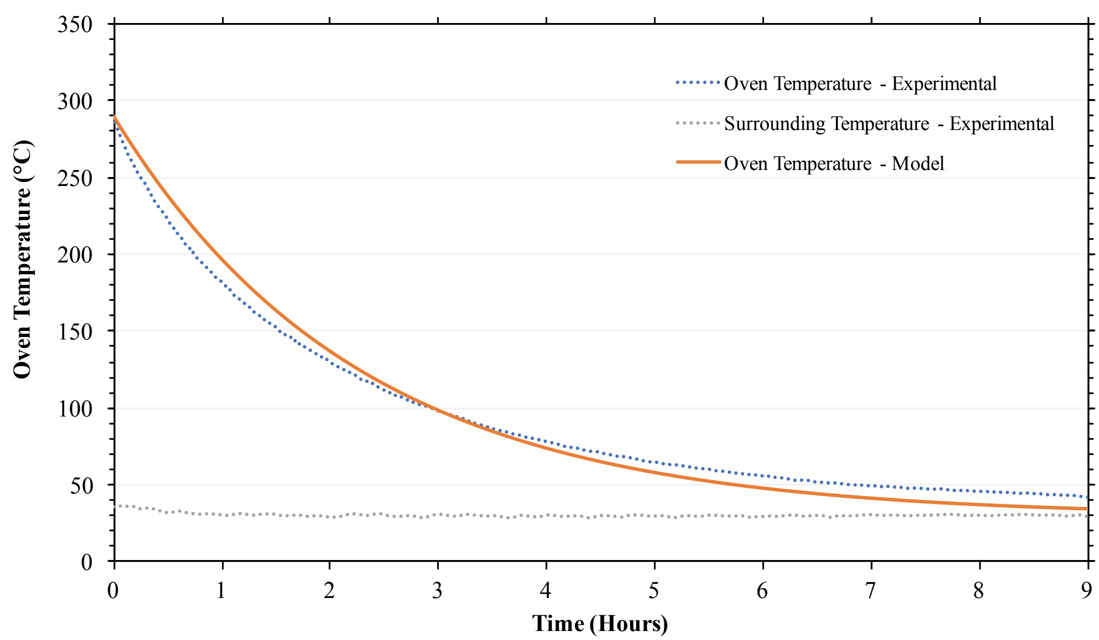

Figure B.6: Oven Cool Down Test – Regression Analysis

The average mass flow rate of air, which was assumed constant, was determined to be 0.012 kg/s, with a resulting coefficient of determination of $R^2 = 0.981$.

Assuming a constant mass flow rate introduced an error to the model, since the air mass flow rate is actually proportional to the oven temperature. This explains why the model underpredicted the rate of cooling in the first few hours of the experiment, when the mass flow rate of air was actually higher than 0.012 kg/s, and overpredicted the rate of cooling in the later hours of the experiment, when the mass flow rate of air was actually lower than 0.012 kg/s. For comparison, conducting a simple steady state energy balance on the independent oven introduced in in Table B.2 operating at 288°C (550°F) using equation (B.1) produces an air mass flow rate of 0.031 kg/s. Regardless, the model was able to provide a reasonably good fit to the experimental data.

The model was then modified to predict the rate of cooling for the insulated oven with a sealed door (sealed and insulted case), and the insulated oven with a fully sealed exhaust vent (sealed exhaust vent case). For the sealed and insulated oven, the overall heat transfer coefficient was reduced from 3.71 W/K to 0.20 W/K, and the mass flow rate was reduced by 12.8%, from 0.012 kg/s to 0.010 kg/s (since the rate of exfiltration through the oven door was only 12.8% of the total mass flow rate of air through the oven). For the oven with a fully sealed exhaust vent, an overall heat transfer coefficient of 0.20 W/K was used, and the oven was assumed to be perfectly sealed, with mass flow rate of 0 kg/s. The results of the three transient temperature profiles, assuming an initial oven temperature of 288°C (550°F) and a surrounding temperature of 21°C are shown below in Figure B.7.

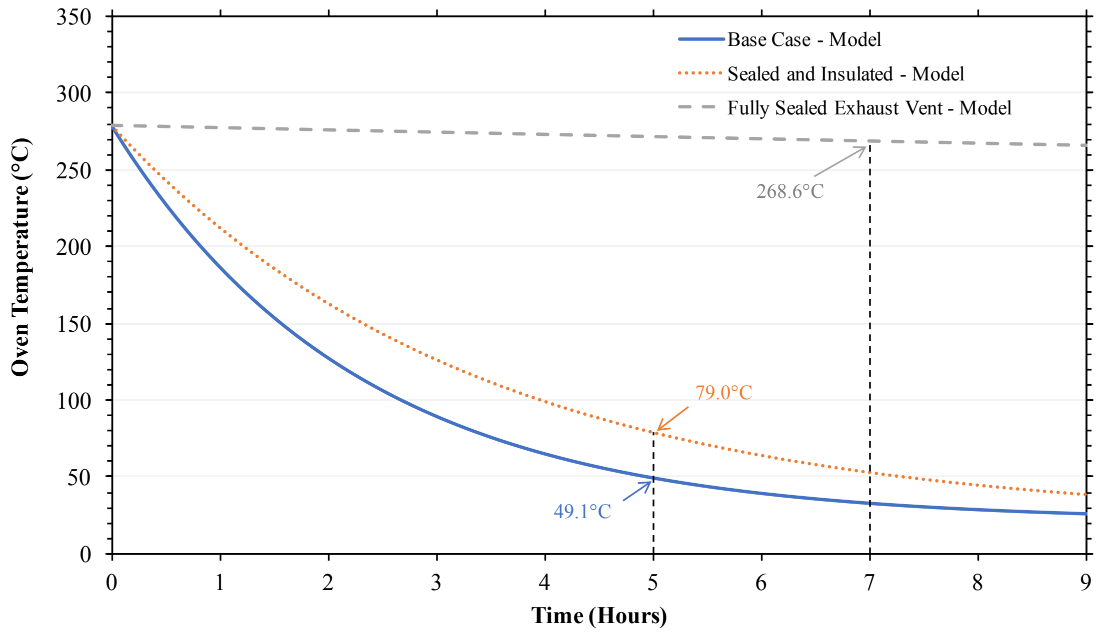

Figure B.7: Oven Temperature Profiles During Shutdown

The results of Figure B.7 show that the solution is relatively insensitive to the parameter changes associated with sealing and insulating the oven, however the act of fully sealing the oven exhaust vent dramatically reduces the rate of heat loss. If the oven was shut down at 2:30 am, by 7:30 am (5 hours later) the oven temperature would have dropped to 49.1°C and 79.0°C for the base case and the sealed and insulated case respectively. Based on the oven startup profiles presented in Figure B.1 and Figure B.2, the settling time would be between 95 minutes and 110 minutes. Therefore, a startup time of 7:30 am would still be recommended, to ensure the oven has reached a steady state before 9:30 am.

However, fully sealing the exhaust vent with the TEG POWER system provides a great benefit, as the oven temperature at 9:30 am (7 hours into cooling) would have only decreased to 268.6°C (515.5°F). As a result, it is proposed that if the oven is insulated, and fully sealed with the TEG POWER system, that the oven may be fully shut down at night, and started remotely at 9:30 am, immediately before cooking commences.

Appendix C
Uncertainty Analysis

The total uncertainty of each measured variable, δx, was calculated using equation (C.1), from each of the individual uncertainties, δ_i, that contributed to the total uncertainty of the measured variable. The calculation was done in accordance with the ASME standard PTC 19.1-2005 [54]:

$$\delta x = \sqrt{\sum_{i=1}^{n} (\delta_i)^2} \tag{C.1}$$

Table C.1 and Table C.2 below present the total absolute and relative uncertainties associated with each measured variable, based on the specifications stated by the instrument manufacturers.

Table C.1: Uncertainty of Measured Variables – Part 1

Measurement	Device	Individual Uncertainties		Total Uncertainty	
		Uncertainty Type	Value	Absolute	Relative
Room Temperatures	Wall Mounted Thermocouple Sensor (Omega EWS-TC-T)	Accuracy Cold-junction compensation accuracy Temperature measurement accuracy	±1.1°C ±0.8°C ±0.02°C	±1.4°C	(@21°C) ±6.7%
Kitchen Temperature	Solid State Temperature Sensor (Omega EWS-RH)	Accuracy Repeatability	±1.4°C ±0.3°C	±1.4°C	(@30°C) ±4.7%
Kitchen Relative Humidity	Thin Film Polymer Capacitor Sensor (Omega EWS-RH)	Accuracy (from 20 to 80% RH) Repeatability	±3% RH ±1% RH	±3.2% RH	(@50% RH) ±6.4%
Outdoor Temperature	Temperature and Relative Humidity Probe (Cambell Scientific HMP45C-L)	Accuracy (@ 20°C)	±0.2°C	±0.2°C	(@21°C) ±1.0%
Outdoor Relative Humidity	Temperature and Relative Humidity Probe (Cambell Scientific HMP45C-L)	Accuracy (@ 20°C against factory reference)	±1% RH	±1% RH	(@73% RH) ±1.4%
Oven Exhaust Temperature	T-type Thermocouple (Omega TMQSS-125U-6) (Omega TJ60-CPSS-18U-6-CC)	Accuracy Cold-junction compensation accuracy Temperature measurement accuracy	±1.0°C ±0.8°C ±0.02°C	±1.3°C	(@240°C) ±0.5%
Cumulative Natural Gas Use	Positive Displacement Flow Meter (ACM-250 & ACM-425)	Volume of diaphragm	±0.05 m^3	±0.05 m^3	±0.2%

Table C.2: Uncertainty of Measured Variables – Part 2

Measurement	Device	Individual Uncertainties		Total Uncertainty	
		Uncertainty Type	Value	Absolute	Relative
DHW Temperatures	T-type Thermocouple (Omega TMQSS-125U-6)	Accuracy Cold-junction compensation accuracy Temperature measurement accuracy	±1.0°C ±0.8°C ±0.02°C	±1.3°C	max(@10°C) ±13.0% min(@58°C) ±2.2%
DHW Flow Rate	Turbine Flow Meter (Omega FTB- 4605)	Accuracy	±1.5% of rate	(@6.5L/min) ±0.10 L/min	±1.5%
DHW Electrical Power Input	AC Power Transducer (CR Magnetics CR6210-250-20)	Accuracy	±0.5%	±10 W	±0.5%
HVAC Electric Current	Current Transducer (CR9580-20-M)	Accuracy	±0.5%	0.1 A	±0.5%
Pitot-static Tube Differential Pressure	Differential Pressure Transducer (Fluke 922 Airflow Meter)	Accuracy	±1Pa	±1 Pa	max(@12 Pa) ±7.7% min(@93 Pa) ±1.1%
Natural Gas Flow Rate	Laminar Flow Meter (Alicat M-50SLMP-D)	Accuracy Repeatability	±(0.4% of Reading + 0.2% of FS) ±0.2% of FS	(@17.5 L/min) ±0.2 L/min	(@17.5 L/min) ±1.1%
Oven Temperature	E-type Thermocouple (Omega EMQSS-125U-24)	Accuracy Cold-junction compensation accuracy Temperature measurement accuracy	±1.7°C ±0.8°C ±0.02°C	±1.9°C	(@287°C) ±0.7%
Coolant Water Flow Rate	Coriolis Flowmeter (Endress+Hauser Promass 80E)	Accuracy Repeatability	±0.20% of Reading ±0.10% of Reading	(@6 L/min) ±0.01 L/min	(@6 L/min) ±0.2%
Coolant Water Temperatures	T-type Thermocouple (Omega TMQSS-125U-6)	Accuracy Cold-junction compensation accuracy Temperature measurement accuracy	±1.0°C ±0.8°C ±0.02°C	±1.3°C	max(@69.5°C) ±1.9% min(@74.4°C) ±1.7%
Natural Gas Flow Rate	Thermal Dispersion Flow Meter (McMillian 50D-13)	Accuracy Repeatability	±1.5% of FS ±0.25% of FS	±1.52 L/min	(@12 L/min) ±12.7%

The uncertainties in the dependent variables, δy, were then considered. The procedure used to determine the propagation of uncertainty from the measured variables into the dependent variables, established by Kline and McClintock, is described with equation (C.2) below [55].

$$\delta y = \sqrt{\left(\frac{\partial y}{\partial x_1}\,\delta x_1\right)^2 + \left(\frac{\partial y}{\partial x_2}\,\delta x_2\right)^2 + \cdots + \left(\frac{\partial y}{\partial x_n}\,\delta x_n\right)^2} \tag{C.2}$$

Where:

δy: uncertainty in dependent variable

δx: uncertainty in measured variable

$\frac{\partial y}{\partial x}$: partial derivative of dependent variable with respect to each independent variable

Table C.3: Propagation of Uncertainty

Dependent Variable		Total Uncertainty	
Name	Symbol	Absolute	Relative
Building Temperature Difference	$T_{out} - T_{in}$	±1.4°C	@ $(T_{out} - T_{in}) = 13°C$ ±10.8%
Heat Transfer Through Building Skin	$\dot{Q}_{Building\ Skin}$	±0.27 kW	@ $\dot{Q}_{Building\ Skin} = 2.38\ kW$ ±11.3%
Ventilation Mass Flow Rate	$\dot{m}_{total\ ventilation}$	±0.02 kg/s	@ $\dot{m}_{total\ ventilation} = 1.69\ kg/s$ ±1.2%
Ventilation Sensible Energy	$\dot{Q}_{Ventilation\ Sensible}$	±1.85 kW	@ $\dot{Q}_{Ventilation\ Sensible} = 17.01\ kW$ ±10.9%
Water Vapour Saturation Pressure	p_{ws}	±0.12 kPa	@ $p_{ws} = 2.55\ kPa$ ±4.9%
Partial Pressure of Water Vapour	p_w	±0.084 kPa	@ $p_w = 1.58\ kPa$ ±5.3%
Humidity Ratio	W	±0.00053 kg/kg	@ $W = 0.0098\ kg/kg$ ±5.3%
Humidity Ratio Difference	$W_{out} - W_{in}$	±0.00087 kg/kg	@ $W_{out} - W_{in} = 0.0042\ kg/kg$ ±20.6%
Ventilation Latent Energy	$\dot{Q}_{Ventilation\ Latent}$	±1.60 kW	@ $\dot{Q}_{Ventilation\ Latent} = 7.75\ kW$ ±20.7%
Oven Temperature Difference	$T_{oven} - T_{room}$	±2.36°C	@ $(T_{oven} - T_{room}) = 267°C$ ±0.9%
Conduction Through Oven Structure	$\dot{Q}_{oven,structure}$	±0.01 kW	@ $\dot{Q}_{oven,structure} = 0.99\ kW$ ±1.3%
Radiation from Oven Structure	$\dot{Q}_{oven,structure\ (rad)}$	±0.05 kW	@ $\dot{Q}_{oven,structure\ (rad)} = 0.78\ kW$ ±6.4%
DHW Thermal Energy	$\dot{Q}_{water,thermal}$	±0.03 kW	@ $\dot{Q}_{water,thermal} = 0.61\ kW$ ±4.1%
Rate of Exhaust Gas Energy Recovery	$\dot{Q}_{recovered}$	±0.73 kW	@ $\dot{Q}_{recovered} = 1.95\ kW$ ±37.3%

Appendix D
Utility Measurements

Utility measurements of natural gas and electricity were obtained from a full year's worth of bills collected from Union Gas and Alectra Utilities (Formerly Horizon Utilities). Table D.1 and Table D.2 below summarize the natural gas and electricity measurements respectively.

Table D.1: Natural Gas Utility Bill Summary [56]

Billing Month	Natural Gas Consumption (m^3)	
	Store A	Store B
Jan, 2016	3,604	3,161
Feb, 2016	3,950	3,021
Mar, 2016	2,928	2,572
Apr, 2016	2,468	2,186
May, 2016	1,815	1,526
Jun, 2016	1,801	1,830
Jul, 2016	1,236	1,558
Aug, 2016	1,341	1,765
Sep, 2016	1,832	1,489
Oct, 2016	2,092	1,691
Nov, 2016	2,249	1,532
Dec, 2016	3,961	2,862
Total	29,276	25,194

Table D.2: Electricity Utility Bill Summary [57]

Billing Month	Electricity Consumption (kWh)	
	Store A	Store B
Mar, 2016	8,647	9,203
Apr, 2016	8,831	9,287
May, 2016	11,077	13,392
Jun, 2016	12,269	14,261
Jul, 2016	17,222	19,337
Aug, 2016	16,757	18,116
Sep, 2016	9,105	10,132
Oct, 2016	10,268	12,231
Nov, 2016	8,794	9,277
Dec, 2016	11,430	9,535
Jan, 2017	9,392	8,556
Feb, 2017	8,572	9,100
Total	132,362	142,429

References

[1] United Nations Population Division, "The world at 6 Billion."

[2] "BP Energy Outlook | Energy economics | BP Global." [Online]. Available: http://www.bp.com/en/global/corporate/energy-economics/energy-outlook.html. [Accessed: 16-Jun-2017].

[3] Canada Energy Systems Analysis Research, "Sankey diagrams of Canada's energy systems," *Canada's Energy Systems in 2013*. [Online]. Available: http://www.cesarnet.ca/visualization/sankey-diagrams-canadas-energy-systems?scope=Canada&year=2013&modifier=none&display=value&hide=exp&scalevalue=0.017967697941545933#chart-form. [Accessed: 16-Jun-2017].

[4] A. Molson, "Natural Gas Account Summary."

[5] Statistics Canada, "Households and the Environment: Energy Use," 2011.

[6] D. Finnerty, "The Development of Methodologies and a Novel Test Facility for the Characterisation of Thermoelectric Generators," M.A.Sc Thesis, McMaster, 2013.

[7] J. Girard, "The investigation of exhaust control strategies and waste heat recovery practices of naturally-ventilated exhaust streams," M.A.Sc Thesis, McMaster, 2016.

[8] J. P. Waltz, "Practical Experience in Achieving High Levels of Accuracy in Energy Simulations of Existing Buildings," in *ASHRAE Transactions*, 1992, vol. 98, pp. 606–617.

[9] D. B. Crawley, J. W. Hand, M. Kummert, and B. T. Griffith, "Contrasting the capabilities of building energy performance simulation programs," *Build. Environ.*, vol. 43, no. 4, pp. 661–673, Apr. 2008.

[10] M. Trcka, J. L. M. Hensen, and M. Wetter, "Co-simulation of innovative integrated HVAC systems in buildings," *J. Build. Perform. Simul.*, vol. 2, no. 3, pp. 209–230, Sep. 2009.

[11] "ESP-r." [Online]. Available: http://www.buildingenergysoftwaretools.com/software/esp-r-0. [Accessed: 19-Jun-2017].

[12] I. Beausoleil-Morrison, F. Macdonald, M. Kummert, T. McDowell, and R. Jost, "Co-simulation between ESP-r and TRNSYS," *J. Build. Perform. Simul.*, vol. 7, no. 2, pp. 133–151, Apr. 2013.

[13] University of Wisconsin, "TRNSYS 18," Mar-2017. [Online]. Available: http://sel.me.wisc.edu/trnsys/index.html. [Accessed: 19-Jun-2017].

[14] D. B. Crawley *et al.*, "EnergyPlus: creating a new-generation building energy simulation program," *Energy Build.*, vol. 33, no. 4, pp. 319–331, Apr. 2001.

[15] M. J. Witte, "EnergyPlus Development: 2016 Building Technologies Office Peer Review," U.S. Department of Energy Office of Energy Efficiency & Renewable Energy.

[16] G. N. Walton, *Thermal Analysis Research Program reference manual*. National Bureau of Standards.

[17] R. Strand *et al.*, "Enhancing and extending the capabilities of the building heat balance simulation technique for use in EnergyPlus," in *Proceedings of Building Simulation'99, IBPSA*, Kyoto, Japan, 1999, vol. II, pp. 653–660.

[18] Y. J. Huang *et al.*, “Linking the COMIS multi-zone airflow model with the EnergyPlus building energy simulation program,” in *Proceedings of Building Simulation’99, IBPSA*, Kyoto, Japan, 1999, vol. II, pp. 1065–1070.

[19] D. K. Arasteh, E. U. Finlayson, and C. Huizenga, “Window 4.1: Program Description,” Lawrence Berkeley Laboratory, Berkeley, CA, LBL-35298, Mar. 1994.

[20] Blodgett Oven Company, “Gas Deck Oven: Installation - Operation - Maintenance.” 2015.

[21] *Building Code Act, 1992*, vol. O. Reg. 332/12. 2014.

[22] ASHRAE Standing Standard Project Committee 90.1, “ANSI/ASHRAE/IES Standard 90.1-2016: Energy Standard for Buildings Except Low-Rise Residential Buildings (I-P Edition).” ASHRAE, 2016.

[23] National Fire Protection Association, “NFPA 96: Standard for Ventilation Control and Fire Protection of Commercial Cooking Operations,” Aug. 2004.

[24] *Technical Standards and Safety Act, 2000*, vol. S.O. 2000, c. 16. 2017.

[25] “B149.1-10 (R2015) - Natural gas and propane installation code.” CSA, 2010.

[26] “Standard 154-2003, Ventilation for Commercial Cooking Operations.” ASHRAE.

[27] G. Brohard, R. Swierczyna, P. Sobiski, V. Smith, and D. Fisher, “Makeup Air Effects on Kitchen Exhaust Hood Performance,” Dec. 2002.

[28] “UL 710: Standard for Exhaust Hoods for Commercial Cooking Equipment,” UL, Sep. 2012.

[29] M. P. Foster and M. J. Down, “Ventilation of Livestock Buildings by Natural Convection,” *J. Agric. Eng. Res.*, vol. 37, 1987.

[30] American Society of Heating, Refrigeration and Air-Conditioning Engineers, *2009 ASHRAE Handbook: Fundamentals*. Atlanta, GA, 2009.

[31] ISO/TC 163/SC 2, "ISO 6946:2007(en) Building components and building elements - Thermal resistance and thermal transmittance - Calculation Method," International Organization for Standardization, Dec. 2007.

[32] ISO/TC 160/SC 2, "ISO 10292:1994 Glass in building -- Calculation of steady-state U values (thermal transmittance) of multiple glazing," International Organization for Standardization, Jun. 1994.

[33] M. J. Moran, H. N. Shapiro, D. D. Boettner, and M. B. Bailey, *Fundamentals of Engineering Thermodynamics*, 7th ed. John Wiley & Sons, Inc., 2011.

[34] J. H. Keenan, F. G. Keyes, P. G. Hill, and J. G. Moore, *Steam Tables: Thermodynamic Properties of Water Including Vapor, Liquid and Solid Phases*. New York: Wiley, 1969.

[35] L. C. Nelson and E. F. Obert, "Generalized Compressibility Charts," *Chem. Eng.*, p. 61:203, 1954.

[36] T. H. Kuehn, J. W. Ramsey, and J. L. Threlkeld, *Thermal Environmental Engineering*, 3rd ed. Pearson, 1998.

[37] R. W. Hyland and A. Wexler, "Formulations for the thermodynamic properties of the saturated phases of H2O from 173.15 K to 473.15 K," in *ASHRAE Transactions*, Washington DC, 1983, vol. 89, pp. 500–519.

[38] Hydrogen Analysis Resource Center, "Lower and Higher Heating Values of Hydrogen and Other Fuels," Argonne National Laboratory, Jan. 2015.

[39] Union Gas, "Chemical Composition of Natural Gas." [Online]. Available: https://www.uniongas.com/about-us/about-natural-gas/chemical-composition-of-natural-gas. [Accessed: 29-Jun-2017].

[40] American Society of Agronomy, Crop Science Society of America, and Soil Science Society of America, *Micrometeorology in Agricultural Systems*. 677 S. Segoe Rd., Madison, WI 53711, USA, 2005.

[41] York, "Technical Guide 50Hz Predator."

[42] E. Jones, T. Oliphant, and P. Peterson, "SciPy: Open Source Scientific Tools for Python," 2001. [Online]. Available: http://www.scipy.org.

[43] P. J. Pritchard, *Fox and McDonald's Introduction to Fluid Mechanics*, 8th ed. 111 River Street, Hoboken, NJ: John Wiley & Sons, Inc., 2011.

[44] L. R. Austin and J. D. Seader, "Entry region for steady viscous flow in coiled circular pipes," *AIChE J.*, vol. 20, no. 4, p. 820, Jul. 1974.

[45] S. V. Patankar, V. S. Pratap, and D. B. Spalding, "Prediction of laminar flow and heat transfer in helically coiled pipes," *J. Fluid Mech.*, vol. 62, no. 3, pp. 539–551, Feb. 1974.

[46] A. Kalpakli, "Experimental Study of Turbulent Flows Through Pipe Bends," M.A.Sc Thesis, Royal Institute of Technology, Stockholm, Sweden, 2012.

[47] York, "Technical Guide Sunline 2000," 1997.

[48] M. Zaher, "The Integration of Annular Thermoelectric Generators in a Heat Exchanger for Waste Heat Recovery Applications," M.A.Sc Thesis, McMaster, 2017.

[49] W. Wagner and A. Pruß, "The IAPWS Formulation 1995 for the Thermodynamic Properties of Ordinary Water Substance for General and Scientific Use," International Association for the Properties of Water and Steam, Jun. 2002.

[50] Environment and Climate Change Canada, “Canadian Climate Normals 1981-2010 Station Data - Climate - Environment and Climate Change Canada,” 25-Sep-2013. [Online]. Available: http://climate.weather.gc.ca/climate_normals/results_1981_2010_e.html?searchType=stnName&txtStationName=hamilton&searchMethod=contains&txtCentralLatMin=0&txtCentralLatSec=0&txtCentralLongMin=0&txtCentralLongSec=0&stnID=4932&dispBack=0. [Accessed: 10-May-2017].

[51] Independent Electricity System Operator, “Ontario Planning Outlook: A technical report on the electricity system prepared by the IESO,” 1600–120 Adelaide Street West Toronto, ON M5H 1T1, Sep. 2016.

[52] U.S. Energy Information Administration, “Carbon Dioxide Emissions Coefficients,” U.S. Department of Energy, 1000 Independence Ave., SW Washington, DC 20585, Feb. 2016.

[53] Alicat Scientific, “Technical Data for Alicat M-Series Mass Flow Meters.”

[54] The American Society of Mechanical Engineers, “ASME PTC 19.1-2005,” Oct. 2006.

[55] S. J. Kline and F. A. McClintock, “Describing Uncertainties in Single-Sample Experiments,” *Mech. Eng.*, vol. 75, pp. 3–8, Jan. 1953.

[56] Union Gas, “Account Summary.”

[57] Horizon Utilities, “Your Bill: Electricity Charges.”